

# **Assessing the Feasibility of Using Statistical Shape Modelling to Detect Pulmonary Hypertension**

By George Moodley

## Abstract

Pulmonary Hypertension (PH) is a cardiovascular disorder marked by elevated pulmonary arterial pressure. It presents significant diagnostic challenges due to its symptom overlap with other conditions. This dissertation explores the feasibility of using Statistical Shape Modelling (SSM) to enhance the detection of PH through medical imaging data analysis. The study identifies shape variations in the pulmonary artery and aorta that correlate with PH, utilising Principal Component Analysis (PCA) and Partial Least Squares (PLS) regression.

The research involves preparing a comprehensive dataset by smoothing, denoising, and aligning surface meshes derived from segmented CT scans. PCA and PLS techniques are applied to capture the geometric variability within the pulmonary artery and aorta, identifying significant shape modes associated with PH. The diagnostic performance of these shape modes is assessed using Receiver Operating Characteristics (ROC) and Precision-Recall Curves (PRC), determining sensitivity, specificity, and classification rates.

The results indicate that specific shape modes within the pulmonary artery, particularly PCA Shape Mode 1 and PLS Shape Mode 1, exhibit moderate to strong correlations with mean pulmonary arterial pressure (mPAP). These findings suggest that an enlarged pulmonary artery diameter is a crucial indicator of PH. The significant shape modes demonstrated acceptable discriminative power, with AUCROC values of 0.718 and 0.734, respectively, and relatively good sensitivity of 0.744 and 0.837. However, the specificity in correctly classifying healthy patients was limited.

Validation studies on unseen data confirm the potential of SSM as a diagnostic tool for PH, though performance varied with different definitions of PH ( $mPAP \geq 25\text{mmHg}$  and  $mPAP \geq 20\text{mmHg}$ ). The study underscores the importance of a balanced dataset and the need for further refinement to enhance model accuracy and robustness.

In conclusion, SSM shows promise as a non-invasive and reliable method for detecting PH, potentially reducing diagnostic intervals and improving patient outcomes. Future work should optimise data preparation techniques, increase dataset size, and combine shape modes with other diagnostic metrics to improve the model's generalizability and accuracy.

## Acknowledgements

I want to thank my supervisor, Dr. Andrew Cookson, for his support and guidance throughout this project. Additionally, I wish to express my appreciation to the clinicians who assisted in preparing the dataset. Special thanks to Liam Burrows, undertaking his PhD at the University of Bath, for his continuous support throughout the project. Additionally, Liam supplied the dataset used within the project through a machine learning segmentation algorithm he formulated. He has always been available to address any queries or help I needed, and his assistance has been invaluable.

## Table of Contents

<b><u>ASSESSING THE FEASIBILITY OF USING STATISTICAL SHAPE MODELLING TO DETECT PULMONARY HYPERTENSION.....</u></b>	<b><u>1</u></b>
<b><u>ABSTRACT.....</u></b>	<b><u>2</u></b>
<b><u>ACKNOWLEDGEMENTS.....</u></b>	<b><u>3</u></b>
<b><u>TABLE OF CONTENTS .....</u></b>	<b><u>4</u></b>
<b><u>LIST OF FIGURES.....</u></b>	<b><u>8</u></b>
<b><u>LIST OF TABLES.....</u></b>	<b><u>12</u></b>
<b><u>ABBREVIATIONS AND ACRONYMS .....</u></b>	<b><u>14</u></b>
<b><u>UNITS .....</u></b>	<b><u>14</u></b>
<b><u>1    INTRODUCTION.....</u></b>	<b><u>15</u></b>
1.1    ANATOMY OF THE PULMONARY CIRCULATION SYSTEM.....	15
1.2    DEFINITION AND CLASSIFICATION OF PULMONARY HYPERTENSION .....	16
1.3    CURRENT PULMONARY HYPERTENSION DIAGNOSTIC METHODOLOGIES .....	17
1.4    THE DIAGNOSIS PROBLEM .....	18
1.5    PROJECT AIMS AND OBJECTIVES.....	20
<b><u>2    LITERATURE REVIEW .....</u></b>	<b><u>21</u></b>
2.1    DATA PREPARATION .....	24
2.1.1    SEGMENTATION .....	24
2.1.2    DENOISING AND SMOOTHING.....	24
2.1.3    ALIGNMENT.....	24
2.2    ATLAS CONSTRUCTION .....	25
2.2.1    MEAN TEMPLATE FORMATION AND DEFORMATIONS.....	25

2.2.2	DETERMINISTIC ATLASES OR BAYESIAN ATLASES .....	27
2.2.3	ATLAS PARAMETERS.....	27
<b>2.3</b>	<b>STATISTICAL ANALYSIS.....</b>	<b>29</b>
2.3.1	PRINCIPAL COMPONENT ANALYSIS (PCA).....	29
2.3.2	PARTIAL LEAST SQUARES (PLS) REGRESSION.....	31
2.3.3	CORRELATING TO PULMONARY HYPERTENSION (PH).....	33
<b>2.4</b>	<b>MODEL VALIDATION .....</b>	<b>34</b>
2.4.1	RECEIVER OPERATING CHARACTERISTIC CURVE AND AREA UNDER CURVE (AUCROC)	
	34	
2.4.2	YOUNDEN'S INDEX (J-STATISTIC) .....	36
2.4.3	PRECISION-RECALL CURVE (PRC) AND AREA UNDER CURVE (AUC – PRC) .....	36
2.4.4	F $\beta$ SCORE .....	38
<b>3</b>	<b>METHODOLOGY .....</b>	<b>39</b>
<b>3.1</b>	<b>PRE-PROCESSING.....</b>	<b>39</b>
3.1.1	SEGMENTATION .....	39
3.1.2	SURFACE MESH CONVERSION.....	40
3.1.3	SMOOTHING, DENOISING AND DECIMATING .....	41
3.1.4	ALIGNMENT.....	43
<b>3.2</b>	<b>ATLAS CONSTRUCTION .....</b>	<b>44</b>
3.2.1	PARAMETER SETTINGS.....	44
3.2.2	TEMPLATE FORMATION AND SHAPE DEFORMATIONS.....	46
<b>3.3</b>	<b>STATISTICAL ANALYSIS.....</b>	<b>47</b>
3.3.1	CORRELATION METHODOLOGY .....	47
3.3.2	PRINCIPAL COMPONENT ANALYSIS (PCA).....	47
3.3.3	PARTIAL LEAST SQUARES (PLS) REGRESSION.....	48
3.3.4	NEW PH DEFINITION – MPAP = 20MMHG .....	48
<b>3.4</b>	<b>MODEL FEASIBILITY VALIDATION.....</b>	<b>49</b>
3.4.1	RECEIVER OPERATING CHARACTERISTIC (ROC) CURVE.....	49
3.4.2	PRECISON RECALL CURVE (PRC) .....	49
3.4.3	PH SHAPE MODE CLASSIFICATION & UNSEEN DATA VALIDATION.....	49
<b>4</b>	<b>RESULTS AND ANALYSIS .....</b>	<b>51</b>

<b>4.1</b>	<b>SHAPE VARIANCE IN THE DATASETS .....</b>	<b>51</b>
<b>4.2</b>	<b>PCA SHAPE MODE CLASSIFICATION MAIN PULMONARY ARTERY .....</b>	<b>54</b>
4.2.1	SPEARMAN'S RANK CORRELATION COEFFICIENT .....	54
4.2.2	RECEIVER OPERATING CHARACTERISTIC (ROC) CURVE.....	57
4.2.3	PRECISION-RECALL CURVE (PRC).....	60
4.2.4	DEFINED PH CLASSIFICATION THRESHOLD .....	62
<b>4.3</b>	<b>PLS SHAPE MODE CLASSIFICATION MAIN PULMONARY ARTERY .....</b>	<b>64</b>
4.3.1	SPEARMAN'S RANK CORRELATION COEFFICIENT .....	64
4.3.2	RECEIVER OPERATING CHARACTERISTIC (ROC) CURVE.....	66
4.3.3	PRECISION-RECALL CURVE (PRC).....	68
4.3.4	DEFINED PH CLASSIFICATION THRESHOLD .....	70
<b>4.4</b>	<b>PCA SHAPE MODE CLASSIFICATION AORTA .....</b>	<b>71</b>
4.4.1	SPEARMAN'S RANK CORRELATION COEFFICIENT .....	71
4.4.2	RECEIVER OPERATING CHARACTERISTIC (ROC) CURVE.....	75
4.4.3	PRECISION-RECALL CURVE (PRC).....	77
4.4.4	DEFINED PH CLASSIFICATION THRESHOLD .....	80
<b>4.5</b>	<b>VALIDATION.....</b>	<b>82</b>
4.5.1	MAIN PULMONARY ARTERY (MPA) .....	82
4.5.2	AORTA.....	84
<b>4.6</b>	<b>CURRENT DIAGNOSTIC METHODS PERFORMANCE .....</b>	<b>85</b>
4.6.1	PULMONARY ARTERY TO AORTA RATIO (PA:A) .....	85
4.6.2	PULMONARY VASCULAR RESISTANCE (PVR).....	87
<b>4.7</b>	<b>COMPARING NEW &amp; OLD PH DEFINITIONS .....</b>	<b>88</b>
<b>5</b>	<b><u>DISCUSSION .....</u></b>	<b><u>91</u></b>
<b>5.1</b>	<b>PROJECT EVALUATION .....</b>	<b>91</b>
<b>5.2</b>	<b>PROJECT UNCERTAINTY.....</b>	<b>92</b>
<b>5.3</b>	<b>PROJECT LIMITATIONS .....</b>	<b>92</b>
<b>6</b>	<b><u>FUTURE DIRECTIONS .....</u></b>	<b><u>93</u></b>
<b>7</b>	<b><u>CONCLUSION .....</u></b>	<b><u>94</u></b>
<b>8</b>	<b><u>BIBLIOGRAPHY.....</u></b>	<b><u>95</u></b>

<b>9 APPENDIX .....</b>	<b>102</b>
<b>9.1 APPENDIX A – DATASET.....</b>	<b>102</b>
<b>9.2 APPENDIX B – NORMALITY TEST MATLAB FILE .....</b>	<b>105</b>
<b>9.3 APPENDIX C – PCA MATLAB FILE .....</b>	<b>106</b>
<b>9.4 APPENDIX D – PLS MATLAB FILE .....</b>	<b>111</b>
<b>9.5 APPENDIX E – SCATTER PLOTS MATLAB FUNCTION FILE .....</b>	<b>116</b>
<b>9.6 APPENDIX F – ROC &amp; PRC MATLAB FUNCTION FILE.....</b>	<b>126</b>
<b>9.8 APPENDIX G – CURRENT DIAGNOSTIC METHODS PERFORMANCE MATLAB FILE ....</b>	<b>129</b>
<b>9.9 APPENDIX H – VALIDATION MATLAB FILE.....</b>	<b>140</b>
<b>9.10 APPENDIX I – DEFORMETRICA FILE .....</b>	<b>149</b>
<b>9.11 APPENDIX J – NEW PH DEFINITION RESULTS - PCA MAIN PULMONARY ARTERY ..</b>	<b>151</b>
9.11.1 RECEIVER OPERATING CHARACTERISTIC (ROC).....	151
9.11.2 PRECISON RECALL CURVE (PRC) .....	153
<b>9.12 APPENDIX K – NEW PH DEFINITION RESULTS - PLS MAIN PULMONARY ARTERY ..</b>	<b>155</b>
9.12.1 RECEIVER OPERATING CHARACTERISTIC (ROC).....	155
9.12.2 PRECISON RECALL CURVE (PRC) .....	156
<b>9.13 APPENDIX L – NEW PH DEFINITION RESULTS - PCA AORTA.....</b>	<b>157</b>
9.13.1 RECEIVER OPERATING CHARACTERISTIC (ROC).....	157
9.13.2 PRECISON RECALL CURVE (PRC) .....	159
<b>9.14 APPENDIX M – EXTRA INFORMATION.....</b>	<b>161</b>
9.14.1 PH CLASSIFICATIONS.....	161
9.14.2 SEGMENTATION .....	161
9.14.3 MESH GENERATION.....	162
9.14.4 BAYESIAN Vs DETERMINISTIC ATLASES.....	162
9.14.5 LARGE DEFORMATION DIFFEOMORPHIC METRIC MAPPING (LDDMM) .....	163
9.14.6 LAPLACIAN AND TAUBIN FILTERING .....	163
9.14.7 KERNEL WIDTH .....	165
9.14.8 DEFORMETRICA.....	165
9.14.9 CORRELATION COEFFICIENTS .....	166
9.14.10 ALIGNMENT .....	166
<b>9.15 APPENDIX N – PVR EFFECTIVE ROC CURVE AND PRC.....</b>	<b>168</b>
<b>9.16 APPENDIX O – PAA EFFECTIVE ROC CURVE AND PRC .....</b>	<b>169</b>

## List of Figures

FIGURE 1. DIAGRAM OF THE PULMONARY CIRCULATORY SYSTEM. THE POINTS OF INTEREST FOR THIS STUDY ARE THE AORTA, “RED ARCH”, AND MAIN PULMONARY ARTERY, “BLUE Y-BRANCH”. (“PULMONARY CIRCULATION   DEFINITION, FUNCTION, DIAGRAM, & FACTS   BRITANNICA,” 2024).....	16
FIGURE 2. ENLARGEMENT OF THE PULMONARY ARTERY AT A MORE SIGNIFICANT MPAP VALUE, INDICATIVE OF PH (MELZIG ET AL., 2019).....	17
FIGURE 3. FLOWCHART DEMONSTRATING THE DIAGNOSIS PROBLEM WITH PH. IT SHOWS THE CONVOLUTED ROUTE TO GETTING DIAGNOSED (FROST ET AL., 2019). .....	19
FIGURE 4. THE DATA INFORMATION KNOWLEDGE WISDOM (DIKW) PYRAMID. REPRESENTS THE RELATIONSHIPS BETWEEN EACH ONE, ILLUSTRATING THE PROGRESSION OF RAW DATA TO VALUABLE INSIGHTS (BRUSE, 2017). .....	21
FIGURE 5. 2D ATLAS CREATED FROM FIVE INSTANCES OF THE DIGIT “2” FROM THE MNIST (BÔNE ET AL., 2018).....	22
FIGURE 6. SHAPE ANALYSIS OF THE MAIN PULMONARY ARTERY, USING THE CENTRELINE TOOLKIT IN 3D SLICER (SABRY ET AL., 2024).....	23
FIGURE 7. ALIGNMENT OF FOUR SKULLS AT DIFFERENT POSITIONS IN SPACE TRANSLATED ALL TO THE SAME PLACE USING THE PROCRUTES ALGORITHM (DAHDOUH ET AL., 2014). .....	25
FIGURE 8. COMPUTED TEMPLATE SHAPE (BLUE) BASED ON THE TWENTY INPUT CoA MODELS, ADAPTED FROM (BRUSE ET AL., 2016). .....	26
FIGURE 9. LARGE DEFORMATION DIFFEOMORPHIC METRIC MAPPING (LDDMM) OF AORTAS FROM THE TEMPLATE TO SUBJECTS WITHIN THE ATLAS (LEFT). EACH SUBJECT SHAPE IS UNIQUELY PARAMETERISED BY ITS DEFORMATION FUNCTION $\varphi$ ; ALL DEFORMATIONS CONCATENATED IN A MATRIX DESCRIBE ALL 3D SHAPE INFORMATION WITHIN THE POPULATION (RIGHT) (BRUSE ET AL., 2016).....	27
FIGURE 10. EFFECT OF KERNELS TO CAPTURE FEATURES OF A DISTRIBUTION (COARSE TO SMOOTH) ADAPTED FROM (IZENMAN, 2008).....	28
FIGURE 11. SHAPE MODEL OF AN AORTA REPRESENTED BY CURRENTS; CHANGING RESOLUTION $\lambda w$ (BRUSE, 2017). .....	28
FIGURE 12. SIX PCA SHAPE MODES AND THE COMPUTED ESTIMATED MEAN TEMPLATE FROM THE FOUNDING ATLAS (CUTUGNO ET AL., 2021).....	31
FIGURE 13. THE FIRST MODE FROM A PLS ANALYSIS, ADAPTED FROM (SUINESIAPUTRA ET AL., 2018).....	33
FIGURE 14. CONFUSION MATRIX (“WHAT IS A CONFUSION MATRIX IN MACHINE LEARNING?,” N.D.).....	35
FIGURE 15. A TYPICAL ROC CURVE WITH THE YOUNDEN’S INDEX (J STATISTIC) PLOTTED ON IT (XU ET AL., 2014).....	36
FIGURE 16. A TYPICAL PRC (“PRECISION-RECALL,” N.D.). .....	37
FIGURE 17. GENERAL SSM PIPELINE FROM SEGMENTATION OF THE STRUCTURE OF INTEREST TO ANATOMICAL MEAN SHAPE (TEMPLATE) COMPUTATION AND 3D SHAPE VARIABILITY DESCRIPTION VIA PRINCIPAL COMPONENT ANALYSIS (PCA), ADAPTED FROM (BIGLINO ET AL., 2017).....	39

FIGURE 18. SEGMENTATION OF THE MAIN PULMONARY ARTERY (RED, TOP), AORTA (GREEN, TOP) AND PULMONARY ARTERY CAPILLARY NETWORK (BOTTOM).....	40
FIGURE 19. SURFACE MESH GENERATED FROM SEGMENTATION IN FIGURE 18 OF THE MAIN PULMONARY ARTERY AND ITS CAPILLARY NETWORK.....	40
FIGURE 20. SURFACE MESH EXPORTED FROM THE SEGMENTATION IN FIGURE 18 OF THE MAIN PULMONARY ARTERY AND AORTA AND THEIR SUBSEQUENT SEPARATION.....	41
FIGURE 21. SMOOTHING (TOP) AND DENOISING (BOTTOM) PROCESSES UNDERTOOK. ....	42
FIGURE 22. THE DECIMATION THAT WAS UNDERTAKEN IN THE PROJECT. THE LEFT DECIMATED MESH HAS MORE CELLS AND NODES THAN THE RIGHT DECIMATED MESH. ....	43
FIGURE 23. ALIGNMENT OF THREE MESHES FROM THE MAIN PULMONARY ARTERY AND AORTA DATASETS AT THREE DIFFERENT VIEWPOINTS.....	44
FIGURE 24. EXAMPLE OF PROTRUSION WHICH WAS APPEARING ON SOME ATLAS DEFORMATIONS.....	45
FIGURE 25. THE ESTIMATED MAIN PULMONARY ARTERY AND AORTA TEMPLATES WERE COMPUTED IN THE ATLAS FROM THREE DIFFERENT VIEWPOINTS. ....	46
FIGURE 26. THE ITERATIVE RECONSTRUCTION DEFORMATION PROCESS IS UNDERTAKEN WHEN FORMULATING THE ATLAS. THE PURPLE REPRESENTS THE IITAL SHAPE, WHILE THE LILAC REPRESENTS THE FIRST ITERATIVE DEFORMATION, AND THE PINK REPRESENTS THE SECOND ITERATIVE DEFORMATION.....	47
FIGURE 27. THE AMOUNT OF SHAPE VARIANCE IN THE DATASET CAPTURED CUMULATIVELY BY THE PCA (TOP) AND PLS (BOTTOM) MODES FOR THE MAIN PULMONARY ARTERY. ....	51
FIGURE 28. THE AMOUNT OF SHAPE VARIANCE IN THE DATASET CAPTURED CUMULATIVELY BY THE PCA (TOP) AND PLS (BOTTOM) MODES FOR THE AORTA. ....	52
FIGURE 29. ROC CURVES FOR PCA SHAPE MODES 1 (TOP) AND 6 (BOTTOM) AND THEIR REPRESENTATIVE YOUDEN INDEX VALUES, THE RED DASHED LINE. THE BLACK DASHED LINE IS THE RANDOM CLASSIFIER LINE. ....	57
FIGURE 30. THE QUANTITY OF PCA SHAPE MODES 1 (TOP) AND 6 (BOTTOM) IN EACH SUBJECT WITHIN THE DATASET PLOTTED AGAINST EACH SUBJECT'S ASSOCIATED MPAP. THE RED DASHED IS THE MPAP DEFINITION FOR PH AND THE BLACK DASHED LINE IS THE SHAPE MODE QUANTITY THRESHOLD FOR CLASSIFYING PH, DEFINED BY YOUDEN'S INDEX.....	58
FIGURE 31. PRC CURVES FOR PCA SHAPE MODES 1 (TOP) AND 6 (BOTTOM) AND THEIR REPRESENTATIVE MAXIMUM $F\beta$ SCORE, THE RED DOT. THE BLACK DASHED LINE IS THE BASELINE CLASSIFIER LINE. ....	60
FIGURE 32. THE QUANTITY OF PCA SHAPE MODES 1 (TOP) AND 6 (BOTTOM) IN EACH SUBJECT WITHIN THE DATASET WAS PLOTTED AGAINST EACH SUBJECT'S ASSOCIATED MPAP. THE RED DASHED IS THE MPAP DEFINITION FOR PH, AND THE BLACK DASHED LINE IS THE SHAPE MODE QUANTITY THRESHOLD FOR CLASSIFYING PH, DEFINED BY THE MAXIMUM $F\beta$ SCORE. ....	61
FIGURE 33. THE QUANTITY OF PCA SHAPE MODES 1 (TOP) AND 6 (BOTTOM) IN EACH SUBJECT WITHIN THE DATASET PLOTTED AGAINST EACH SUBJECT'S ASSOCIATED MPAP. THE RED DASHED IS THE MPAP DEFINITION FOR PH AND THE BLACK DASHED LINE IS THE SHAPE MODE QUANTITY THRESHOLD FOR CLASSIFYING PH, DEFINED BY THE OPTIMAL VALUE AT A COMPROMISE BETWEEN THE TWO THRESHOLDS. ....	63

FIGURE 34. ROC CURVES FOR PLS SHAPE MODE 1 AND ITS REPRESENTATIVE YOUDEN INDEX VALUE, THE RED DASHED LINE. THE BLACK DASHED LINE IS THE RANDOM CLASSIFIER LINE.....	66
FIGURE 35. THE QUANTITY OF PLS SHAPE MODE 1 IN EACH SUBJECT WITHIN THE DATASET WAS PLOTTED AGAINST EACH SUBJECT'S ASSOCIATED MPAP. THE RED DASHED IS THE MPAP DEFINITION FOR PH AND THE BLACK DASHED LINE IS THE SHAPE MODE QUANTITY THRESHOLD FOR CLASSIFYING PH, DEFINED BY YOUDEN'S INDEX.....	67
FIGURE 36. PRC CURVES FOR PLS SHAPE MODE 1 AND ITS REPRESENTATIVE MAXIMUM $F\beta$ SCORE, THE RED DOT. THE BLACK DASHED LINE IS THE BASELINE CLASSIFIER LINE.....	68
FIGURE 37. THE QUANTITY OF PLS SHAPE MODE 1 IN EACH SUBJECT WITHIN THE DATASET WAS PLOTTED AGAINST EACH SUBJECT'S ASSOCIATED MPAP. THE RED DASHED IS THE MPAP DEFINITION FOR PH, AND THE BLACK DASHED LINE IS THE SHAPE MODE QUANTITY THRESHOLD FOR CLASSIFYING PH, DEFINED BY THE MAXIMUM $F\beta$ SCORE.....	68
FIGURE 38. THE QUANTITY OF PLS SHAPE MODE 1 IN EACH SUBJECT WITHIN THE DATASET PLOTTED AGAINST EACH SUBJECT'S ASSOCIATED MPAP. THE RED DASHED IS THE MPAP DEFINITION FOR PH AND THE BLACK DASHED LINE IS THE SHAPE MODE QUANTITY THRESHOLD FOR CLASSIFYING PH, DEFINED BY THE OPTIMAL VALUE AT A COMPROMISE BETWEEN THE TWO THRESHOLDS.....	70
FIGURE 39. ROC CURVES FOR PCA SHAPE MODES 20 (TOP) AND 22 (BOTTOM) AND THEIR REPRESENTATIVE YOUDEN INDEX VALUES, THE RED DASHED LINE. THE BLACK DASHED LINE IS THE RANDOM CLASSIFIER LINE.....	75
FIGURE 40. THE QUANTITY OF PCA SHAPE MODES 20 (TOP) AND 22 (BOTTOM) IN EACH SUBJECT WITHIN THE DATASET WAS PLOTTED AGAINST EACH SUBJECT'S ASSOCIATED MPAP. THE RED DASHED IS THE MPAP DEFINITION FOR PH AND THE BLACK DASHED LINE IS THE SHAPE MODE QUANTITY THRESHOLD FOR CLASSIFYING PH, DEFINED BY YOUDEN'S INDEX.....	76
FIGURE 41. PRC CURVES FOR PCA SHAPE MODES 20 (TOP) AND 22 (BOTTOM) AND THEIR REPRESENTATIVE MAXIMUM $F\beta$ SCORE, THE RED DOT. THE BLACK DASHED LINE IS THE BASELINE CLASSIFIER LINE.....	77
FIGURE 42. THE QUANTITY OF PCA SHAPE MODES 20 (TOP) AND 22 (BOTTOM) IN EACH SUBJECT WITHIN THE DATASET WAS PLOTTED AGAINST EACH SUBJECT'S ASSOCIATED MPAP. THE RED DASHED IS THE MPAP DEFINITION FOR PH, AND THE BLACK DASHED LINE IS THE SHAPE MODE QUANTITY THRESHOLD FOR CLASSIFYING PH, DEFINED BY THE MAXIMUM $F\beta$ SCORE.....	78
FIGURE 43. THE QUANTITY OF PCA SHAPE MODES 20 (TOP) AND 22 (BOTTOM) IN EACH SUBJECT WITHIN THE DATASET WAS PLOTTED AGAINST EACH SUBJECT'S ASSOCIATED MPAP. THE RED DASHED IS THE MPAP DEFINITION FOR PH AND THE BLACK DASHED LINE IS THE SHAPE MODE QUANTITY THRESHOLD FOR CLASSIFYING PH, DEFINED BY THE OPTIMAL VALUE AT A COMPROMISE BETWEEN THE TWO THRESHOLDS.....	80
FIGURE 44. BAR CHART OF PCA SHAPE MODE 1'S UNSEEN DATA VALIDATION STUDY RESULTS AND ITS SUCCESSFUL CLASSIFICATION RATE. SUCCESSFUL CLASSIFICATIONS ARE ON THE LEFT, AND INCORRECT CLASSIFICATIONS ARE ON THE RIGHT. THE CHART ALSO SHOWS THE SPLIT OF HEALTHY PATIENTS TO PATIENTS WITH PH.....	82

FIGURE 45. BAR CHART OF PLS SHAPE MODE 1'S UNSEEN DATA VALIDATION STUDY RESULTS AND ITS SUCCESSFUL CLASSIFICATION RATE. SUCCESSFUL CLASSIFICATIONS ARE ON THE LEFT, AND INCORRECT CLASSIFICATIONS ARE ON THE RIGHT. THE CHART ALSO SHOWS THE SPLIT OF HEALTHY PATIENTS TO PATIENTS WITH PH.....	83
FIGURE 46. BAR CHART OF PCA SHAPE MODE 6'S UNSEEN DATA VALIDATION STUDY RESULTS AND ITS SUCCESSFUL CLASSIFICATION RATE. SUCCESSFUL CLASSIFICATIONS ARE ON THE LEFT, AND INCORRECT CLASSIFICATIONS ARE ON THE RIGHT. THE CHART ALSO SHOWS THE SPLIT OF HEALTHY PATIENTS TO PATIENTS WITH PH.....	83
FIGURE 47. BAR CHART OF PCA SHAPE MODE 20'S UNSEEN DATA VALIDATION STUDY RESULTS AND ITS SUCCESSFUL CLASSIFICATION RATE. SUCCESSFUL CLASSIFICATIONS ARE ON THE LEFT, AND INCORRECT CLASSIFICATIONS ARE ON THE RIGHT. THE CHART ALSO SHOWS THE SPLIT OF HEALTHY PATIENTS TO PATIENTS WITH PH.....	84
FIGURE 48. THE PA:A RATIO FOR EACH SUBJECT WITHIN THE DATASET PLOTTED AGAINST EACH SUBJECT'S ASSOCIATED MPAP. THE RED DASHED IS THE MPAP DEFINITION FOR PH, AND THE BLACK DASHED LINE IS THE PA:A CURRENT CLASSIFICATION FOR A PATIENT SUSPECTED OF HAVING PH, 1.....	85
FIGURE 49. BAR CHART OF PA:A'S CLASSIFICATION RESULTS AND ITS SUCCESSFUL CLASSIFICATION RATE. SUCCESSFUL CLASSIFICATIONS ARE ON THE LEFT, AND INCORRECT CLASSIFICATIONS ARE ON THE RIGHT. THE CHART ALSO SHOWS THE SPLIT OF HEALTHY PATIENTS TO PATIENTS WITH PH. ....	86
FIGURE 50. THE PVR QUANTITY FOR EACH SUBJECT WITHIN THE DATASET WAS PLOTTED AGAINST EACH SUBJECT'S ASSOCIATED MPAP. THE RED DASHED IS THE MPAP DEFINITION FOR PH AND THE BLACK DASHED LINE IS THE PVR CURRENT CLASSIFICATION FOR A PATIENT SUSPECTED OF HAVING PH, 3 .....	87
FIGURE 51. BAR CHART OF PVR'S CLASSIFICATION RESULTS AND ITS SUCCESSFUL CLASSIFICATION RATE. SUCCESSFUL CLASSIFICATIONS ARE ON THE LEFT, AND INCORRECT CLASSIFICATIONS ARE ON THE RIGHT. THE CHART ALSO SHOWS THE SPLIT OF HEALTHY PATIENTS TO PATIENTS WITH PH. ....	88

## List of Tables

TABLE 1. THE THREE DIFFERENT DEFINITIONS OF PH.....	17
TABLE 2. RANGE OF CORRELATION COEFFICIENTS AND THEIR REPRESENTATIVE MEANING.....	34
TABLE 3. PARAMETER SETTINGS.....	45
TABLE 4. THE SIGNIFICANT SHAPE MODES ASSOCIATED WITH THE PRESENCE OF PH ARE BASED ON SPEARMAN'S RANK CORRELATION COEFFICIENT AND SPEARMAN'S RANK CORRELATION COEFFICIENT P-VALUE.....	54
TABLE 5. VISUALISATION OF PCA SHAPE MODE 1 FOR THE MAIN PULMONARY ARTERY AND ITS VARIATION ACROSS $\pm 2\sigma$ AND ITS VARIANCE OF THE DATASET.....	55
TABLE 6. VISUALISATION OF PCA SHAPE MODE 6 FOR THE MAIN PULMONARY ARTERY AND ITS VARIATION ACROSS $\pm 2\sigma$ AND ITS VARIANCE OF THE DATASET.....	56
TABLE 7. THE AUCROC VALUES FOR PCA SHAPE MODES 1 AND 6. AND THE CLASSIFICATION SUCCESS RATE OF THE SHAPEN MODES AT THE YOUDEN'S INDEX THRESHOLD.....	58
TABLE 8. THE AUCROC VALUES FOR PCA SHAPE MODES 1 AND 6. THE CLASSIFICATION SUCCESS RATE OF THE SHAPEN MODES AT THE MAXIMUM $F\beta$ SCORE THRESHOLD.....	61
TABLE 9. THE SENSITIVITY, SPECIFICITY, AND CLASSIFICATION SUCCESS RATE OF THE SHAPE MODES AT THE DEFINED OPTIMAL THRESHOLD FOR PCA SHAPE MODES 1 AND 6.....	63
TABLE 10. THE SIGNIFICANT SHAPE MODE ASSOCIATED WITH THE PRESENCE OF PH IS BASED ON SPEARMAN'S RANK CORRELATION COEFFICIENT AND SPEARMAN'S RANK CORRELATION COEFFICIENT P-VALUE.....	64
TABLE 11. VISUALISATION OF PLS SHAPE MODE 1 FOR THE MAIN PULMONARY ARTERY AND ITS VARIATION ACROSS $\pm 2\sigma$ AND ITS VARIANCE OF THE DATASET.....	65
TABLE 12. THE AUCROC VALUES FOR PLS SHAPE MODE 1. AND THE CLASSIFICATION SUCCESS RATE OF THE SHAPE MODE AT THE YOUDEN'S INDEX THRESHOLD.....	67
TABLE 13. THE AUCROC VALUES FOR PLS SHAPE MODE 1. THE CLASSIFICATION SUCCESS RATE OF THE SHAPE MODE AT THE MAXIMUM $F\beta$ SCORE THRESHOLD.....	69
TABLE 14. THE SENSITIVITY, SPECIFICITY, AND CLASSIFICATION SUCCESS RATE OF THE SHAPE MODE AT THE DEFINED OPTIMAL THRESHOLD FOR PLS SHAPE MODE 1.....	70
TABLE 15. THE SIGNIFICANT SHAPE MODES ASSOCIATED WITH THE PRESENCE OF PH ARE BASED ON THEIR SPEARMAN'S RANK CORRELATION COEFFICIENT AND SPEARMAN'S RANK CORRELATION COEFFICIENT P-VALUE.....	71
TABLE 16. VISUALISATION OF PCA SHAPE MODE 20 FOR THE AORTA AND ITS VARIATION ACROSS $\pm 2\sigma$ AND ITS VARIANCE OF THE DATASET.....	72
TABLE 17. VISUALISATION OF PCA SHAPE MODE 22 FOR THE AORTA AND ITS VARIATION ACROSS $\pm 2\sigma$ AND ITS VARIANCE OF THE DATASET.....	73
TABLE 18. THE AUCROC VALUES FOR PCA SHAPE MODES 20 AND 22. AND THE CLASSIFICATION SUCCESS RATE OF THE SHAPEN MODES AT THE YOUDEN'S INDEX THRESHOLD.....	76
TABLE 19. THE AUCROC VALUES FOR PCA SHAPE MODES 20 AND 22. THE CLASSIFICATION SUCCESS RATE OF THE SHAPEN MODES AT THE MAXIMUM $F\beta$ SCORE THRESHOLD. ....	79

TABLE 20. THE SENSITIVITY, SPECIFICITY, AND CLASSIFICATION SUCCESS RATE OF THE SHAPE MODES AT THE DEFINED OPTIMAL THRESHOLD FOR PCA SHAPE MODES 20 AND 22.....	80
TABLE 21.THE UNSEEN DATA VALIDATION STUDY PERFORMANCE METRICS FOR EACH SIGNIFICANT SHAPE MODE RELATED TO THE MAIN PULMONARY ARTERY.....	82
TABLE 22. THE UNSEEN DATA VALIDATION STUDY PERFORMANCE METRICS FOR EACH SIGNIFICANT SHAPE MODE RELATED TO THE AORTA.....	84
TABLE 23.THE EFFECTIVE AUCROC AND AUC – PRC AND SENSITIVITY AND SPECIFICITY FOR THE PA:A CLASSIFICATION THRESHOLD.....	85
TABLE 24. THE EFFECTIVE AUCROC AND AUC – PRC AND SENSITIVITY AND SPECIFICITY FOR THE PVR CLASSIFICATION THRESHOLD.....	87
TABLE 25. THE PERFORMANCE CHARACTERISTICS AT THE NEW PH DEFINITION OF mPAP = 20MMHG FOR THE REMAINING DOMINANT SHAPE MODES, WITH AN ASSOCIATION WITH THE PRESENCE OF PH, .....	89

## Abbreviations and Acronyms

AUC	Area Under the Curve
AUC – PRC	Area Under the Precision-Recall Curve
AUCROC	Area Under the Receiver Operating Characteristic Curve
CT	Computed Tomography
CTEPH	IP{Chronic Thromboembolic Pulmonary Hypertension
IPAH	Idiopathic Pulmonary Arterial Hypertension
LDDMM	Large Deformation Diffeomorphic Metric Mapping
mPAP	Mean Pulmonary Arterial Pressure
MRI	Magnetic Resonance Imaging
NIfTI	Neuroimaging Informatics Technology Initiative
PA:A	Pulmonary Artery to Aorta Ratio
PAH	Pulmonary Arterial Hypertension
PAP	Pulmonary Arterial Pressure
PCA	Principal Component Analysis
PH	Pulmonary Hypertension
PLS	Partial Least Squares (Regression)
PRC	Precision-Recall Curve
PVR	Pulmonary Vascular Resistance
RHC	Right Heart Catheterisation
ROC	Receiver Operating Characteristic Curve
SSM	Statistical Shape Modelling
SSMs	Statistical Shape Models
VTK	Visualisation Toolkit
WSPH	World Symposium on Pulmonary Hypertension

## Units

mmHg	Millimetres of Mercury (A unit of Pressure)
WU	Wood Units (A unit of Resistance)

# 1 Introduction

According to the World Health Organisation, cardiovascular diseases are the leading causes of deaths globally, responsible for millions of deaths each year (“Cardiovascular diseases (CVDs),” n.d.). The British Heart Foundation also claims cardiovascular diseases are estimated to cost the UK economy £25 billion annually (“bhf-cvd-statistics-uk-factsheet.pdf,” n.d.). One of these diseases is Pulmonary Hypertension (PH), which in the UK alone has shown an increase in the number of patients, from 1539 in 2004 to 8589 in 2020 (“Pulmonary hypertension,” n.d.). PH poses a significant worldwide health concern, impacting individuals across all age brackets. Its prominence is notably increasing among the elderly population, especially in nations with ageing demographics. Current estimates indicate a prevalence of approximately 1% of the global population, rising to 10% in individuals aged 65 years and older (Hooper et al., 2016).

PH is a pathophysiological disorder which may be encompassed within various other clinical conditions and potentially an underlying factor in the early stages of the majority of cardiovascular and respiratory diseases (Galie et al., 2009). Historically, the diagnosis of PH has faced challenges arising from a convoluted and manual process, primarily constrained by technological limitations, leading to considerable delays in diagnosis. However, recent technological advancements have paved the way for substantial improvements. Current research endeavours are dedicated to enhancing the diagnostic process by integrating machine learning with medical imaging data. This project seeks to contribute to these advancements by employing statistical shape modelling (SSM) to facilitate the accurate detection of PH.

## 1.1 Anatomy of the Pulmonary Circulation System

The pulmonary circulation system is essential for the gas exchange process, facilitating the transfer of oxygen and carbon dioxide between the lungs and the bloodstream. It starts from the heart's right ventricle, where deoxygenated blood is forced into the pulmonary artery, transporting deoxygenated blood to the lungs. This artery, the blue “y-shaped” blood vessel in Figure 1, divides into left and right branches for each lung and continues to subdivide into smaller arteries and capillaries in the lung tissue. In the pulmonary capillaries, oxygen is absorbed, and carbon dioxide is expelled. Oxygen-rich blood flows back to the heart via the pulmonary veins, into the left atrium, and then to the left ventricle. The left ventricle then pumps it into the aorta, the red “arched” blood vessel in Figure 1, which distributes it throughout the body.

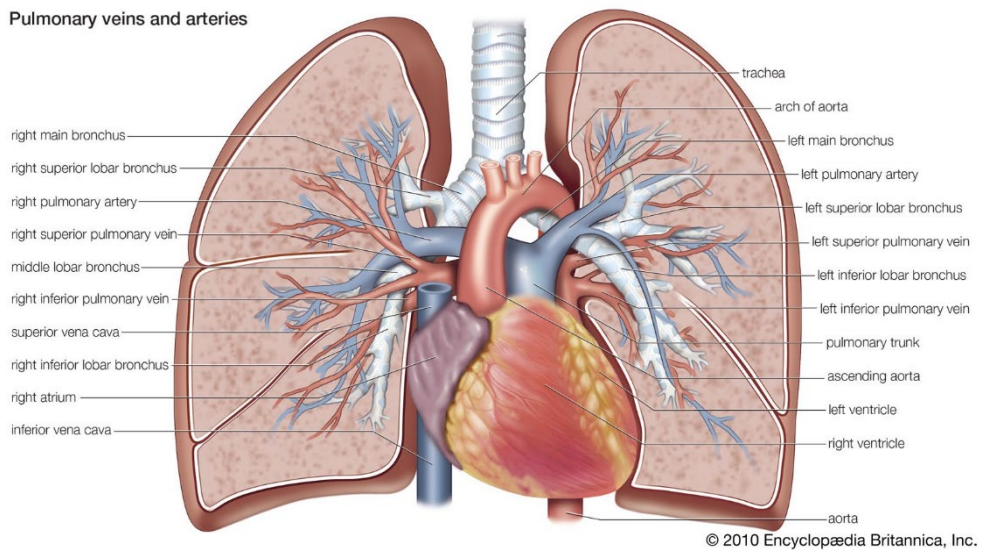


*Figure 1. Diagram of the pulmonary circulatory system. The points of interest for this study are the aorta, “red arch”, and main pulmonary artery, “blue y-branch”. (“Pulmonary circulation | Definition, Function, Diagram, & Facts | Britannica,” 2024)*

## 1.2 Definition and Classification of Pulmonary Hypertension

The medical definition of PH has remained controversial since the most recent World Symposium on Pulmonary Hypertension (WSPH), with debates still ongoing (Hooper et al., 2013). According to data from healthy subjects, the normal mean pulmonary arterial pressure (mPAP) at rest is approximately  $14.0 \pm 3.3$  mmHg (Simonneau et al., 2019). The criterion for abnormal pulmonary arterial pressure (above the 97.5th percentile) would be a mPAP  $\geq 20$  mmHg, two standard deviations above this mean value (Galiè et al., 2019). Nevertheless, this mPAP level alone is insufficient for defining PH, as it might be attributed to elevated cardiac output or pulmonary artery wedge pressure. Consequently, current recommendations advocate incorporating a pulmonary vascular resistance (PVR)  $\geq 3$  Wood Units (WU) into the definition of pre-capillary PH associated with an mPAP  $\geq 20$  mmHg, irrespective of aetiology (Simonneau et al., 2019). However, the approved haemodynamic definition of PH currently is mPAP  $\geq 25$  mmHg at rest, as assessed by right heart catheterisation (RHC) (Galiè et al., 2019). Thus, both definitions will be investigated for the project. A visual representation is shown in Figure 2.

*Table 1. The three different definitions of PH.*

Index	Pulmonary Hypertension Definitions
<b>1</b>	mPAP $\geq$ 25 mmHg
<b>2</b>	mPAP $\geq$ 20 mmHg
<b>3</b>	mPAP $\geq$ 20mmHg & PVR $\geq$ 3 WU

### 1.3 Current Pulmonary Hypertension Diagnostic Methodologies

The diagnosis of PH begins with a detailed clinical evaluation, where doctors assess a patient's symptoms, medical history and physical examination findings. Non-invasive tests follow, including echocardiography, to estimate pulmonary artery pressure and assess right ventricular function and imaging studies like chest X-rays and CT scans, which may reveal enlarged pulmonary arteries or other abnormalities (Humbert et al., 2022). For example, a pulmonary artery-to-aorta (PA:A) ratio, which, if greater than 1, may suggest PH. The definitive diagnosis is made through right heart catheterisation (RHC), an invasive procedure that directly measures PAP and other haemodynamic parameters. These include the PVR, calculated using the other haemodynamic, with a PVR  $\geq$  3 WU indicating pre-capillary PH (Rajagopal et al., 2023).

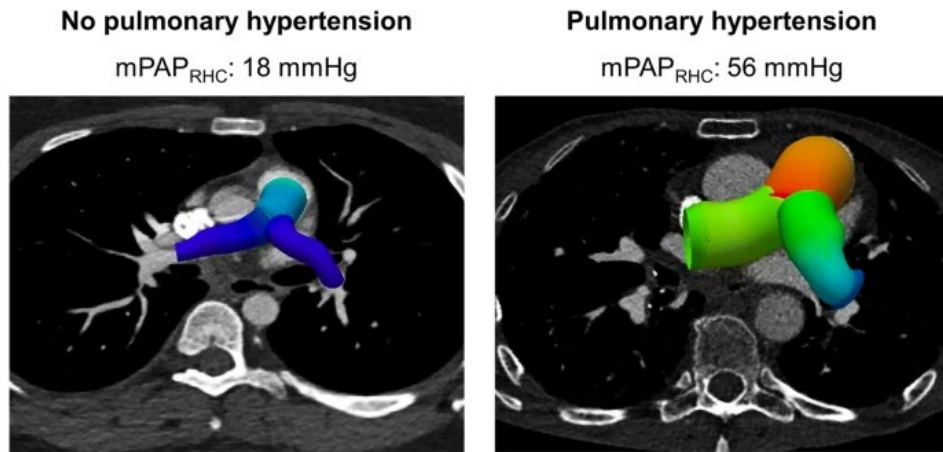


*Figure 2. Enlargement of the pulmonary artery at a more significant mPAP value, indicative of PH (Melzig et al., 2019).*

## 1.4 The Diagnosis Problem

At greater mPAPs, the pulmonary artery enlarges, as seen in Figure 2. This growth is viewed on medical imaging scans, as mentioned previously. From the scans, measurements for the mean diameter of the pulmonary artery and aorta are taken. If the ratio of the pulmonary artery diameter to aorta diameter is greater than 1 ( $PA:A > 1$ ), the patient is suspected, but not confirmed, of having PH and is sent for further testing (Freed et al., 2016). The necessity for additional testing constitutes one of the contributing factors to potential delays in diagnosing patients with PH. Furthermore, further testing in current diagnostic methods involves invasive strategies to diagnose a patient with PH. This is not ideal, especially in the scenario where a patient does not have PH, as they have undergone unnecessary surgery.

The delay in diagnosis of PH is a multifaceted problem. The contributing variables include a complex diagnostic process due to PH symptoms mimicking those of other cardiovascular or respiratory disorders. This results in the potential for misdiagnosis, hence the requirement for further testing. Consequently, various echocardiograms and RHC assessments are required, which may be inaccessible due to the sparsity of specialised PH centres. Additionally, attributable to the early stage asymptomatic nature of PH symptoms and gradual onset, individuals may adapt to the symptoms over time without realising the severity of their condition. Therefore, due to a lack of general population awareness of PH, delays in seeking medical attention and, thus, diagnosis are present (Mandras et al., 2016). Moreover, PH is not curable, emphasising the importance of introducing new methodologies to aid reliable recognition of PH at the earliest opportunity so that the disease can be managed appropriately.

A recent study in New Zealand and Australia found a mean diagnostic interval of 2.5 years between symptom onset and an RHC diagnosis, consistent with data from the USA, Europe and China. An older study in Australia, with a differing methodology, found a mean interval of  $47 \pm 34$  months (Khouri et al., 2020). Both studies demonstrate longevity within the diagnosis process; thus, given the ubiquity of PH, it is essential to refine the diagnosis process. Furthermore, studies indicate a correlation between longer diagnosis intervals and higher mortality rates, highlighting the importance of reducing the diagnosis time (Khouri et al., 2020). The complicated diagnostic process is encapsulated by the flowcharts in Figure 3.

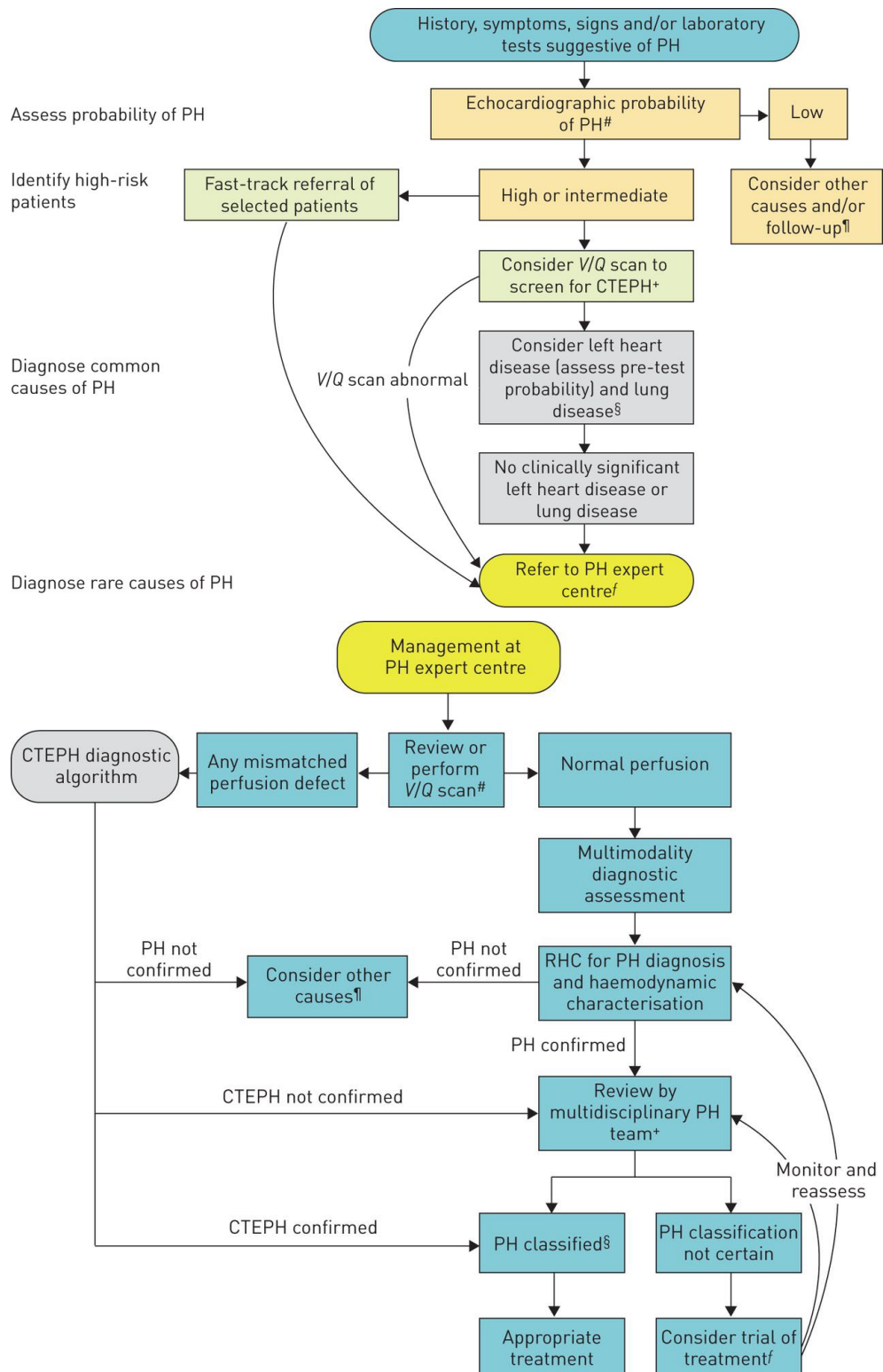


Figure 3. Flowchart demonstrating the diagnosis problem with PH. It shows the convoluted route to getting diagnosed (Frost et al., 2019).

The evolution of machine learning, particularly SSM, offers an avenue to accurately enhance the diagnosis process through potential automated detection of PH (Pesapane et al., 2018). This will reduce the diagnosis time and, therefore, the improved survival rate of patients diagnosed with PH.

## 1.5 Project Aims and Objectives

This study aims to develop a model to reliably and accurately detect the likelihood of PH in a patient from their medical imaging scans. Thus, this aims to contribute to a broader issue of reducing the diagnosis interval between symptoms and diagnosis of PH. The aim will look to be accomplished through achieving the following objectives throughout the project:

- Obtain an aligned dataset of surface meshes emulating the main pulmonary artery and aorta of requisite quality.
- Obtain detailed shape variability within the pulmonary artery and aorta datasets.
- Obtain correlation of particular shape variabilities to the presence of Pulmonary Hypertension.
- Obtain validation of the correlation between the particular correlating shape variabilities and the presence of Pulmonary Hypertension.

## 2 Literature Review

SSM is a sophisticated machine learning technique employed mainly in the field of medical imaging. It is used to analyse and represent the geometric variation of shapes within a population, focusing on extracting useful, structured information and knowledge. In the context of clinical research, the overarching objective is to ascend the Data, Information, Knowledge, and Wisdom (DIKW) pyramid, as seen in Figure 4, aiming for greater significance and value in clinical decision-making (Young and Frangi, 2009).



Figure 4. The Data Information Knowledge Wisdom (DIKW) pyramid. Represents the relationships between each one, illustrating the progression of raw data to valuable insights (Bruse, 2017).

The method involves succinctly describing a preprocessed dataset of semantically similar two or three-dimensional objects through geometric representations, deforming a computed mean shape of the dataset population to every object within the population, as shown in Figure 5. Through the deformation, the shape variability within the population is captured (Ambellan et al., 2019). The separate variations can be associated with an outcome, like the presence of a disease, through various statistical analysis techniques. Given the nature of human anatomy, the vast majority of human anatomical structures are the same but with slight variations. Thus, SSM offers a very credible option for medical applications and has already been shown to produce results in similar problems related to cardiovascular diseases, like in Frank Agyei-NTIM's thesis (Agyei-Ntim, n.d.).

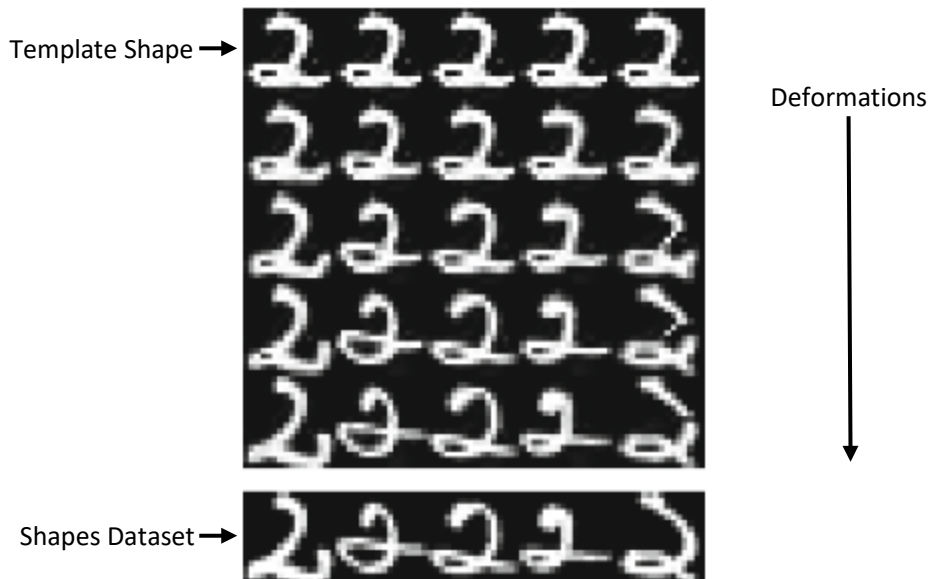


*Figure 5. 2D Atlas created from five instances of the digit "2" from the MNIST (Bône et al., 2018)*

SSM was selected for this project over alternative methods like morphometry and deep learning-based approaches, as despite its heavy dependence on the quality and diversity of the training data and is computationally intensive, SSM demonstrates incredibly strong interpretability to capture an extensive range of different feature variations ("Dryden-Mardia-Slides-04.pdf," n.d.). This allows a greater scope of variations to be analysed for an association with PH. Additionally, SSM is a logical progression from the machine learning advancements in segmenting medical image data and can be used on a smaller dataset, unlike its counterparts. This is important given that PH is a relatively rare condition; thus, a high volume of clinical data is difficult to come by.

In the existing literature, SSM has been employed to delineate the progression of PH and cardiovascular diseases by modelling the heart's ventricles. SSM has identified the ventricles' principal shape features, both among asymptomatic individuals and in correlation to cardiovascular diseases or failings, like PH (X. Zhang et al., 2017). This application extends to identifying the presence of PH, monitoring its advancement, and prognosticating patient outcomes (Di Folco et al., 2020). However, the reliability of studies concerning PH can be scrutinised due to their reliance on relatively small datasets. While investigations tracing its progression and forecasting patient prognosis utilised datasets greater than 250 subjects, those identifying the presence of PH were

based on a dataset a fifth of that size (Addetia et al., 2016; Dawes et al., 2017). These datasets appear diminutive when juxtaposed with studies related to similar objectives for other cardiovascular diseases, with databases of almost 2000 subjects (Medrano-Gracia et al., 2014). This further highlights the lack of high volumes of data.

Most shape analyses pertinent to PH conducted in studies were centred on modelling the heart's ventricles, with one focusing on the pulmonary artery "y-branch". In this particular study by Sabry et al., the shape analysis was conducted using visualisation toolkit software, extracting the centre line of the main pulmonary artery, and conducting shape analysis on the variations between subjects' centrelines, as seen in Figure 6 (Sabry et al., 2024). However, this approach can potentially miss features that may otherwise be captured by analysing the whole blood vessels' surface mesh. Examples of studies analysing blood vessels include the Bruse et al. study assessing aortic arch morphology and the Cosentino et al. study assessing ascending thoracic aortic aneurysms, indicating that detailed useful information can be extracted by extending this type of methodology to the main pulmonary artery (Bruse et al., 2016; Cosentino et al., 2020).

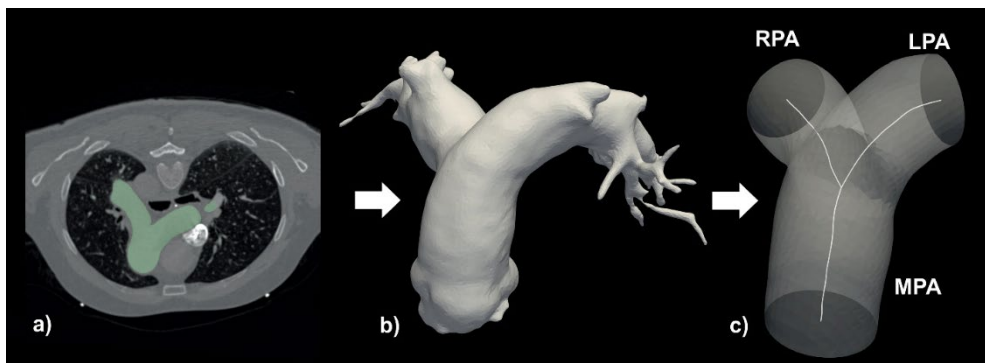


*Figure 6. Shape Analysis of the main pulmonary artery, using the centreline toolkit in 3D Slicer (Sabry et al., 2024).*

## 2.1 Data Preparation

### 2.1.1 Segmentation

SSM tends to begin with segmentation. However, it is not in the scope of this project, and more information can be found in Appendix 9.13.2.

### 2.1.2 Denoising and Smoothing

Surface meshes derived from segmented medical imaging data often contain noise, artefacts, or inconsistencies, which can hinder the quality of the SSM findings. Thus, denoising and smoothing techniques play a critical role in keeping the models able to reliably and accurately capture the intrinsic shape variations (Taubin et al., 1996). Denoising involves removing unwanted artefacts or noise that may have been introduced during the data acquisition process, which helps preserve the structural features of the studied shapes. Smoothing, on the other hand, refines the geometric surfaces, reducing irregularities and inconsistencies to reveal a more precise, more representative depiction of the shape (“Mesh Smoothing.pdf,” n.d.). Taubin and Laplacian filters were chosen over alternative methods for the project. See Appendix 9.13.6 for the reasons why and the mathematical theory.

### 2.1.3 Alignment

In SSM, alignment refers to the process of standardising the global positions, orientations, and scales of shapes within a dataset so they can be meaningfully compared and analysed, as in Figure 7. This preprocessing step is critical as it ensures that shape variability captured in the model reflects inherent anatomical differences rather than arbitrary spatial discrepancies (Da Fontoura Costa and Cesar Jr., 2010). Proper alignment maximises the accuracy of subsequent shape analyses by reducing noise introduced by the inconsistencies above, ensuring that the statistical model captures actual structural variation, thus enabling reliable comparisons, classification, and predictions across the population (Davies et al., 2001). From the literature, the Procrustes algorithm, in conjunction with fiducial landmarks, was selected for the study as used by Medrano-Gracia et al. (Medrano-Gracia et al., 2014). For more information on why, see Appendix 9.13.10.

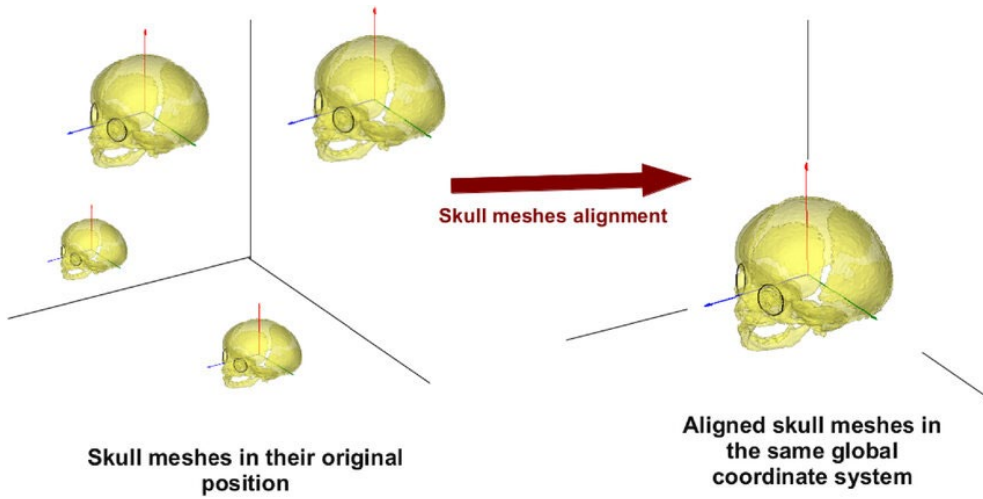


*Figure 7. Alignment of four skulls at different positions in space translated all to the same place using the Procrustes algorithm (Dahdouh et al., 2014).*

## 2.2 Atlas Construction

The SSM methodology fundamentally involves constructing atlases from a template that is deformed to fit the shapes of various subjects in a dataset. An atlas, according to the definition of Young and Frangi, is “an alignment of data maps from different domains, either population or individualised, which enables querying of relations [...] to construct the ‘big picture’” (Young and Frangi, 2009). They are comprehensive representations that capture the average anatomical structure, a standardised reference template, and its variations to each subject in the dataset population, which are captured in the form of momenta vectors outputted from the model, an example of which is shown in Figure 8. The reasons why the Deformetrica software package was chosen to construct the atlas over other options can be found in Appendix 9.13.8.

### 2.2.1 Mean Template Formation and Deformations

Atlases achieve this by first aligning individual subjects to a chosen template subject within the dataset to formulate the mean template. Depending on the specific application, the representation of this mean template can vary, ranging from landmarks and surface meshes to volumetric grids. Once all shapes in the dataset have been aligned, an average shape, or atlas, is computed by averaging the corresponding points across the dataset. From this point, a statistical shape model is constructed, either from the deformation fields or directly from the aligned shapes (Heimann and Meinzer, 2009). The mean template is then deformed to each subject to quantify the variability

across the dataset in the form of momenta vectors. Thus, every subject in the dataset can be described mathematically as a function of the mean template.

$$T = \phi(\bar{T}) + \varepsilon$$

$$\text{Subject} = \text{Deformed Template} + \text{Residuals}$$

Where  $\phi$  is a diffeomorphism transformation. A Diffeomorphism transformation, part of Large Deformation Diffeomorphic Metric Mapping (LDDMM), is a smooth, invertible function, with a smooth inverse, hence crucial to smooth one-to-one mapping of two shapes, like in Figure 9 (Durrleman, 2010). An example mean template of a dataset can be seen in Figure 8 (Styner et al., 2003). More theory behind LDDMM can be found in Appendix 9.13.5.



Figure 8. Computed template shape (blue) based on the twenty input CoA models, adapted from (Bruse et al., 2016).

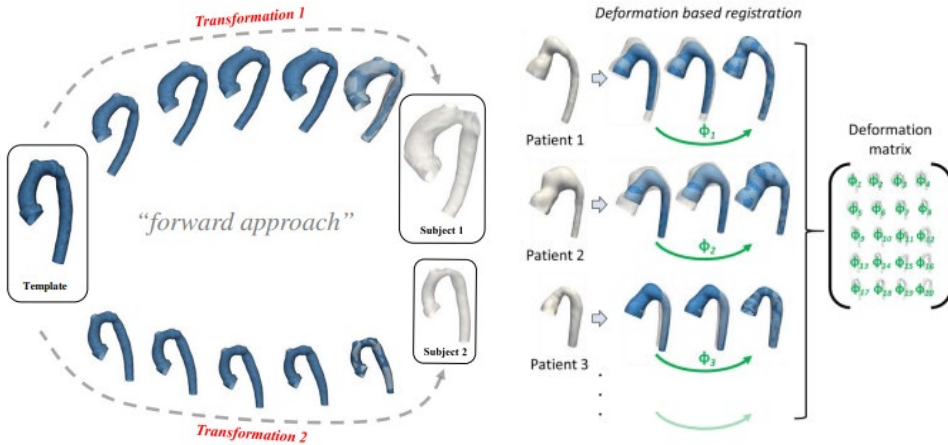


Figure 9. Large Deformation Diffeomorphic Metric Mapping (LDDMM) of aortas from the template to subjects within the atlas (left). Each subject shape is uniquely parameterised by its deformation function  $\varphi$ ; all deformations concatenated in a matrix describe all 3D shape information within the population (right) (Bruse et al., 2016).

## 2.2.2 Deterministic Atlases or Bayesian Atlases

There are two types of atlases. Information regarding their differences can be found in Appendix 9.13.4. In this project, a deterministic atlas will be used.

## 2.2.3 Atlas Parameters

Deformetrica's atlas construction requires various important parameters to be set to optimise the modelling process of creating an estimated mean template and subsequent deformation to the other population subjects (Durrleman et al., 2014).

These parameters are:

- Template Kernel Width (Gaussian Kernel),  $\lambda_{w_T}$
- Model Kernel Width (Gaussian Kernel),  $\lambda_{w_M}$
- Noise Standard Deviation,  $n_{std}$

In the univariate case, kernels are often used to obtain a smoother probability density estimate of a distribution than the histogram representation, as seen in Figure 10 (Izenman, 2008). This parameter is important because it is the typical scale at which the coordinate vector fields vary spatially and, therefore, defines the smoothness of the captured features (Bruse, 2017). A general trend is that the lower the kernel width, the better, as more features and a better representation of the shape are captured, as seen in Figure 11. However, if the kernel width is too small, too many features are picked up, and noise dominates, thus the widths need to be iteratively decreased, checking how

the meshes are being deformed at each iteration to determine the optimal kernel widths (Durrleman et al., 2014).

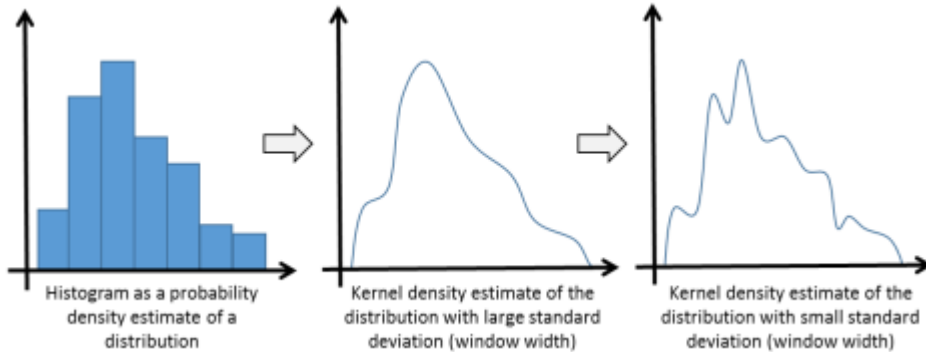


*Figure 10. Effect of kernels to capture features of a distribution (coarse to smooth) adapted from (Izenman, 2008).*

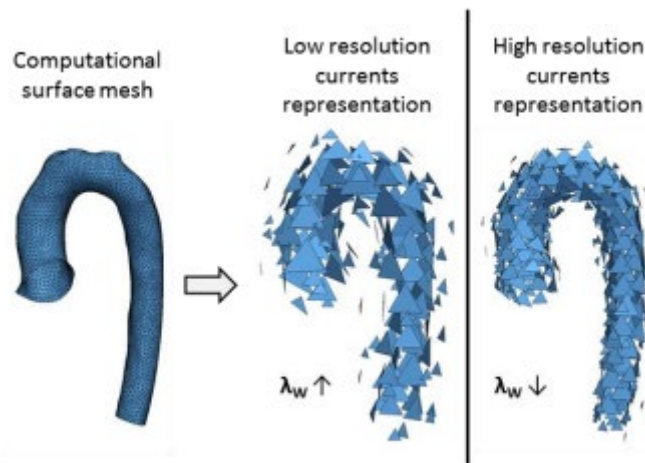


*Figure 11. Shape model of an aorta represented by currents; changing resolution  $\lambda_w$  (Bruse, 2017).*

Noise standard deviation controls how accurate the template is to be fitted to the other subjects in the dataset. A lower value of  $nstd$  gives more importance to the data fitting cost for this object (Mansi, 2010).

## 2.3 Statistical Analysis

Once the SSM has been conducted, forming the atlas and momenta vectors for each shape variability outputted, the individual variations require analysis to determine whether any of the shape modes are associated with a particular disease. The analytical methods can be classified into two categories: supervised and unsupervised learning, both of which will be used to investigate any findings and compare the results.

Principal Component Analysis (PCA) serves as the primary unsupervised analysis technique, revealing the most significant shape modes that encapsulate the majority of variance within the dataset. Conversely, an alternative method, Partial Least Squares Regression (PLS) functions, is the primary supervised analysis technique, pinpointing the critical shape modes contributing to a variable, which indicates, for example, the likelihood of a disease. While PLS effectively captures a significant portion of the variance in the data using a relatively small number of shape modes, it typically captures less variance than PCA using the same number of shape modes. This discrepancy arises from PLS prioritising the maximal covariance between shape alterations and the indicator variable, alongside identifying the most significant shape changes (Mansi et al., 2011).

Studies have found that both PCA and PLS are solely engaged in dimensionality reduction within the analytical domain. For instance, when analysing momenta vectors generated by an atlas model, both PCA and PLS yield new sets of momenta vectors delineating the most prominent shape variations within the population. Subsequent steps are necessary to convert these momenta vectors into 3D shape meshes for visualisation purposes (Di Folco et al., 2020).

### 2.3.1 Principal Component Analysis (PCA)

In shape modelling, each anatomical or geometric structure is often represented as a set of landmark coordinates or vertices, creating a high-dimensional feature space (Cootes et al., 1995). The displacement deformations of each geometric structure from the template structure are captured in the output momenta vector from the shape modelling. Applying PCA transforms this vector space into a reduced set of orthogonal principal components that capture the most significant patterns of variation, called shape modes. These modes are ordered based on the amount of variance they explain,

with the first few modes often capturing the majority of the meaningful shape variation (Harris et al., 2013).

Mathematically, PCA begins by assembling a matrix,  $X$ , of each shape's deformation momenta vectors, where each row corresponds to a different shape in the dataset. The mean momenta vector,  $\mu$ , is computed:

$$\mu = \frac{1}{n} \sum_{i=1}^n X_i$$

Where  $n$  is the number of shapes in the dataset. The mean vector is subtracted from each shape to form the mean-centered matrix,  $\hat{X}$ :

$$\hat{X} = X - \mu$$

From which the covariance matrix,  $C$ , is computed:

$$C = \frac{1}{n-1} \hat{X}^T \hat{X}$$

And can be decomposed into eigenvectors,  $V$ , and eigenvalues,  $\lambda$ :

$$CV = V\Lambda$$

Where  $\Lambda$  is a diagonal matrix containing the eigenvalues, which are to be sorted into descending order of magnitude, leaving the dominant modes of variation,  $k$  eigenvectors at the top (Bonaretti, n.d.). Subsequently, the eigenvector matrix can be ordered into the order of the descending eigenvalues,  $V'$  (Heimann and Meinzer, 2009). From this, the amount of each shape mode present within each subject in the dataset can be calculated using the dot product between the mean-centred momenta vector matrix and the PCA eigenvector matrix. This produces a matrix,  $Z$ , with each row representing the shape mode amounts for a single subject, which can be analysed for correlations to PH (Hollenbeck et al., 2018).

$$Z = \hat{X} \cdot V'$$

In Mansi et al. study, Mansi et al. utilised both PCA and PLS to contrast the outcomes, acknowledging PCA's inherent constraint stemming from its unsupervised nature. This limitation arises because "insignificant" shape modes may still contain pertinent associations concerning a disease, for example, yet PCA disregards them (Mansi et al., 2011). Despite this, Susinesiaputra et al. found in their study, attempting to use different methods for classifying myocardial infarction, PCA classification accuracy levels of 0.95, which is very successful; thus, PCA can produce valuable insights (Susinesiaputra et al., 2018).

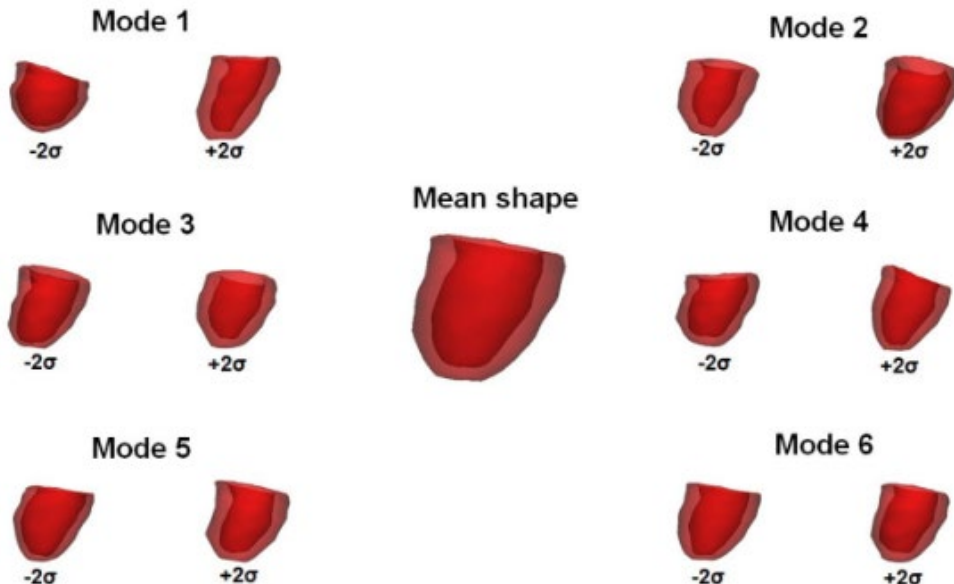


Figure 12. Six PCA shape modes and the computed estimated mean template from the founding atlas (Cutugno et al., 2021).

### 2.3.2 Partial Least Squares (PLS) Regression

PLS is particularly useful when dealing with high-dimensional data, like shape data, where the number of predictor variables, in this case shape features, exceeds the number of observations, leading to issues like multicollinearity. The application of PLS regression analyses the relationship between a set of predictor variables, such as shape modes in the form of momenta vectors in our case, and a response variable, like a clinical outcome. It aims to find the latent variable, or shape modes in our study, that capture the maximum covariance between the predictor variables and the response variable (Cootes et al., 1995).

Mathematically, PLS regression is conducted through an iterative algorithm taking predictor variables,  $X$ , the dataset subjects momenta vectors matrix outputted from the SSM, and response variables,  $Y$ , the corresponding subject mPAP data as inputs. PLS regression decomposes the predictors and responses into a set of components or "Shape Modes". These components are derived to capture the maximum covariance between predictors and responses (Chin and Marcoulides, 1998). The decomposition of  $X$  and  $Y$  matrices into the components is as expressed as:

$$X = TP^T + E_X$$

$$Y = UQ^T + E_Y$$

Where:

- $T$  is the score matrix for  $X$ , containing the scores of each sample on each component.
- $P$  is the loading matrix for  $X$ , containing the weights for each predictor on each component.
- $E_X$  is the residual matrix for  $X$ , containing the unexplained variance.
- $U$  is the score matrix for  $Y$ , containing the scores of each sample on each component.
- $Q$  is the loading matrix for  $Y$ , containing the weights for each response on each component.
- $E_Y$  is the residual matrix for  $Y$ , containing the unexplained variance.

PLS regression builds a predictive model by iteratively constructing these components, or “Shape Modes”, in terms of SSM. Each component is a linear combination of the original predictors and responses (Chin and Marcoulides, 1998). The model produces a matrix,  $V$ , where each row contains coefficients that define a linear combination of PLS components approximating the original predictor variable, the momenta vectors. Similarly to the PCA, the amount of each shape mode present within each subject in the dataset can be calculated using the dot product between  $V$  and the momenta vector matrix. This produces a matrix,  $Z$ , Each row represents the shape mode amounts for a single subject, which can be analysed for correlations to PH.

$$Z = X \cdot V$$

Studies like Zhang et al. and Susinesiaputra et al. have utilised iterative forms of the PLS regression algorithm, allowing them to characterise the shape modes to known variations indicative of the disease they were attempting to classify (Susinesiaputra et al., 2018). Having these specific types of variations, like sphericity and conicity, related to the disease and the dataset anatomies allows the results to be interpreted much more effectively, rather than dealing with generalised “Shape Modes” (X. Zhang et al., 2017). Plus, the results can be communicated coherently to relevant industry professionals. Another key feature of PLS regression is that each component is orthogonal, meaning uncorrelated, to the previous ones, ensuring that each successive component captures a different source of variation. This means every shape mode found in the post-SSM PLS regression would be distinct, improving the findings' robustness (Cootes et al., 1995).

The Susinesiaputra et al. study found that the SSM PLS method produced an accuracy of 0.98, which was greater than the PCA method, showing excellent performance. Hence, it is logical to predict that the supervised PLS regression technique will be better

equipped for applications with indicator variables linked to shape variations. Although given that PCA did not perform poorly, it is worth exploring both methods and comparing them similarly to the Susinesiaputra et al. study (Susinesiaputra et al., 2018). Despite the convincing results from this study's utilisation of PLS regression, the methodology needs to be used carefully with data likely to produce outliers, as PLS can be extremely sensitive to such inconsistencies (James et al., 2022).

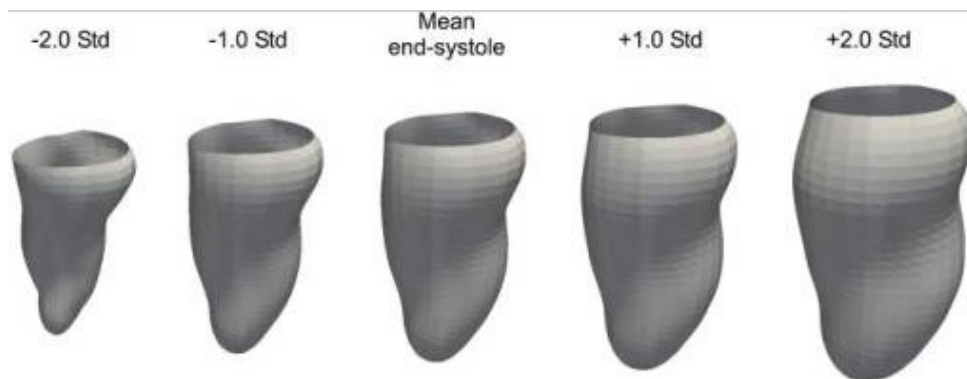


*Figure 13. The first mode from a PLS analysis, adapted from (Susinesiaputra et al., 2018).*

### 2.3.3 Correlating to Pulmonary Hypertension (PH)

Correlation coefficients will be calculated using either Pearson's Correlation Coefficient or Spearman's Rank Correlation Coefficient. Refer to Appendix 9.13.9 to see which scenarios each would be used in. Once the coefficients are calculated, the shape modes will be filtered for correlation coefficients  $\geq 0.3$  or  $\leq -0.3$ , as the general rule for correlation coefficients is that values beyond these constraints indicate a greater positive or negative correlation (Ratner, 2009). Table 2 provides the correlation coefficients and their corresponding meaning (Akoglu, 2018). They also require filtering for a  $p$ -value  $< 0.05$  to indicate that the correlation coefficient is statistically significant at a 95% confidence interval. The  $p$ -value is defined as the “probability that you would have found the current result if the correlation coefficient were, in fact, zero” (Shreffler and Huecker, 2024).

*Table 2. Range of Correlation Coefficients and their representative meaning.*

Correlation Coefficient (CC)	Direction	Strength
- 1	Negative	Perfect
- 1 < CC ≤ - 0.8	Negative	Very Strong
- 0.8 < CC ≤ - 0.6	Negative	Moderate
- 0.6 < CC ≤ - 0.3	Negative	Fair
- 0.3 < CC < 0	Negative	Poor
0	None	None
0 < CC < 0.3	Positive	Poor
0.3 ≤ CC < 0.6	Positive	Fair
0.6 ≤ CC < 0.8	Positive	Moderate
0.8 ≤ CC < 1	Positive	Very Strong
1	Positive	Perfect

## 2.4 Model Validation

This project aims to determine the feasibility of this method as a binary classifier for PH. Thus, the statistical analysis findings require validation to quantify the results' reliability and the method's feasibility. Validation ensures that the model's predictions are accurate, robust, and generalisable to new, unseen data. A model might appear effective without proper validation but fail to perform well in real-world scenarios, leading to incorrect classifications and potentially harmful decisions. Potential methods for validating the model as a binary classifier include Receiver Operating Characteristic (ROC) curves, Precision-Recall curves (PRC) and k-Fold cross-validation. Although k-Fold cross-validation offers a more robust validation by mitigating bias within the dataset, its computational expense and more convoluted mechanism were deemed factors too time-consuming to overcome for the project; hence, ROC and PRC validation will be explored (Tibshirani et al., 2001). The binary classifier metrics are designed for classification where there are 2 distinctive separate outcomes; hence, given that this study relates to the diagnosis classification of PH, treating the study as a binary classifier was acceptable.

### 2.4.1 Receiver Operating Characteristic Curve and Area Under Curve (AUCROC)

A ROC curve is a graphical plot, like in Figure 15, used to evaluate the performance of binary classifiers by illustrating the trade-offs between sensitivity, true positive rate and 1-specificity false positive rate. How to calculate both are listed below, where sensitivity

measures a diagnostic test's ability to identify the presence of a disease correctly, and specificity measures its ability to identify the absence of a disease correctly (Ujj, 2022). The curve is created by utilising a confusion matrix, varying the decision threshold of the classifier, and plotting sensitivity against 1-specificity across multiple thresholds. The Area Under the Curve (AUC) serves as a summary metric, with values ranging from 0.5, no discrimination, to 1.0, perfect discrimination. A high AUC indicates that the model is effective at distinguishing between the positive and negative classes. This makes the ROC curve an essential tool in assessing classifier models' overall discriminative power (Nahm, 2022). Given the project's diagnostic element, using ROC curves for validation also allowed the use of Youden's Index as a method for defining the classification thresholds for PH of the significant shape modes.

		True Class	
		Positive	Negative
Predicted Class	Positive	TP	FP
	Negative	FN	TN

Figure 14. Confusion Matrix ("What is A Confusion Matrix in Machine Learning?," n.d.).

- Sensitivity, *True Positive Rate*,  $TPR = \frac{\text{True Positives (TP)}}{\text{TP}+\text{False Negatives (FN)}}$
- 1-Specificity, *False Positive Rate*,  $FPR = \frac{\text{False Positives (FP)}}{\text{FP}+\text{True Negatives (TN)}}$

Susinesiaputra et al. found in their study AUC validation results of 0.994 and 0.996 for geometric morphometric PCA and SSM PLS methods, respectively (Suinesiaputra et al., 2018). Demonstrating the capacity of this study to find convincing results.

#### 2.4.2 Youden's Index (J-Statistic)

Youden's Index, also known as Youden's J Statistic, is a metric extension of the ROC curve, used to evaluate the effectiveness of a binary diagnostic test and determine the optimal decision threshold for binary classification. The index considers both sensitivity and specificity, true negative rate, giving equal weighting to true positives and false positives and is defined as:

$$J = \text{Sensitivity} + \text{Specificity} - 1 = TPR - FPR$$

The value ranges between 0 and 1, where a value closer to 1 indicates an optimal combination of sensitivity and specificity and the optimal point is considered where  $J$  is the maximum. A graphical interpretation of the metric is shown in Figure 15. Used frequently in medical capacities, to ensure maximum correct classification rate, while minimising errors (Youden, 1950).

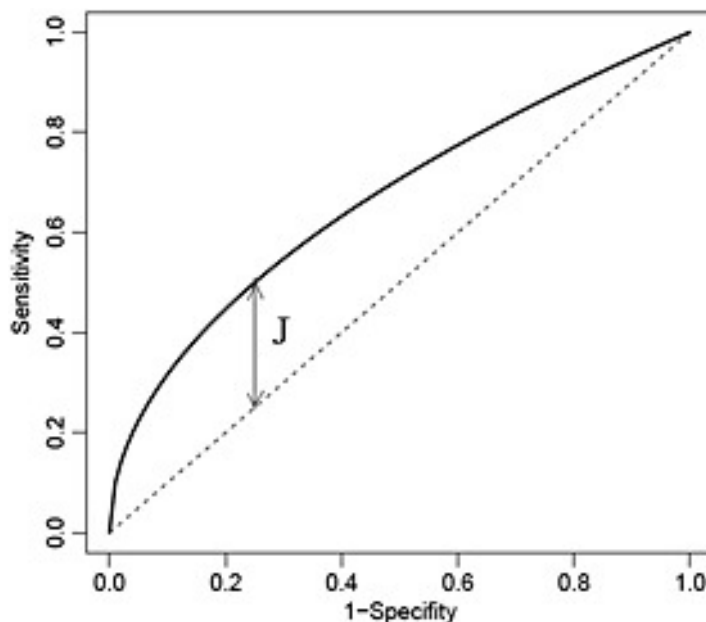


Figure 15. A typical ROC curve with the Youden's Index (J Statistic) plotted on it (Xu et al., 2014).

Despite Youden's Index's beneficial characteristics, other factors need to be considered, when defining a classification threshold (Fluss et al., 2005). One of these factors is whether an imbalance in the predictor outcomes is desired rather than them being weighted equally, as Youden's Index is limited to. PRCs and the related  $F\beta$  score can address this issue.

#### 2.4.3 Precision-Recall Curve (PRC) and Area Under Curve (AUC – PRC)

Precision-recall curves are graphical representations, as seen in Figure 16, that illustrate the trade-off between precision and recall (sensitivity) across different classification thresholds. They provide valuable insights into the performance of a model, especially

in cases of class imbalance (Saito and Rehmsmeier, 2015). Precision measures the proportion of true positives out of all predicted positives, while recall (or sensitivity) measures the proportion of true positives out of all actual positives:

- $Precision = \frac{TP}{TP+FP}$
- $Recall = Sensitivity$

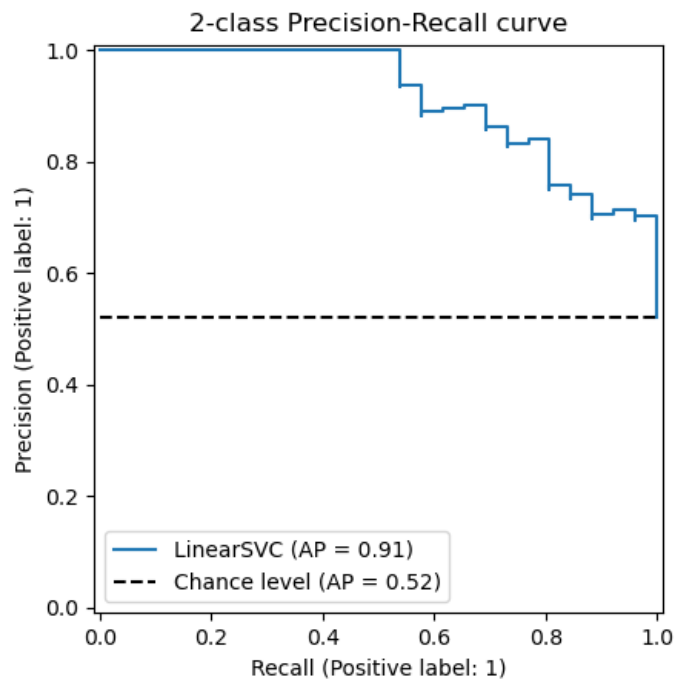


Figure 16. A typical PRC (“Precision-Recall,” n.d.).

Precision is plotted on the y-axis and recall on the x-axis, offering a nuanced view of how effectively the model distinguishes positive instances. High precision with low recall indicates that the model confidently predicts a small subset of positive instances, whereas high recall with low precision indicates that many instances are classified as positive, albeit with lower accuracy. The Area Under the Precision-Recall Curve (AUC-PRC) summarises the overall performance, with higher values signifying better discrimination of positive cases. PRCs need to be used carefully, however, as they are extremely sensitive to misclassifications with data skewed for negative cases. Plus, they can be difficult to interpret for the diagnosis classification compared to ROC curves (Davis and Goadrich, 2006).

#### 2.4.4 $F\beta$ Score

The  $F\beta$  score is a performance metric that balances precision and recall, providing a single measure of a classifier's effectiveness. It is the harmonic mean of precision and recall, offering a comprehensive assessment of classification performance (Sokolova and Lapalme, 2009). The  $F\beta$  score is calculated using:

$$F\beta = \frac{(1 + \beta^2) \times Precision \times Recall}{(\beta^2 \times Precision) + Recall}$$

Where:

- $\beta$  is a weighting parameter that, when greater than 1, places greater emphasis on recall and, when less than 1, prioritises precision.

$F\beta$  has an optimal score when equal to 1 and a worst score when equal to 0. This score exhibits greater versatility than Youden's Index, allowing for the user to prioritise a particular element of the confusion matrix and thus is particularly useful in applications involving imbalanced datasets. This makes it more suitable for applications like medical diagnostics or safety-critical systems, where in the case of  $\beta > 1$ , false negatives carry a high cost. The harmonic mean penalises extreme values more strongly than the arithmetic mean, ensuring that high scores are achieved only when both precision and recall are balanced (Powers, 2008). The diagnostic classification threshold is determined by where  $F\beta$  is maximum.  $F\beta$  needs to be used carefully, as it has the pretty clear limitation of having the potential to obscure broader performance trends by reducing the evaluation to a single composite metric (Sokolova and Lapalme, 2009).

### 3 Methodology

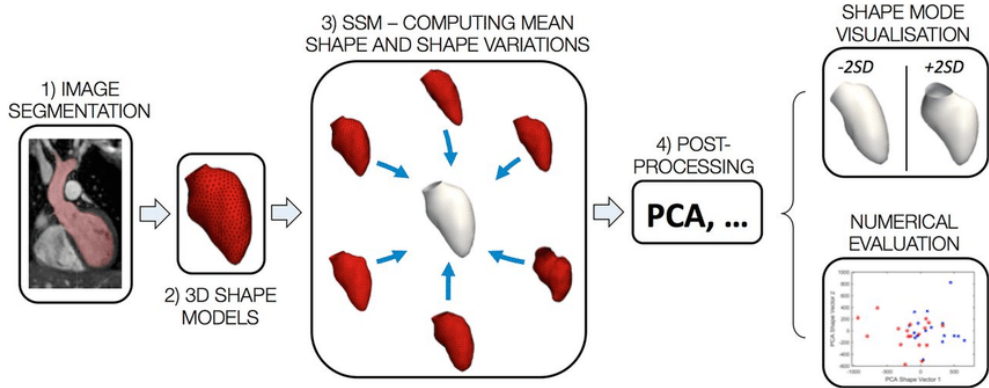


Figure 17. General SSM pipeline from segmentation of the structure of interest to anatomical mean shape (template) computation and 3D shape variability description via principal component analysis (PCA), adapted from (Biglino et al., 2017).

#### 3.1 Pre-processing

For this project, two sets of data were provided from a segmenting machine learning algorithm produced by PhD Liam Burrows: one training set to optimize the model and a clinical set to perform the statistical analysis studies. Both datasets had pre-processing techniques applied to them, such that they were of the requisite quality to perform the shape modelling, thus meeting the first objective.

##### 3.1.1 Segmentation

Segmentation, as alluded to in 2.1.1, was not within the scope of the project as the segmentations were provided. The Segmentations provided included segmentations for both the main pulmonary artery and aorta for 95 different patients within the clinical dataset, as well as 225 pulmonary artery capillary network segmentations in the training dataset. An example of each of these segmentations provided is shown below in Figure 18.

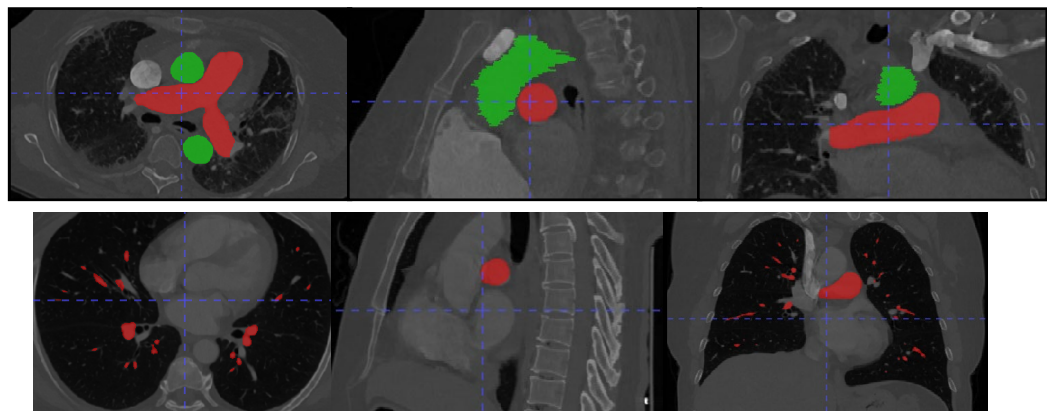


Figure 18. Segmentation of the main pulmonary artery (red, top), aorta (green, top) and pulmonary artery capillary network (bottom).

### 3.1.2 Surface Mesh Conversion

The segmentations were all converted into surface meshes of each anatomy in .vtk format, as explained in Appendix 9.13.3. Examples of the exported surface meshes can be seen below in Figure 19 and Figure 20.

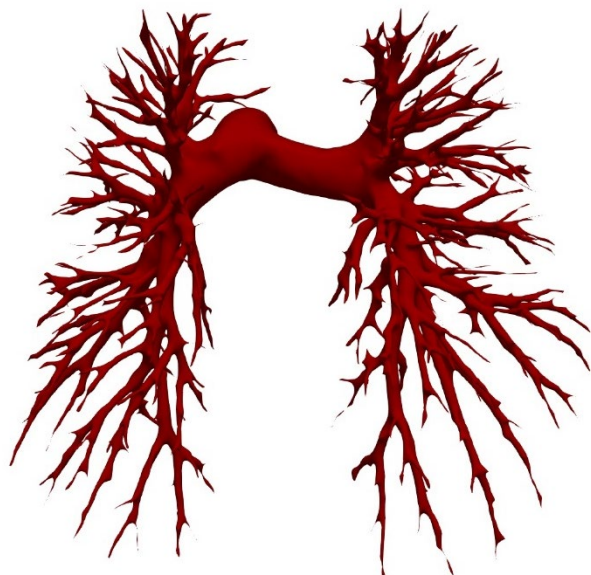
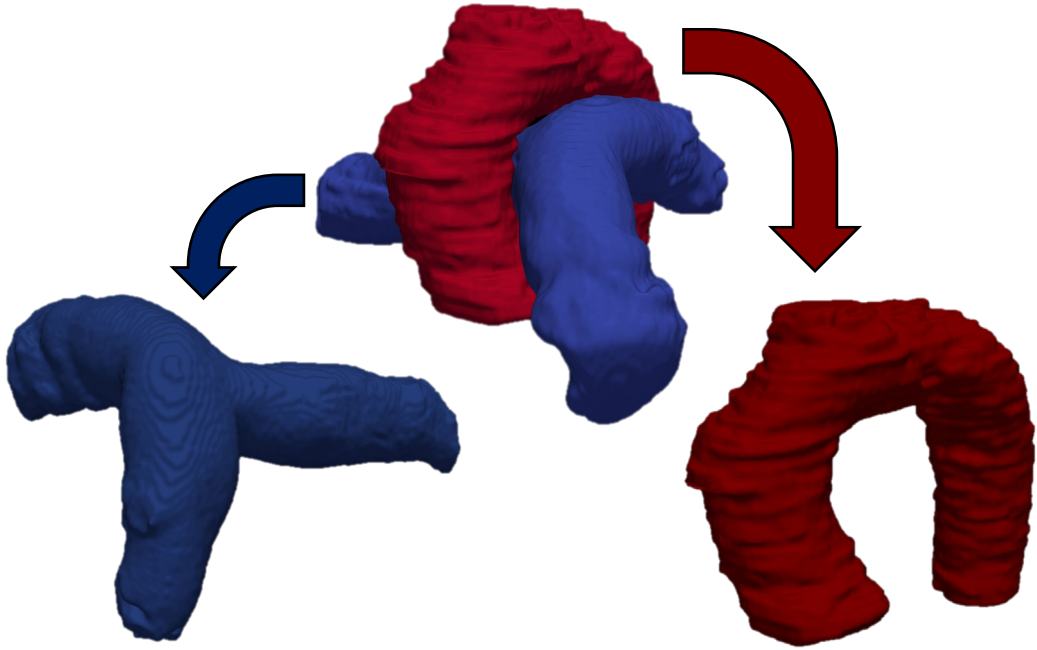


Figure 19. Surface Mesh generated from segmentation in Figure 18 of the main pulmonary artery and its capillary network.



*Figure 20. Surface Mesh exported from the segmentation in Figure 18 of the main pulmonary artery and aorta and their subsequent separation.*

### 3.1.3 Smoothing, Denoising and Decimating

From Figure 20 it is clear to see that the surface meshes produced contained a lot of noise and surface roughness. These potentially disruptive artefacts were removed individually for each surface mesh using smoothing and denoising techniques explored in 2.1.2. The Laplacian and Taubin filters were applied to the surface meshes using the smoothing feature in the 3D Slicer software (“3D Slicer,” n.d.). As mentioned in 2.1.2 the Laplacian filter has a tendency to scale down the size of the surface meshes, potentially removing features we would want to be picked up in the shape modelling. Therefore, the Laplacian was chosen to be utilised first, and then the Taubin filter was used to rescale any areas of the surface mesh which had been scaled down. To find the optimal smoothing factors for each filter, such that the meshes were smoothed and denoised to the required quality and reducing the scale-down effect, the smoothing parameters and iteration numbers were iteratively increased until an optimal point was reached. The optimal parameters found were a smoothing (shrinking) factor,  $\lambda$ , of 0.1 and an inflating factor,  $\mu$ , of 0.0005. These parameters were applied to the whole dataset, running the Laplacian filter first for 100 iterations and the Taubin filter for 100 iterations. The effect this had on the surface meshes can be seen in Figure 21.

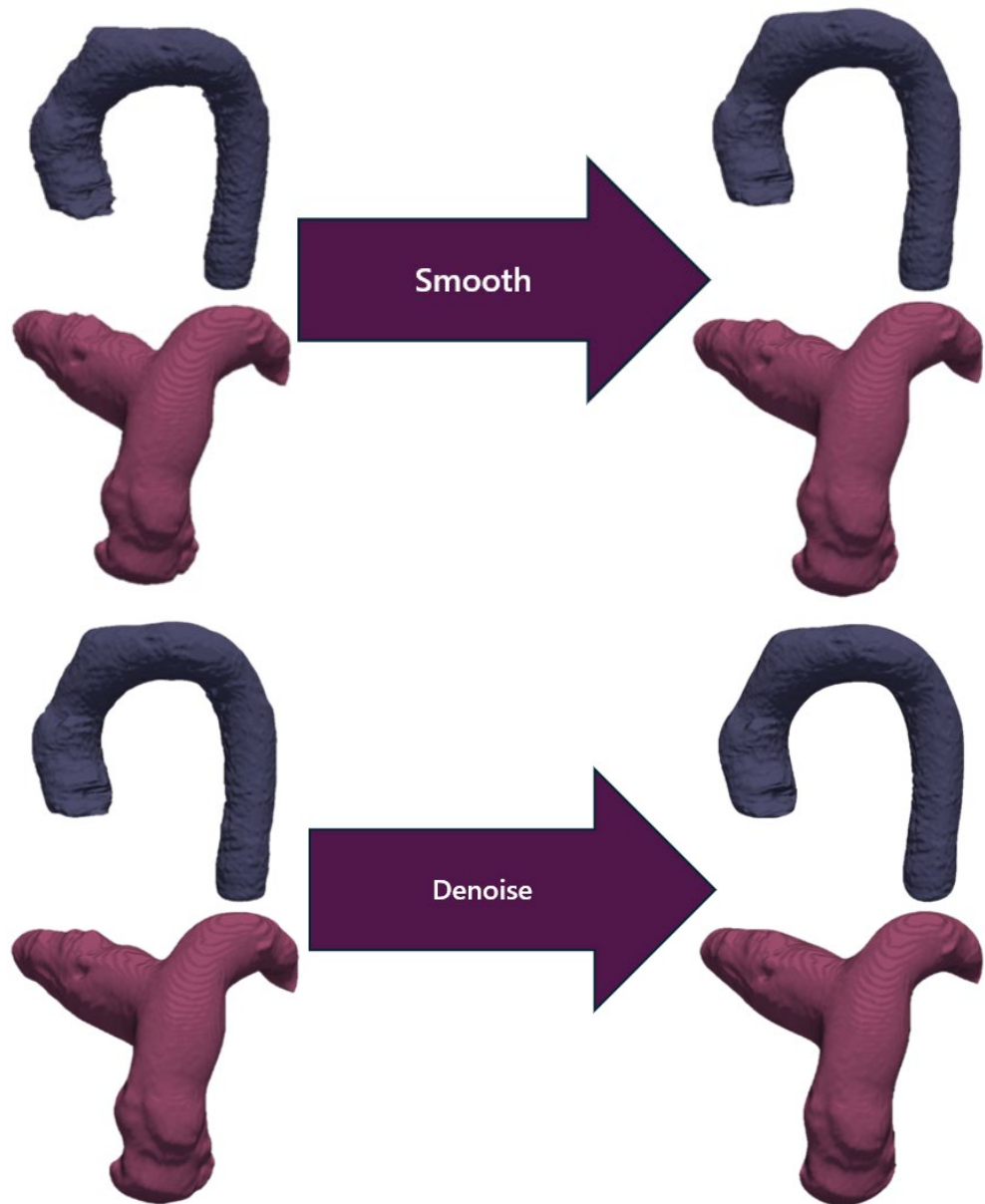
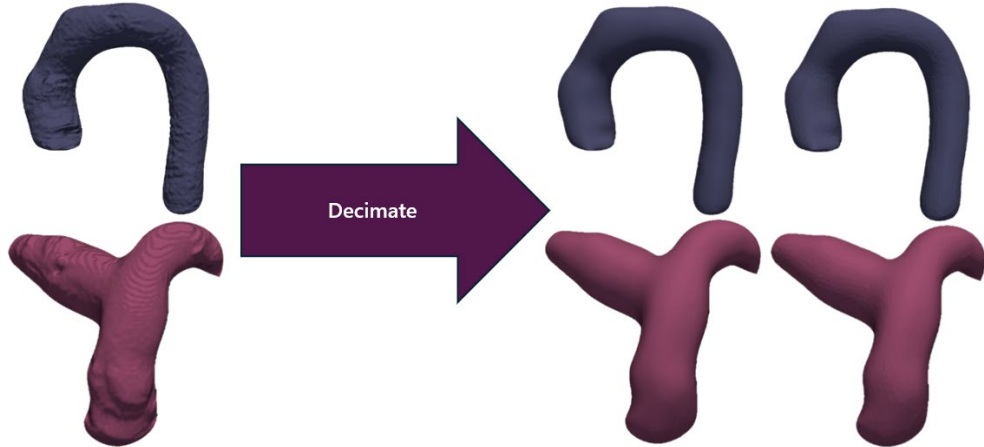


Figure 21. Smoothing (top) and Denoising (bottom) processes undertook.

Once the smoothing and denoising had been completed, the meshes required decimating to reduce the number of cells and nodes within the mesh. This was a computational limitation, given the quality of resolution of the meshes from the segmentation. When the meshes, prior to decimation, were tested on the shape modelling framework, the framework could not run due to the computer's lack of memory capacity. Thus, the meshes were decimated using the decimation feature in the 3D slicer ("3D Slicer," n.d.). Each mesh required decimation to approximately 0.004 of their original resolution in order for the framework to run, taking the cells and nodes

from approximately 500000 and 200000 to 2000 and 800, respectively. The effect this had on the surface meshes can be seen in Figure 22.



*Figure 22. The decimation that was undertaken in the project. The left decimated mesh has more cells and nodes than the right decimated mesh.*

The decimation of the more intricate pulmonary artery capillary network resulted in the complete loss of features. Therefore, the decision was made to remove its use within the project. Some of the individual meshes within the clinical datasets also developed corrupted meshes from the decimation and, therefore, were removed from the dataset to avoid the possibility of outliers and improve the runtime of the shape modelling framework by reducing inconsistencies within the dataset.

### 3.1.4 Alignment

2.1.3 details the importance of alignment for the SSM architecture. The alignment of the surface meshes was conducted using the Procrustes algorithm in conjunction with the use of fiducial landmark markers, as used by Medrano-Gracia et al., detailed in 2.1.3. The fiducial registration wizard feature in 3D Slicer was used to accomplish this, by manually selecting the fiducial landmark markers on a chosen template mesh and the corresponding markers on another individual mesh. The software would then run the Procrustes algorithm, mapping the individual mesh to the template mesh. This was repeated for every mesh in the dataset. A few of the aligned meshes can be seen in Figure 23. Once the alignment procedure was completed for both the main pulmonary artery and aorta datasets, the data was of the required quality to proceed with the shape modelling framework.

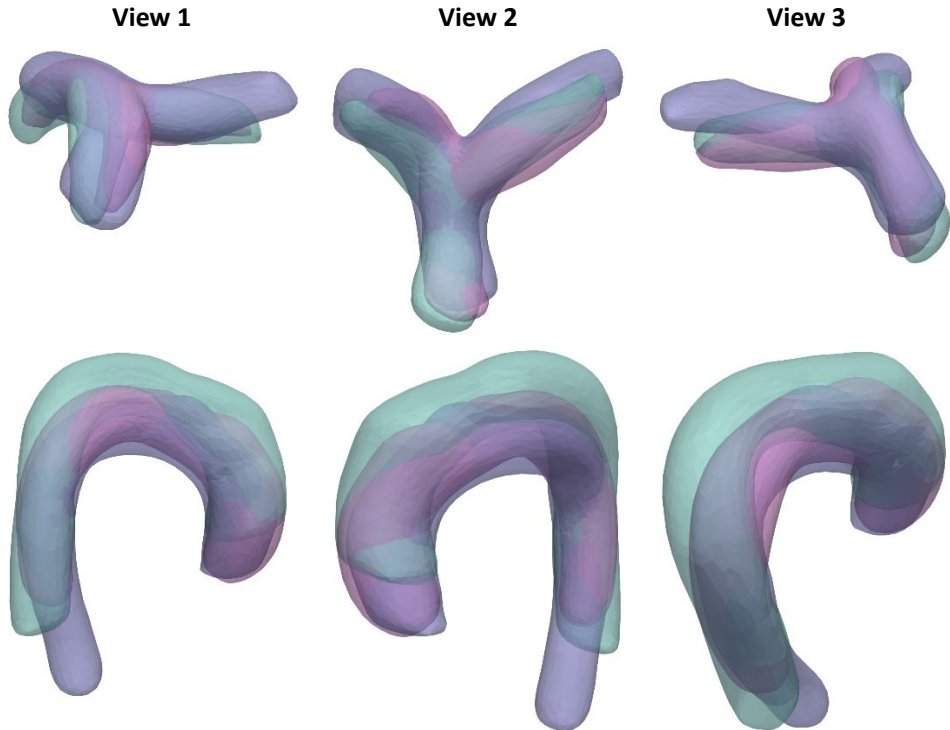


*Figure 23. Alignment of three meshes from the main pulmonary artery and aorta datasets at three different viewpoints.*

### 3.2 Atlas Construction

As mentioned in 2.2, atlas construction forms the fundamental methodology within a shape modelling framework, and the Deformetrica package was used as a tool to complete this. It should be noted that the datasets were split into an almost 80% / 20% split, with 80% for the atlas construction and 20% left for results validation, which will be discussed later. The following section will detail the steps taken in order to formulate an atlas which accurately encapsulates the finite shape feature variability within the dataset. The Jupyter Notebook file used to run the atlas construction with the Python package Deformetrica can be found in Appendix 9.9.

#### 3.2.1 Parameter Settings

As mentioned in 2.2.3, Deformetrica requires various parameters to be set, which will determine the quality of the atlases produced for the main pulmonary artery and aorta. The recommended iterative approach, detailed in 2.2.3, was undertaken to determine the optimal parameters. Starting at kernel widths,  $\lambda wT$  and  $\lambda wM$ , of 40 and noise standard deviation,  $nstd$ , of 10 each parameter was iteratively reduced until either the computational kernel capacity was reached or the deformations within the atlas has

become corrupted. The deformations were checked after every iteration in ParaView (“Paraview,” n.d.). The resulting parameters used were a template kernel width,  $\lambda wT$ , of 10, model kernel width,  $\lambda wM$ , of 11 and noise standard deviation,  $nstd$ , of 1 for the main pulmonary artery dataset and a template kernel width,  $\lambda wT$ , of 10, model kernel width,  $\lambda wM$ , of 14 and noise standard deviation,  $nstd$ , of 1 for the aorta dataset. During this process, it was also noticed that the deformations were producing strange protrusions, as shown in Figure 24; thus, other parameters were altered to combat this issue as recommended by the PhD, Liam Burrows. The final parameter settings used are displayed in Table 3.

*Table 3. Parameter Settings*

Parameter Setting	Pulmonary Artery	Aorta
Template Kernel Wdth, $\lambda_{wT}$	10	10
Model Kerel Wdth, $\lambda_{wM}$	11	14
Noise Standard Deviation, $n_{std}$	1	1
Max Line Search Iterations	20	20
Max Iterations	1000	1000
Convergence Tolerance	1e-9	1e-9
Initial Step Size	0.01	0.01

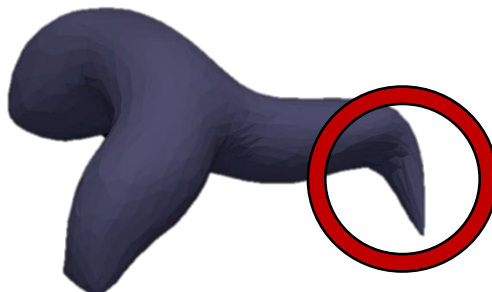


*Figure 24. Example of protrusion which was appearing on some atlas deformations.*

### 3.2.2 Template Formation and Shape Deformations

In order for Deformetrica to formulate the estimated mean template of the dataset, as discussed in 2.2.1, Deformetrica requires a mesh to be selected from the dataset, which will be deformed into the estimated mean template. This mesh was selected by eye, from viewing the meshes in Paraview. Identification of a mesh for each dataset, which was judged to be approximately the mean of the dataset and exhibiting a lack of obtrusive features, was attempted. This was done so Deformetrica would find it easier to deform the mesh to the other meshes in the dataset, as discussed in 2.2.1, reducing the computation intensity. The template selected and subsequently computed mean estimated template is shown in Figure 25.

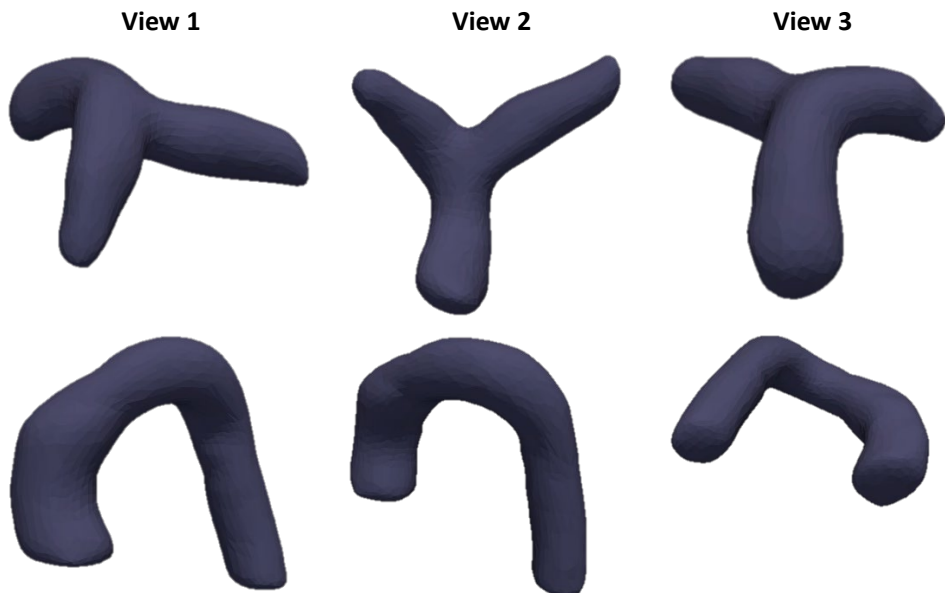


*Figure 25. The estimated main pulmonary artery and aorta templates were computed in the atlas from three different viewpoints.*

Deformetrica utilised the LDDMM methodology, explored in 2.2.1, to deform the templates to the main pulmonary artery and aorta subjects within their respective datasets. The deformations were completed iteratively, producing reconstruction flow surface meshes after every iteration, as well as tracking the displacement changes with momenta vectors. These iterations can be seen in Figure 26. Initially, prior to any reconstructions, Deformetrica defined a number of control points across the template mesh, which was characterised by the parameter settings. These control points are where the displacement differences were captured in the form of momenta vectors, capturing the shape variability within the dataset. These momenta vectors for each

subject in each dataset were outputted in a .txt file format from Deformetrica, as well as the control point and error residuals. Once Deformetrica had completed constructing the atlases for the main pulmonary artery and aorta, the detailed shape variability captured by the atlas was ready to be statistically analysed for any associations to PH.



*Figure 26. The iterative reconstruction deformation process is undertaken when formulating the atlas. The purple represents the initial shape, while the light blue/lilac represents the first iterative deformation, and the pink represents the second iterative deformation.*

### 3.3 Statistical Analysis

As mentioned in 2.3, both PCA and PLS regression statistical techniques were employed to identify potential correlations of particular shape variability to PH. This section will describe the methods used to implement the techniques.

#### 3.3.1 Correlation Methodology

Firstly, the provided mPAP data for each patient was tested for normality using various normality tests to determine the type of correlation coefficient to be used within the investigation. This was conducted due to different correlation coefficients having different conditions of use, as listed in 2.3.3. The tests, which were implemented through a MATLAB code in Appendix 9.2, were the Anderson-Darling, Lilliefors, Shapiro-Wilk and Kolmogorov-Smirnov tests, all of which came up negative. As a result, Spearman's Rank Correlation coefficient was used for the statistical analysis.

#### 3.3.2 Principal Component Analysis (PCA)

The first statistical analysis technique investigated was PCA using the MATLAB code in Appendix 9.3. The mathematical theory explained in 2.3.1 was implemented into the MATLAB code, using a variety of MATLAB functions. The statistical technique was

applied to the shape variability by importing the outputted momenta vector .txt file into MATLAB code. Once the eigenvalues were obtained from applying the covariance matrix to the momenta vectors, the shape variation explained by each principal component, or shape mode, was found. These were plotted cumulatively to find how many shape modes captured 90% of the variance within the dataset. The corresponding eigenvectors were rearranged accordingly to the descending eigenvalues, from which the amount of each shape mode within each subject in the dataset was found using the dot product between them, as detailed in 2.3.1. Now having the shape mode amounts, the MATLAB code in Appendix 9.3 was utilised to import the subject's associated mPAP data and apply Spearman's Rank Correlation to each shape mode quantity data for every subject and the subject's associated mPAP. Doing this produced a Spearman's Rank Correlation Coefficient for each shape mode, from which the shape modes indicating a correlation to PH were found using the correlation classifications in Table 2, 2.3.3. A  $\pm 0.3$  Spearman's Rank Correlation Coefficient classification was used to identify the relevant shape modes indicating an association with PH. This was conducted for both the main pulmonary artery and aorta atlases' momenta vector output files.

### 3.3.3 Partial Least Squares (PLS) Regression

The methodology for PCA was repeated, however, using PLS regression to obtain the components or shape modes. The MATLAB code used to apply PLS regression is in Appendix 9.4 and was again formulated using various MATLAB functions. The differences between PLS and PCA are described in 2.3.2. For PLS, the cumulative dataset variance was found using the outputted component percentage variance from a MATLAB regression function. Additionally, the shape mode amounts within each subject were found using the outputted predictor loading matrix in the dot product calculation rather than the eigenvectors in the PCA, as explained in 2.3.2.

### 3.3.4 New PH Definition – mPAP = 20mmHg

The methodologies for both PCA and PLS were then repeated but using mPAP = 20mmHg as the definition for PH. This was done so that the studies could be compared, given that the literature indicates that the definition of PH is likely to change.

### 3.4 Model Feasibility Validation

Now that the significant shape modes had been distinguished, they required validating as potential binary classifiers for PH, as well as determining an optimal shape mode amount classification for PH. The validation methods explored in 2.4 were used to achieve this. This section will now detail how these techniques were used in the project. All the methods discussed were completed for both PH definitions of mPAP = 25mmHg and mPAP = 20mmHg.

#### 3.4.1 Receiver Operating Characteristic (ROC) Curve

The first validation technique implemented was the ROC curve, where its method, as described in 2.4.1, was implemented using a step variable MATLAB code, to incrementally adjust the classification threshold, as seen in Appendix's 9.5 and 9.6. From this, the sensitivity and specificity at each threshold were plotted, and the area under the curve, AUCROC, was calculated using a MATLAB function for every significant shape mode, as discussed in 2.4.1. Additionally, for each correlating shape mode, Youden's Index was calculated, to determine an estimated PH classification shape mode amount threshold, using the calculation detailed in 2.4.2.

#### 3.4.2 Precision Recall Curve (PRC)

Next, similarly to the implementation of the ROC curve validation technique, the PRC was obtained from plotting precision against recall, and the area under the curve, AUC-PRC, was calculated, as described in 2.4.3. From this, the  $F\beta$  score was found as an alternative estimated classification threshold, with the aim of reducing false negatives, such that people with PH are always identified with a  $\beta$  value of 2. The application of this is detailed in 2.4.4 and can be seen in the Appendix 9.5 and 9.6. A classification threshold and AUC-PRC value were found for every significant shape mode.

#### 3.4.3 PH Shape Mode Classification & Unseen Data Validation

From visualising and calculating the performance of the two estimated classification thresholds, an optimal PH classification threshold was manually defined, whereby reducing false negatives was prioritised, but not with complete disregard for classifying true negatives. The final validation undertaken was using the remaining 20% of the datasets to perform an unseen validation study. The remainder of the dataset was used by inputting the data and estimated atlas templates into the Deformetrica registration feature, which obtained the momenta vectors between the data and templates. The shape mode quantities for each unseen subject data were then calculated. This was

achieved by multiplying the momenta vectors by the computed eigenvector matrix and predictor loading matrix for PCA and PLS analysis validation, respectively, similar to as described in 2.3.1 and 2.3.2.

The study's binary classifier performance metrics were determined for each significant shape mode and analysed. This was conducted using the MATLAB code in Appendix 9.8. The achieved performance statistics were then compared against the performance metrics of current PH diagnostic strategies. The performance indicators for the current diagnostic methods were calculated using the clinical dataset subjects pulmonary artery to aorta ratio, PA:A, and pulmonary vascular resistance, PVR, data and applying the same binary classifier validation techniques through the MATLAB code in Appendix 9.7.

## 4 Results and Analysis

This study produced three sets of results, one concerning the main pulmonary artery PCA and PLS results and the other regarding the aortas. There are three, rather than four, as the PLS study on the clinical aorta dataset produced no significant shape modes correlating to PH. The two sets of results are split into two types: results leading to the evaluation of a shape mode quantity classification for PH, 4.2, 4.3 and 4.4, and validation of this defined classification threshold for both sets of anatomies.

### 4.1 Shape Variance in the Datasets

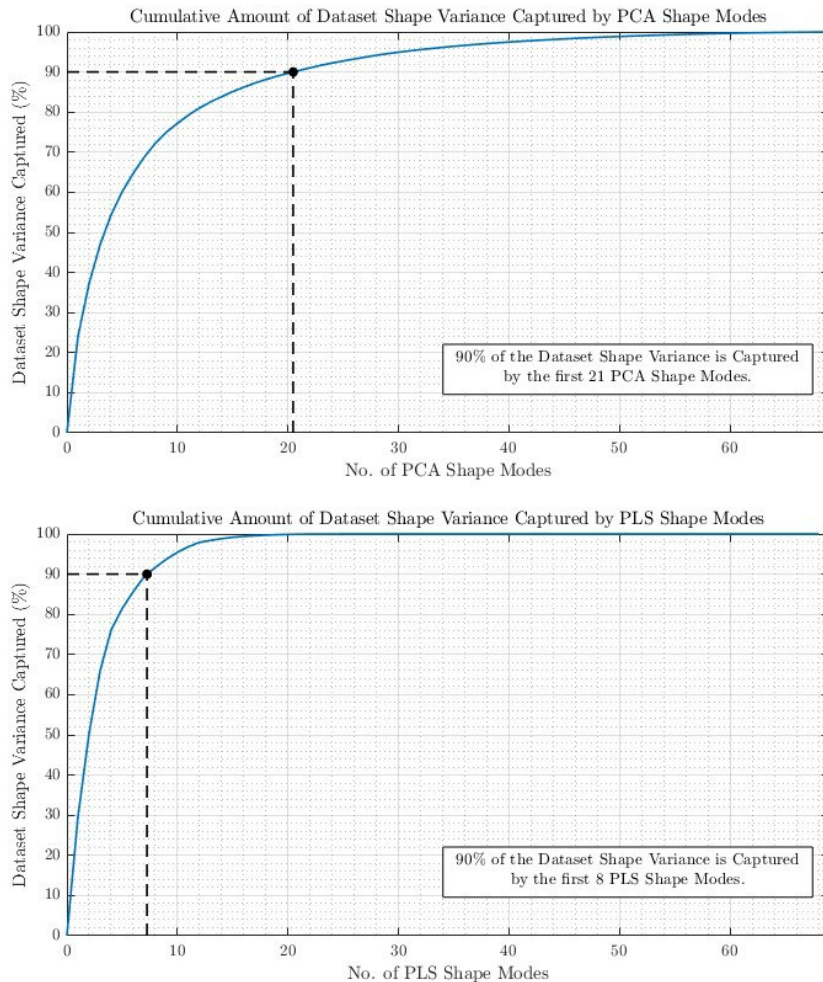


Figure 27. The amount of shape variance in the dataset captured cumulatively by the PCA (top) and PLS (bottom) modes for the main pulmonary artery.

Figure 27 illustrates that 90% of the shape variance is captured by the first 21 PCA shape modes and the first 8 PLS Shape Modes for the main pulmonary artery. This means that we can describe 90% of the whole shape variability within the main pulmonary artery dataset by those PCA and PLS shape modes, respectively.

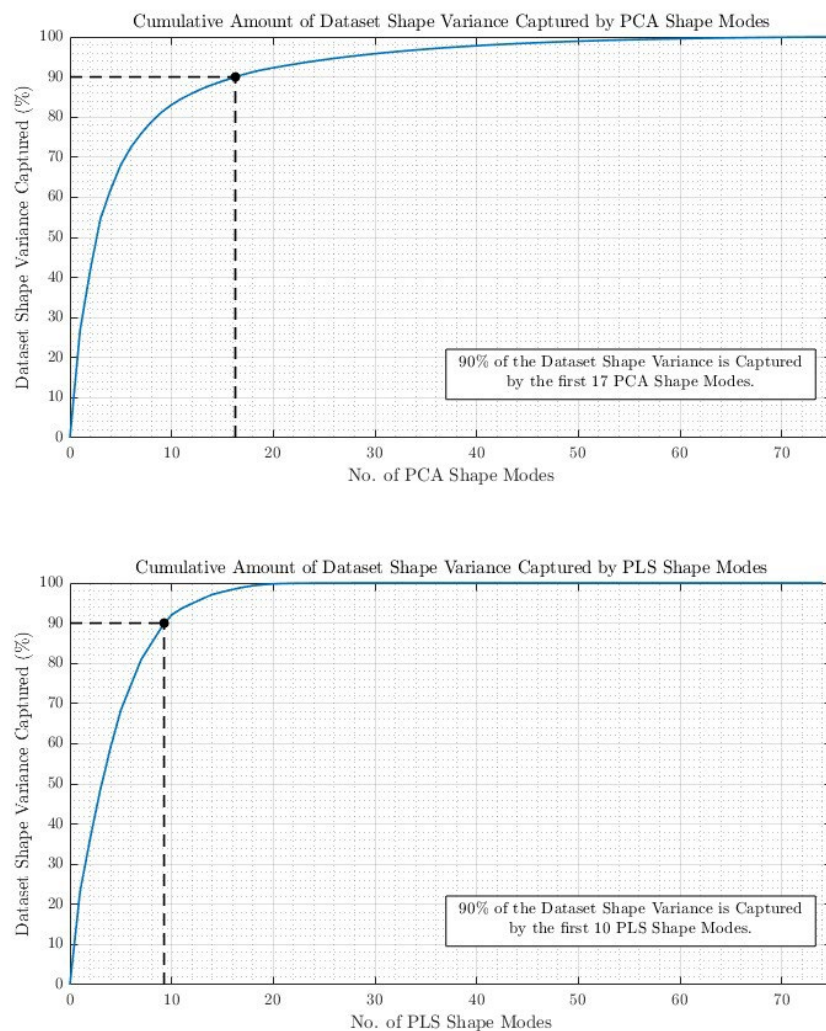


Figure 28. The amount of shape variance in the dataset captured cumulatively by the PCA (top) and PLS (bottom) modes for the aorta.

Figure 28 shows that 90% of the shape variance is captured by the first 17 PCA shape modes and the first 10 PLS Shape Modes for the aorta dataset. This means that we can describe 90% of the whole shape variability within the aorta dataset using those PCA and PLS shape modes, respectively.

Firstly, the fact that the PCA studies required 21 and 17 shapes to capture 90% of the dataset shape variance, respectively, initially suggests that the shape data has significant complexity and a high-dimensional structure. However, in both cases, more PCA shape modes were required than PLS shape modes, indicating that the PLS methodology is more efficient in dimensionality reduction when considering the relationship between the patient's anatomical shape data and mPAP. This was expected, given the supervised nature of the PLS statistical technique, as mentioned in 2.3.2. When discussing dimensionality, this refers to the number of variables described within the shape data. Furthermore, the greater number of PCA modes indicates that the intrinsic geometric variability of the shapes is spread across many dimensions, which PCA captures by focusing purely on the variance within the shape data (Abdi and Williams, 2010). Plus, the fewer PLS modes suggest that there are fewer latent variables that explain most of the covariance between shapes and the response variables, indicating a stronger, more direct relationship (Rosipal and Krämer, 2006).

Moreover, the pulmonary artery dataset required more PCA shape modes to reach 90% variance than the aorta dataset, indicating that the aorta anatomy has less shape complexity, which was as expected. Although the PLS study effectively reduced dimensionality for the aorta dataset, it was less pronounced than in the main pulmonary artery dataset.

Understanding how many shape modes capture 90% of the dataset shape variance is less significant in this study due to the relatively small dataset compared to other similar SSM studies. This is because, its main purpose is to be used to perform dimensionality reduction, reducing the number of shape modes analysed. This is designed to simplify the model, improving the efficiency of data management for large datasets and reducing computational intensity whilst retaining confidence that your model is still representative of the dataset shape variability. Despite this, it also offers an opportunity for future improvements to the model, as new shape instances can be generated by varying along the shape modes, holding 90% of the variance. This would be useful to augment the dataset, given the lack of large data on subjects with PH.

## 4.2 PCA Shape Mode Classification Main Pulmonary Artery

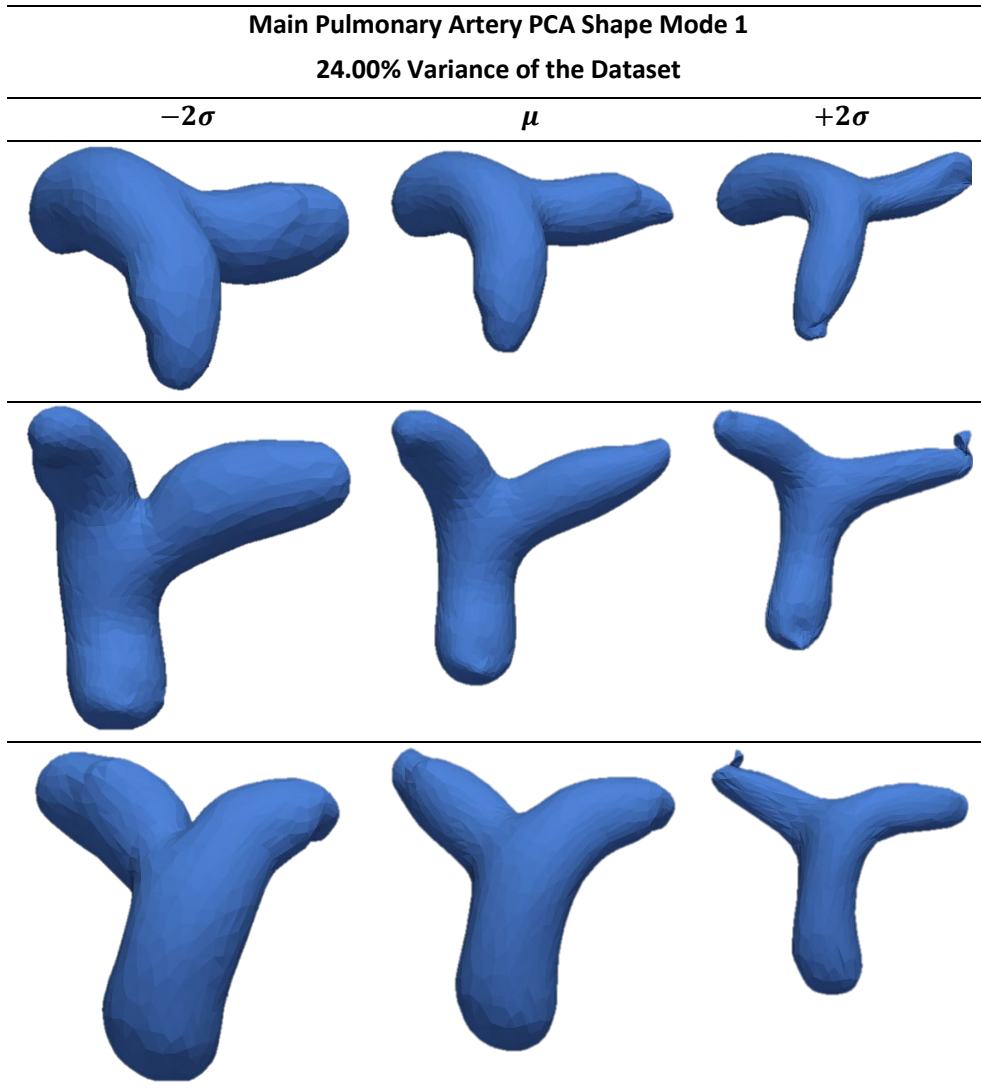
### 4.2.1 Spearman's Rank Correlation Coefficient

*Table 4. The significant shape modes associated with the presence of PH are based on Spearman's Rank Correlation Coefficient and Spearman's Rank Correlation Coefficient P-value.*

Shape Mode No.	Spearman's Rank Correlation	
	Coefficient	Coefficient P-Value
1	-0.4508	0.0001
6	-0.3480	0.0034

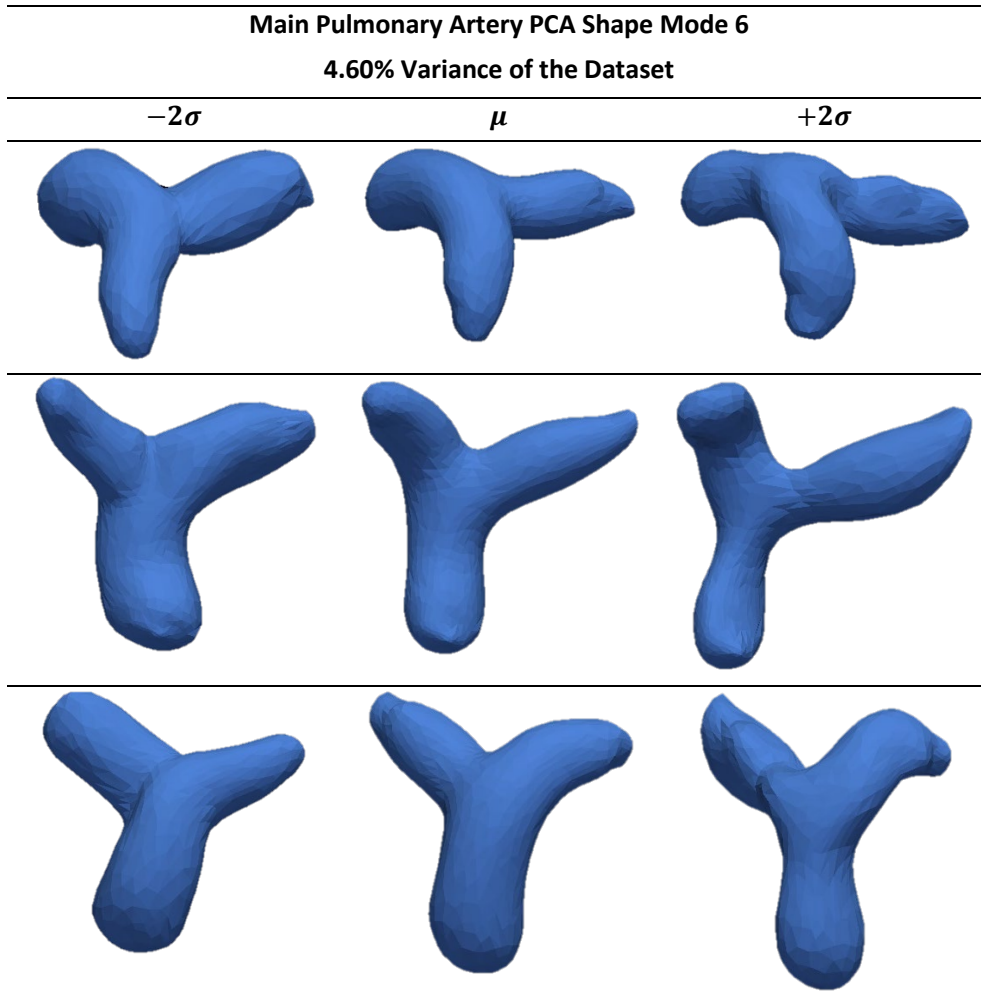
The dominant shape modes possessing at least a “fair” correlation to mPAP, found by applying Spearman’s Rank Correlation, as detailed in 3.3.2, to each shape mode can be seen in Table 4. Table 4 shows that significant PCA shape modes found were shape Mode 1 and 6, both being members of the shape modes, containing 90% of the data. Both hold negative correlations, with shape mode 1, showing a greater correlation to detecting the presence of PH at a greater statistical significance. The negative correlation suggests the lack of a particular shape mode is the classification for PH in both cases. The shape modes can be visualised in Table 5 and Table 6.

*Table 5. Visualisation of PCA Shape Mode 1 for the main pulmonary artery and its variation across  $\pm 2\sigma$  and its Variance of the Dataset.*



As seen in Table 5, PCA Shape Mode 1's variation seems to be a general enlargement of the diameter throughout the anatomy, with  $-2\sigma$  representing the enlarged shape and  $+2\sigma$  representing the shrunken anatomy. This resonates with the literature, given that current diagnostic methods look for expanded pulmonary arteries, like in Figure 2. The shape mode also seems to exhibit greater enlargement on one branch than the other. The shape mode also holds 24% of the total shape variability within the dataset, meaning it is extremely prevalent within the dataset.

*Table 6. Visualisation of PCA Shape Mode 6 for the main pulmonary artery and its variation across  $\pm 2\sigma$  and its Variance of the Dataset.*



As seen in Table 6, PCA Shape Mode 6's variation seems to be an enlargement of one branch plus, increased curvature in the other, with  $+2\sigma$  representing the enlarged branch and increased curvature and  $-2\sigma$  representing the shrunken and straighter anatomy branches. The shape mode also seems to exhibit slightly narrower branches as characteristic at  $+2\sigma$ . The shape mode also accounts for 4.6% of the total shape variability within the dataset, meaning it is fairly prevalent.

#### 4.2.2 Receiver Operating Characteristic (ROC) Curve

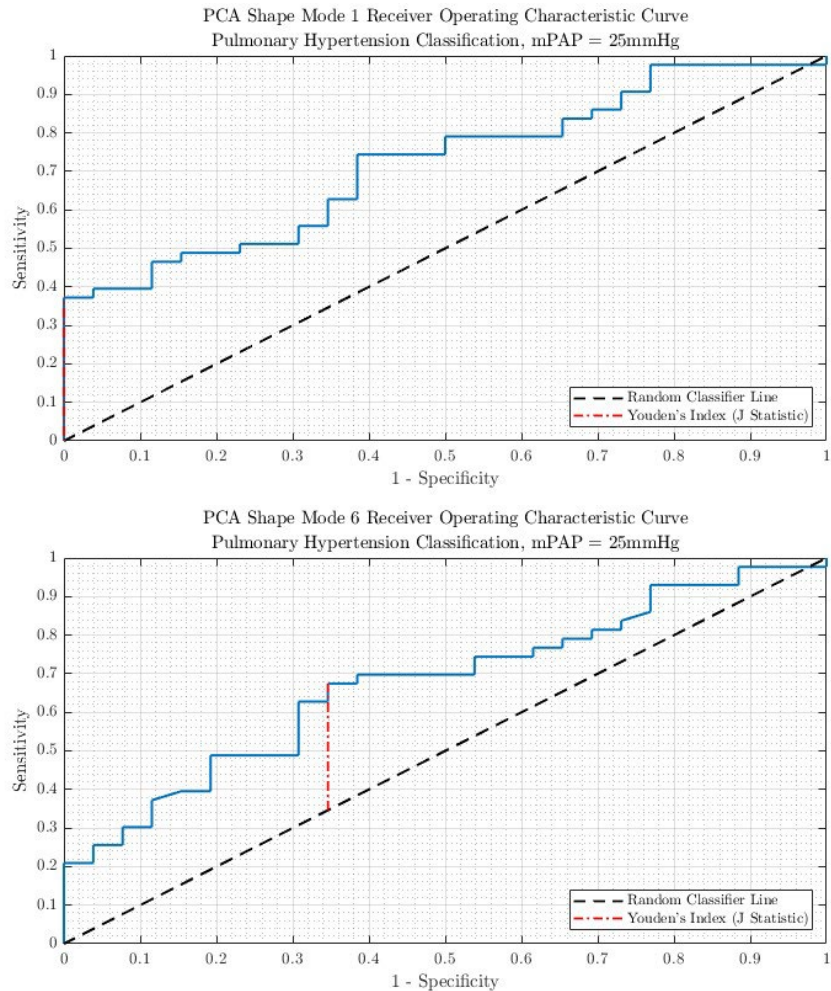


Figure 29. ROC curves for PCA Shape Modes 1 (top) and 6 (bottom) and their representative Youden Index Values, the red dashed line. The black dashed line is the random classifier line.

The ROC curve for Mode 1, as shown in Figure 29, rises prominently above the random classifier line, indicating a better performance. The Youden's Index, the dashed red line, is marked at a point with lower sensitivity and higher specificity. On the other hand, the curve for Mode 6 rises above the random classifier line but less prominently compared to Mode 1. However, Youden's Index for Shape Mode 6 is at a point of greater specificity and sensitivity than Mode 1. Mode 1's ROC curve shows a steeper ascent initially, indicating better performance at higher specificity levels, while Mode 6's ROC curve is less steep, suggesting more balanced sensitivity and specificity. Graphical indications of the Youden's Index classification thresholds are shown for each shape mode in Figure 30.



Figure 30. The quantity of PCA Shape Modes 1 (top) and 6 (bottom) in each subject within the dataset plotted against each subject's associated mPAP. The red dashed is the mPAP definition for PH and the black dashed line is the shape mode quantity threshold for classifying PH, defined by Youden's Index.

Table 7. The AUCROC values for PCA Shape Modes 1 and 6. And the classification success rate of the shapen modes at the Youden's Index threshold.

PCA Shape Mode No.	AUCROC Value	Youden's Index Classification Rate
1	0.718	59.42%
6	0.674	66.67%

As seen in Table 7, Mode 1 has a higher AUCROC than Mode 6. The higher AUC indicates better overall performance in distinguishing between the classes and the presence or absence of PH. Mode 1 demonstrates acceptable discriminatory power,  $AUC > 0.7$ , with Mode 6 performing worse with poor discriminative power (Zweig and Campbell, 1993). The discriminative power of a model refers to its ability to correctly distinguish between different classes. Despite its lesser AUC, Shape Mode 6 has a higher classification rate than Shape Mode 1, as illustrated in Table 7, suggesting it would perform better in industry overall at this classification threshold. This may be attributed to Shape Mode 6's more balanced Youden's Index and could indicate that Mode 6 captures aspects of the shape variability that is more directly useful for making accurate classifications. Mode 1 captures more variance related to the ability to distinguish healthy patients at this threshold, indicated by the higher AUC. This suggests that Mode 1 would be better at ranking patients in terms of their likelihood of having PH if the classification threshold was moved.

#### 4.2.3 Precision-Recall Curve (PRC)

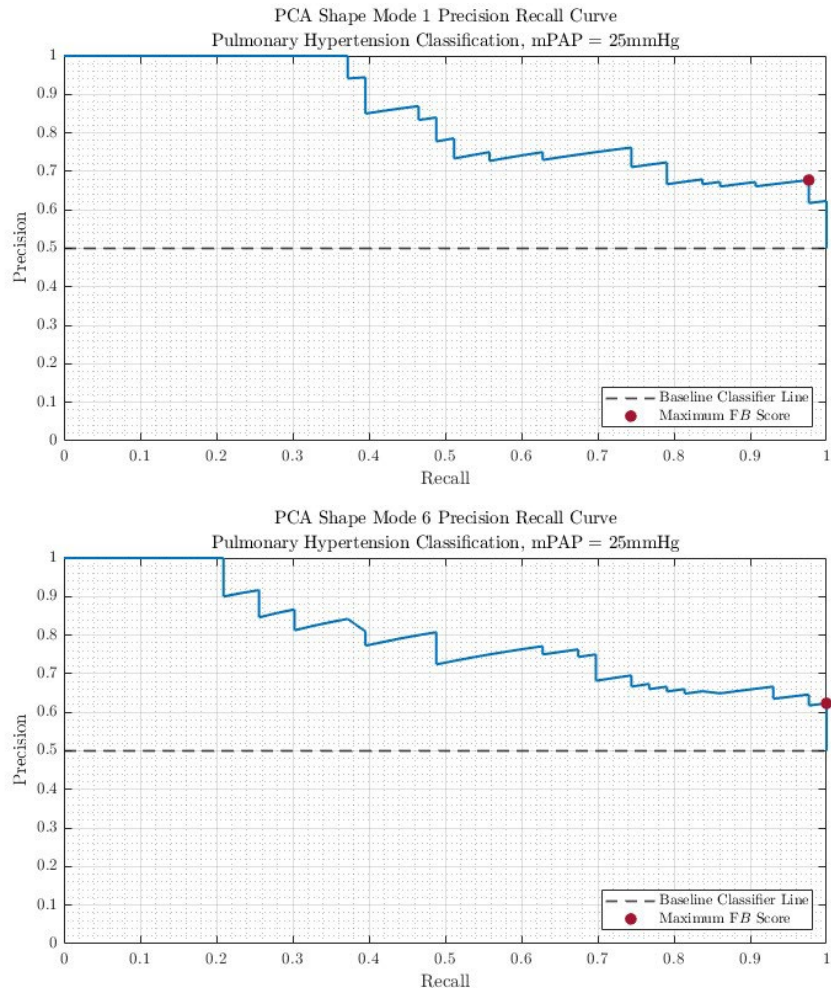
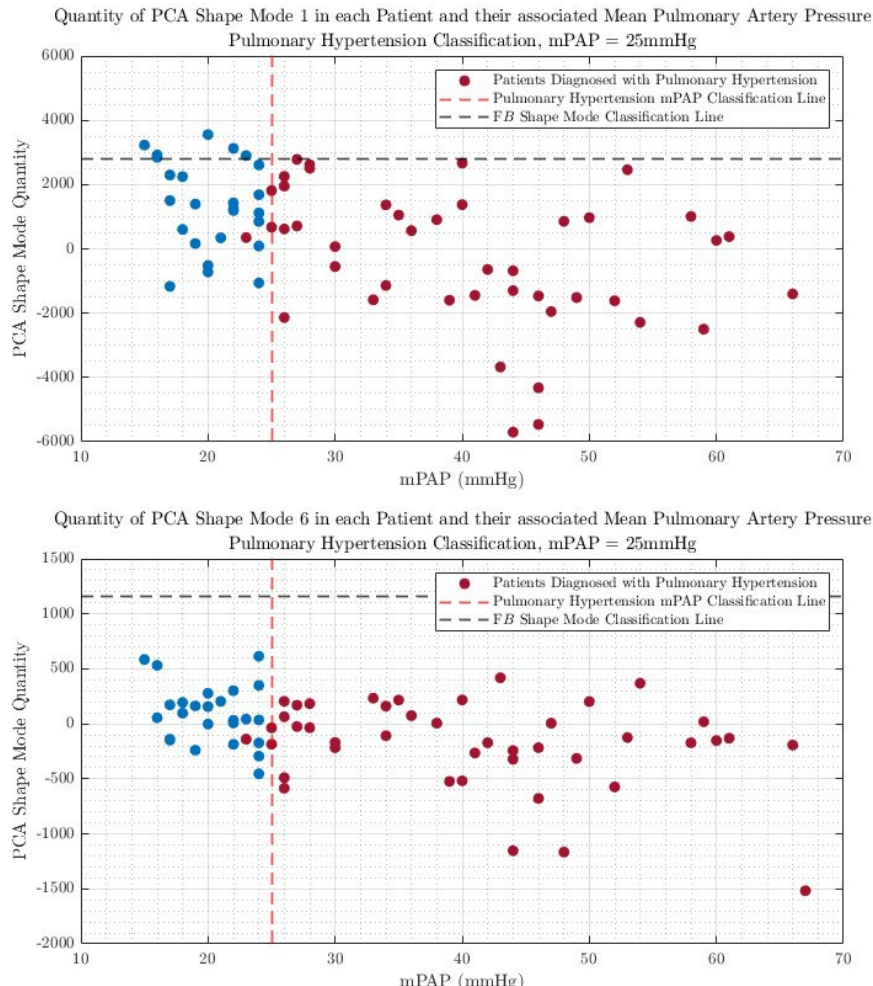


Figure 31. PRC curves for PCA Shape Modes 1 (top) and 6 (bottom) and their representative Maximum  $F\beta$  Score, the red dot. The black dashed line is the baseline classifier line.

As mentioned in 2.4.3 PRC were used to determine a classification threshold more weighted to classifying patients with PH correctly. The red dot in both graphs represents the maximum  $F\beta$  score, indicating this defined classification threshold. As seen in Figure 31, the PRC for Mode 1 starts with high precision and recall values that remain stable before declining, reflecting strong performance until recall reaches higher values. Similar to Mode 1, the curve starts with high precision and recall values but shows a more gradual decline, indicating a steadier trade-off between precision and recall across different thresholds. Graphical indications of the  $F\beta$  Score classification threshold are shown for each mode in Figure 32.



*Figure 32.* The quantity of PCA Shape Modes 1 (top) and 6 (bottom) in each subject within the dataset was plotted against each subject's associated mPAP. The red dashed is the mPAP definition for PH, and the black dashed line is the shape mode quantity threshold for classifying PH, defined by the Maximum F $\beta$  Score.

*Table 8.* The AUCROC values for PCA Shape Modes 1 and 6. The classification success rate of the shape modes at the Maximum F $\beta$  Score threshold.

PCA Shape Mode No.	AUC – PRC Value	F $\beta$ Score Classification Rate
1	0.837	69.57%
6	0.798	62.32%

Mode 1 has a higher AUC – PRC value compared to Mode 6, as seen in Table 8. A higher AUC – PRC indicates better overall performance in terms of maintaining high precision across various recall levels. Both modes demonstrate good performance, with AUC – PRC values  $> 0.75$ , but Mode 1 is slightly superior in balancing precision and recall (Saito and Rehmsmeier, 2015). Mode 1 has a higher classification rate than Mode 6, suggesting that Mode 1 is more effective at correctly classifying instances overall at this classification threshold. Mode 1 achieves a greater  $F\beta$  score, resulting in its more appropriate classification threshold. The  $F\beta$  score thresholds, where in this case,  $\beta = 2$ , are extremely sensitive to outliers relating to subjects with PH. This is because they tend to place their threshold at the extreme values of the subjects with PH so they ensure they classify them correctly; thus, if an outlier is present, it will severely skew the threshold, as in Mode 6's case.

The good AUC – PRC values indicate both modes possess strong discriminative behaviour at this threshold, related to classifying patients with PH. Mode 6's lower classification rate can be attributed to the skewed threshold from the outlier, resulting in no healthy patients being classified correctly, severely decreasing its classification rate. Moreover, the higher AUC – PRC values compared to the AUCROC values suggest that the model's ability to maintain high precision at various recall levels is better than its overall discriminative ability.

#### 4.2.4 Defined PH Classification Threshold

From the graphs in Figure 30 it's clear to see that Youden's Index classification threshold for the presence of PH gives equal weighting to each class, resulting in lots of patients with PH being missed, although the good classification rates. This is not ideal in our case, as we want to reduce false negatives to ensure that as many people with PH are classified correctly without the number of false positives suffering heavily. However, in the case of the  $F\beta$  Score classification threshold, as seen in Figure 32, although the number of false negatives is minimised, it is at too great a cost to the number of false positives. Therefore, the defined classification threshold for each mode was set as a compromise between the two, with greater weighting towards reducing false negatives, as described in 3.4.3. This defined classification threshold can be visualised for each mode in Figure 33.

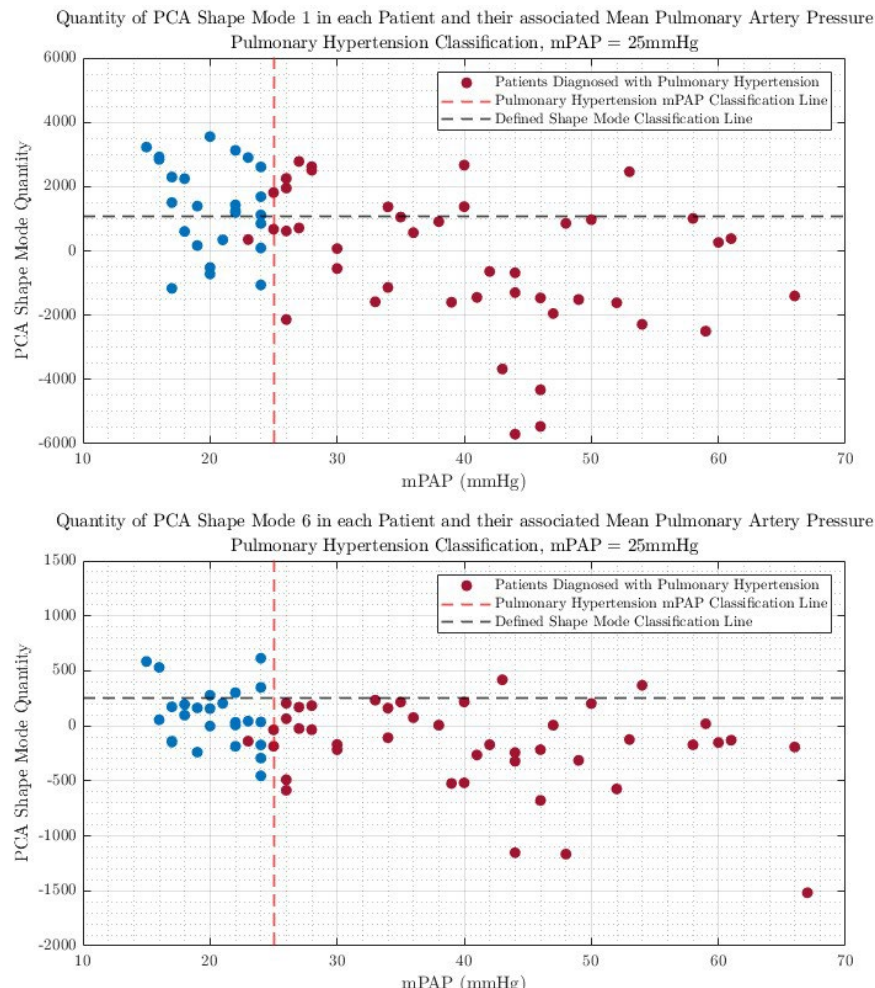


Figure 33. The quantity of PCA Shape Modes 1 (top) and 6 (bottom) in each subject within the dataset plotted against each subject's associated mPAP. The red dashed is the mPAP definition for PH and the black dashed line is the shape mode quantity threshold for classifying PH, defined by the optimal value at a compromise between the two thresholds.

Table 9. The sensitivity, specificity, and classification success rate of the shape modes at the defined optimal threshold for PCA Shape Modes 1 and 6.

PCA Shape Mode No.	Sensitivity	Specificity	Classification Rate
1	0.744	0.615	69.57%
6	0.930	0.231	66.67%

The performance metrics for each mode can be seen in Table 9 and show that Mode 6 has a higher sensitivity but much lower specificity compared to Mode 1. This means Mode 6 is better at detecting PH patients but worse at correctly identifying healthy patients. Mode 1 has a slightly higher classification rate than Shape Mode 6, likely accounted for by the more balanced sensitivity and specificity characteristics. Furthermore, the metrics validated the location of the thresholds, as the classification rates did not decrease while improving specificity for Mode 1 and sensitivity for Mode 6. Mode 1's balanced threshold makes it a reasonable choice for initial screening, where classifying healthy patients is more critical. On the other hand, Mode 6 is more suitable for cases where it's crucial to identify PH patients, even at the cost of higher false positives.

### 4.3 PLS Shape Mode Classification Main Pulmonary Artery

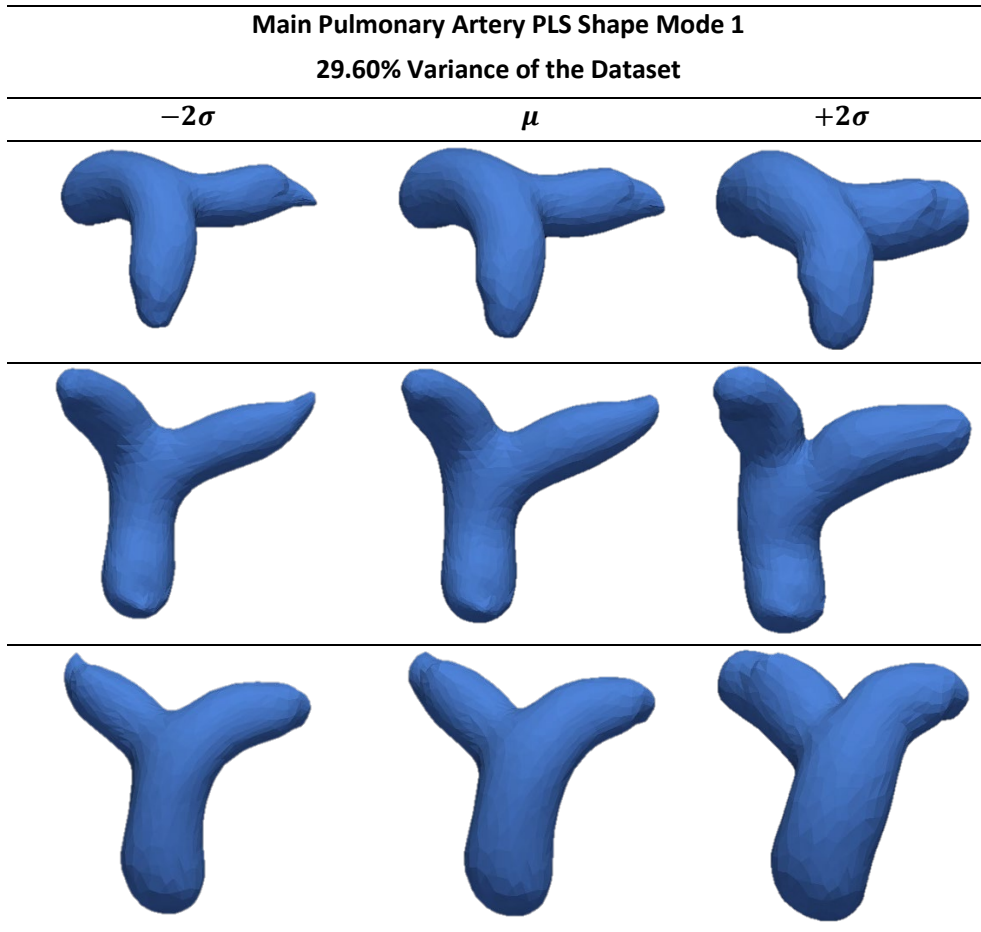
#### 4.3.1 Spearman's Rank Correlation Coefficient

*Table 10. The significant shape mode associated with the presence of PH is based on Spearman's Rank Correlation Coefficient and Spearman's Rank Correlation Coefficient P-value.*

Shape Mode No.	Spearman's Rank Correlation Coefficient	Spearman's Rank Correlation Coefficient P-Value
1	0.4794	3.08e-5

With the same criteria, as explained in 4.2.1, Table 10 shows that a significant shape mode found was PLS Shape Mode 1. Mode 1 belongs to the members of the shape modes, containing 90% of the data. Mode 1 holds a positive correlation with large statistical significance. The positive correlation suggests that the more of the mode present, the more likely the presence of PH. The shape mode can be visualised in Table 11. Compared to the PCA modes in 4.2.1, this PLS shape mode demonstrates a greater magnitude of correlation with greater statistical significance. This suggests that this mode will be more likely and consistently able to detect the presence of PH than the PCA modes.

*Table 11. Visualisation of PLS Shape Mode 1 for the main pulmonary artery and its variation across  $\pm 2\sigma$  and its Variance of the Dataset.*



Similarly to PCA Shape Mode 1, this PLS shape mode, as seen in Table 11, seems to exhibit a general enlargement of the diameter throughout the anatomy, with  $-2\sigma$  representing the enlarged shape and  $+2\sigma$  representing the shrunken anatomy. This enlargement seems to be more balanced across the branches than in PCA Mode 1. This resonates with the literature, given that current diagnostic methods look for expanded pulmonary arteries, like in Figure 2. The shape mode also holds 29% of the total shape variability within the dataset, meaning it is extremely prevalent within the dataset and more prevalent than the PCA modes. Furthermore, given that PLS modes do not share any variability, as detailed in 2.3.2, the variance of the dataset it holds is more significant.

#### 4.3.2 Receiver Operating Characteristic (ROC) Curve

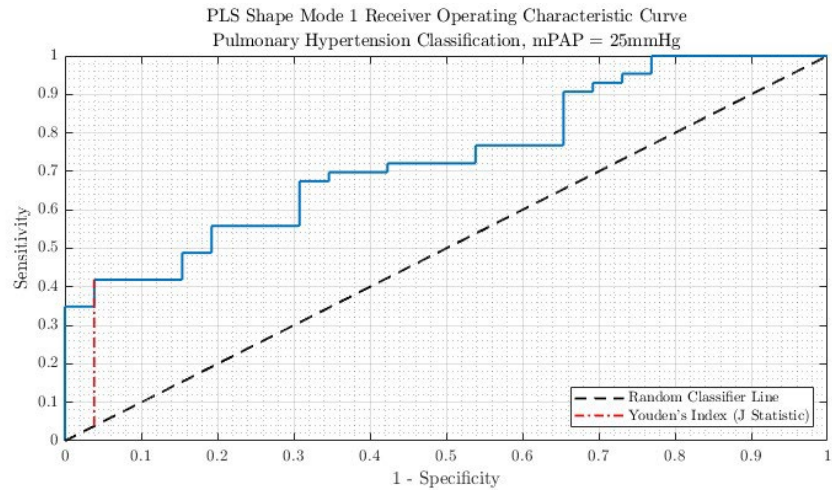
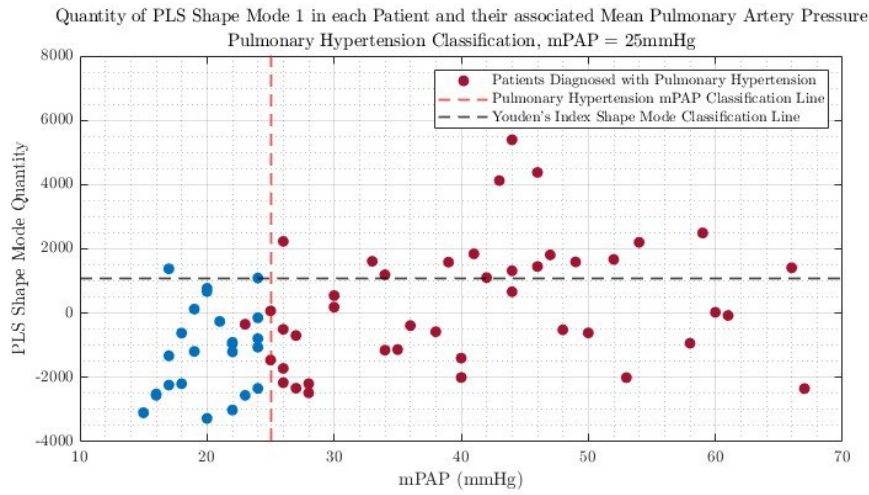


Figure 34. ROC curves for PLS Shape Mode 1 and its representative Youden Index Value, the red dashed line. The black dashed line is the random classifier line.

The ROC curve for Mode 1, as shown in Figure 34, rises prominently above the random classifier line, indicating a better performance. The Youden's Index, the dashed red line, is marked at a point with lower sensitivity and higher specificity. Compared to the PCA modes, this has a slightly higher sensitivity than PCA Mode 1 but a much lower sensitivity than PCA Mode 6. It is also slightly less specific than PCA Mode but much greater specificity than PCA Mode 6. Mode 1's ROC curve shows a steeper ascent initially, indicating better performance at higher specificity levels, similar to the PCA modes. Graphical indications of the Youden's Index classification threshold are shown in Figure 35.



*Figure 35. The quantity of PLS Shape Mode 1 in each subject within the dataset was plotted against each subject's associated mPAP. The red dashed is the mPAP definition for PH and the black dashed line is the shape mode quantity threshold for classifying PH, defined by Youden's Index.*

*Table 12. The AUCROC values for PLS Shape Mode 1. And the classification success rate of the shape mode at the Youden's Index threshold.*

PLS Shape Mode No.	AUCROC Value	Youden's Index Classification Rate
1	0.734	60.87%

As seen in Table 12, Mode 1 has an AUC of 0.734, which is slightly higher than the PCA modes. The higher AUC indicates that the PLS modes' overall performance in distinguishing between the classes is marginally better than that of the PCA modes. The mode has an acceptable discriminatory power, although not good, like the PCA modes (Zweig and Campbell, 1993). The mode's lower classification rate at this threshold suggests it would perform worse than PCA Mode 6 at the industry level. This may be attributed to the mode's imbalanced Youden's Index, which favours higher levels of specificity. Mode 1 captures more variance related to the ability to distinguish PH, indicated by the higher AUC, suggesting that Mode 1 would be better at ranking patients in terms of their likelihood of having PH if the classification threshold was moved, even though the classification rate is lower.

### 4.3.3 Precision-Recall Curve (PRC)

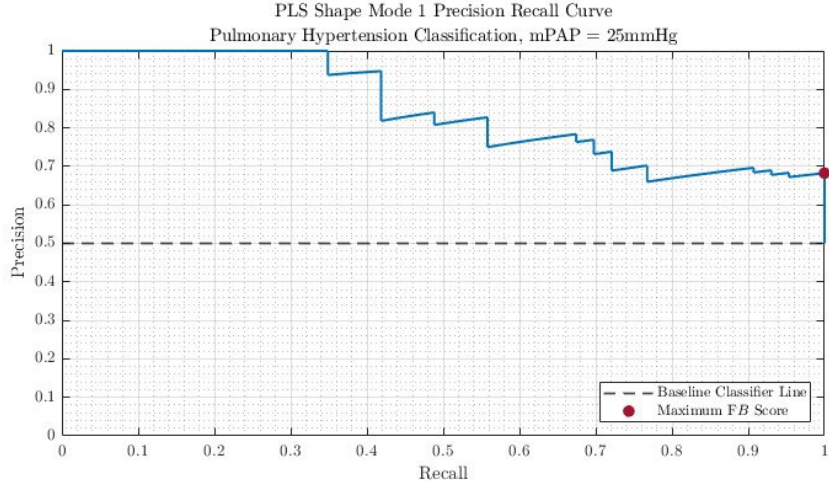


Figure 36. PRC curves for PLS Shape Mode 1 and its representative Maximum  $F\beta$  Score, the red dot. The black dashed line is the baseline classifier line.

Analysing Figure 36, similarly to 4.2.3, Mode 1 starts with high precision and recall values that remain stable for longer than the PCA modes before declining, reflecting strong performance until recall reaches higher values. The decline is more abrupt, suggesting the PCA modes possess a more consistent trade-off between precision and recall across different thresholds. Graphical indications of the  $F\beta$  Score classification thresholds are shown for mode in Figure 37.

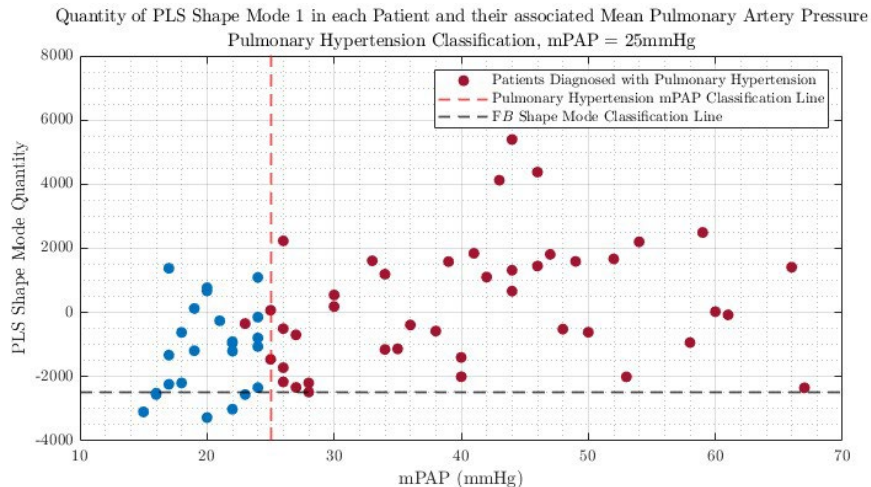


Figure 37. The quantity of PLS Shape Mode 1 in each subject within the dataset was plotted against each subject's associated mPAP. The red dashed is the mPAP definition for PH, and the black dashed line is the shape mode quantity threshold for classifying PH, defined by the Maximum  $F\beta$  Score.

*Table 13. The AUCROC values for PLS Shape Mode 1. The classification success rate of the shape mode at the Maximum F $\beta$  Score threshold.*

PLS Shape Mode No.	AUC – PRC Value	F $\beta$ Score Classification Rate
1	0.844	71.01%

Mode 1 has a marginally higher AUC – PRC value compared to the PCA modes, as seen in Table 8 and Table 13, indicating better overall performance in terms of maintaining high precision across various recall levels. Similarly to the PCA modes, this mode displays good performance, with this mode being slightly superior in balancing precision and recall (Saito and Rehmsmeier, 2015). Mode 1 has a higher classification rate than the PCA modes, suggesting that Mode 1 is more effective at correctly classifying instances overall at this classification threshold. This is likely due to the F $\beta$  Score providing a more appropriate threshold, as can be seen in Figure 37.

The good AUC – PRC values indicate the mode possesses strong discriminative behaviour at this threshold, related to classifying patients with PH. The classification rate achieved at this threshold is the best for the main pulmonary artery out of the ROC and PRC methodologies. Despite this, the classification rate suffers extensively from a large number of false positives. Moreover, the higher AUC – PRC values compared to the AUCROC values suggest that the model's ability to maintain high precision at various recall levels is better than its overall discriminative ability.

#### 4.3.4 Defined PH Classification Threshold

Similarly to 4.2.4 the defined classification threshold for each mode was set as a compromise between Youden's Index and  $F\beta$  Score classification thresholds. This defined classification threshold can be visualised for Mode 1 in Figure 38.

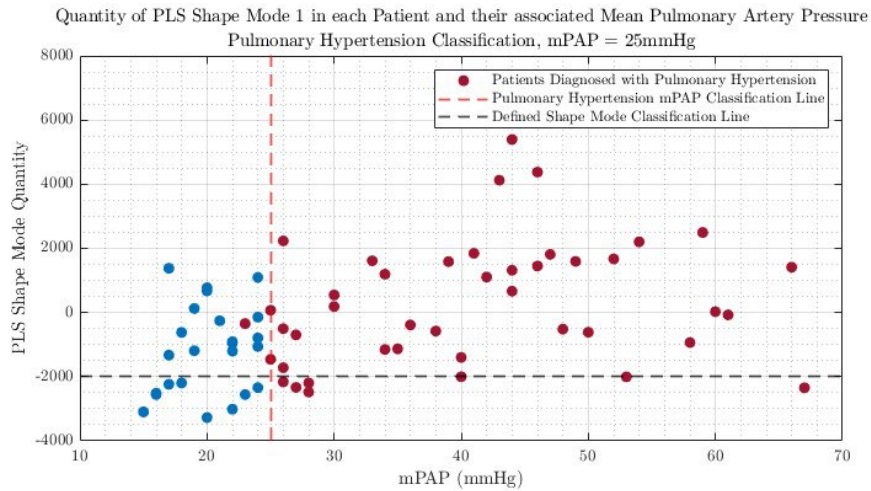


*Figure 38. The quantity of PLS Shape Mode 1 in each subject within the dataset plotted against each subject's associated mPAP. The red dashed is the mPAP definition for PH and the black dashed line is the shape mode quantity threshold for classifying PH, defined by the optimal value at a compromise between the two thresholds.*

*Table 14. The sensitivity, specificity, and classification success rate of the shape mode at the defined optimal threshold for PLS Shape Mode 1.*

PLS Shape Mode No.	Sensitivity	Specificity	Classification Rate
1	0.837	0.346	65.22%

The performance metrics for each mode can be seen in Table 14 and show Mode 1 placed in between the PCA modes for its performance metrics. Mode 1's greater sensitivity over its specificity means it is better at detecting PH patients but worse at correctly identifying healthy patients. The classification rate is worse than in the  $F\beta$  Score case, which seems counter-productive; however, the adjusted threshold allowed for greater specificity, whilst maintaining a large sensitivity. Additionally, the metrics validated the location of the threshold, as the classification rate dropped minimally while improving specificity. It seems this mode would be suitable for cases where it is crucial to identify PH patients and would perform better in the industry than PCA Mode 6 due to its greater specificity.

## 4.4 PCA Shape Mode Classification Aorta

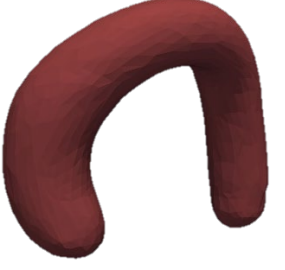
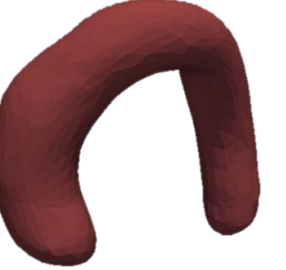
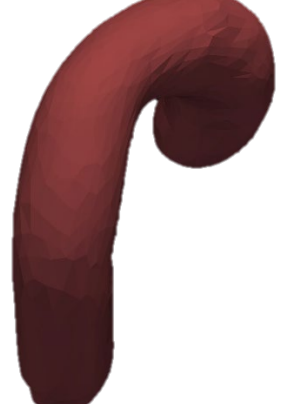
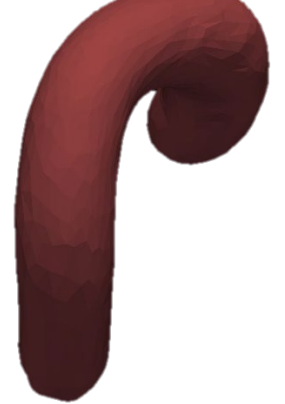
### 4.4.1 Spearman's Rank Correlation Coefficient

*Table 15. The significant shape modes associated with the presence of PH are based on their Spearman's Rank Correlation Coefficient and Spearman's Rank Correlation Coefficient P-value.*

<b>Shape Mode No.</b>	<b>Spearman's Rank Correlation Coefficient</b>	<b>Spearman's Rank Correlation Coefficient P-Value</b>
20	-0.3774	0.0008
22	0.3807	0.0008

With the same criteria but applied to the aorta dataset, as explained in 4.2.1, Table 15 shows that significant PCA shape modes found were shape Mode 20 and 22, neither being members of the shape modes, containing 90% of the data. Hence, confirming the decision does not dimensionally reduce the analysis to those shape modes. Mode 20 elicits a negative correlation, and Mode 22 a positive correlation, both with approximately the same statistical significance. Mode 22 indicates a marginally greater correlation to detect PH than Mode 20, both with the same consistency, given the P-values. The shape modes can be visualised in Table 16 and Table 17.

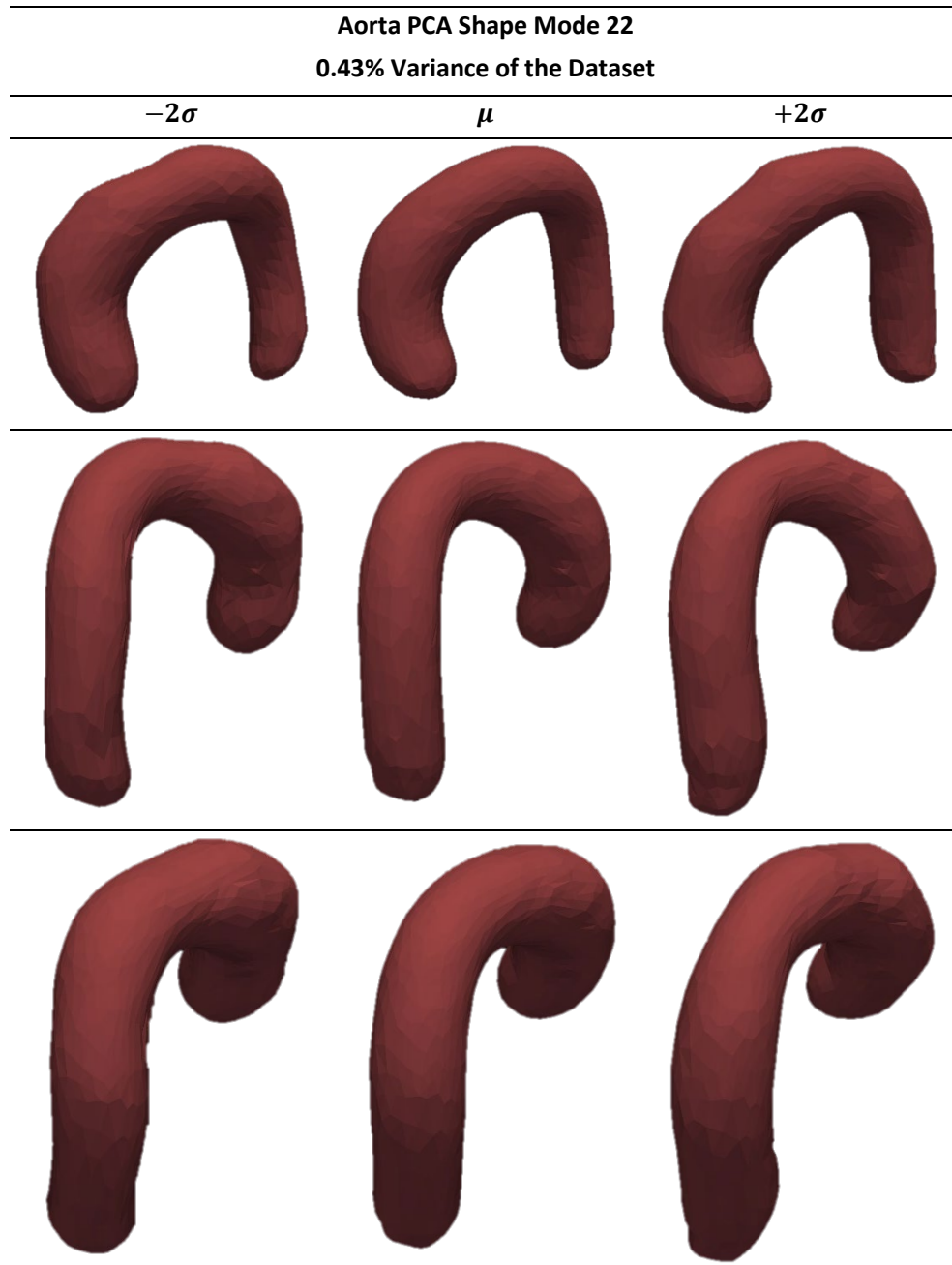
*Table 16. Visualisation of PCA Shape Mode 20 for the aorta and its variation across  $\pm 2\sigma$  and its Variance of the Dataset.*

Aorta PCA Shape Mode 20		
0.47% Variance of the Dataset		
$-2\sigma$	$\mu$	$+2\sigma$
		
		
		

As seen in Table 16, PCA Shape Mode 20's variation seems to be greater curvature in the arch of the aorta, in the "out of page" dimension for the first row of surface meshes. The extent of the curvature can best be seen in the third row, viewing from the "top". It is clear to see that the variation is very minimal between the standard deviations, which aligns with the small variance within the dataset it represents.  $-2\sigma$  seems to

indicate less curvature and  $+2\sigma$  more; therefore, less curvature would be indicative of the presence of PH, given the negative correlation.

*Table 17. Visualisation of PCA Shape Mode 22 for the aorta and its variation across  $\pm 2\sigma$  and its Variance of the Dataset.*



As seen in Table 17, PCA Shape Mode 22's variation seems to be a shrinkage across the top of the arch of the aorta. It is clear to see that the variation is very minimal between the standard deviations, which aligns with the small variance within the dataset it represents.  $-2\sigma$  seems to indicate greater shrinkage and  $+2\sigma$  less; therefore, less shrinkage would be indicative of the presence of PH, given the positive correlation.

For both modes, the variation is very minimal. Thus, the credibility of these modes as being associated with the presence of PH is already questionable. This is because it is difficult to comprehend that such small variations can relate to the presence of PH. The small variations relate to a large range of shape mode amounts, indicating how sensitive the shape mode quantity is to incremental variations. Thus, it is more likely that if any of the modes come out as credible classifiers for PH, it is a coincidental outcome.

#### 4.4.2 Receiver Operating Characteristic (ROC) Curve

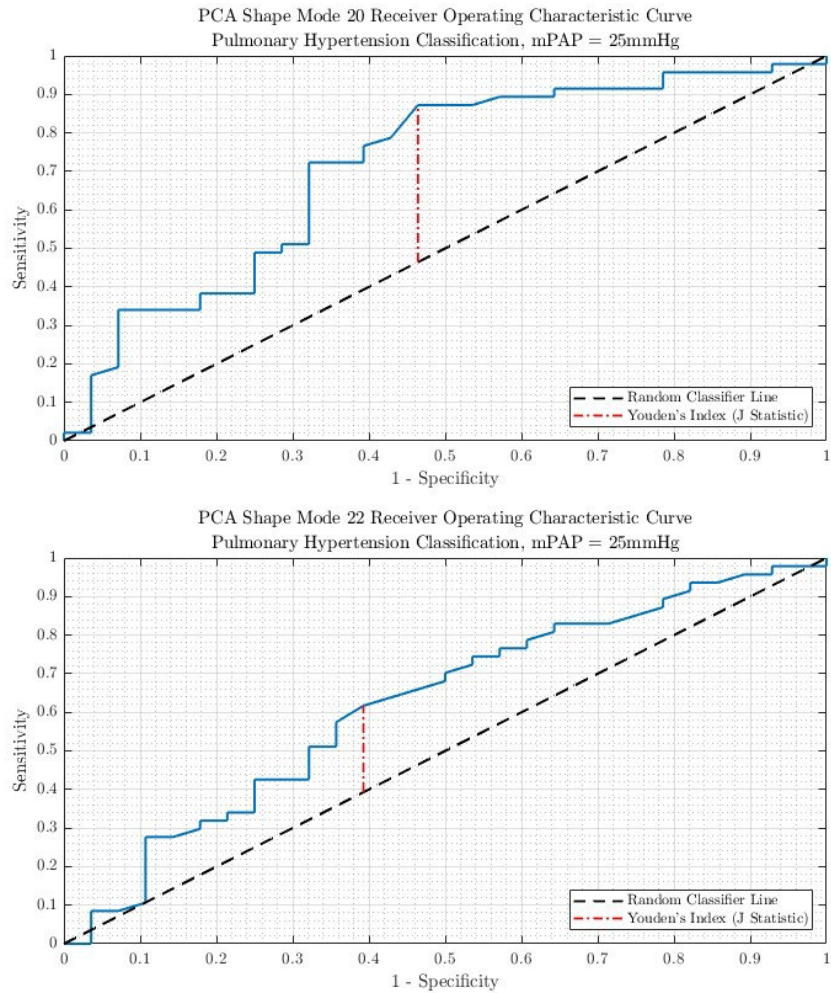
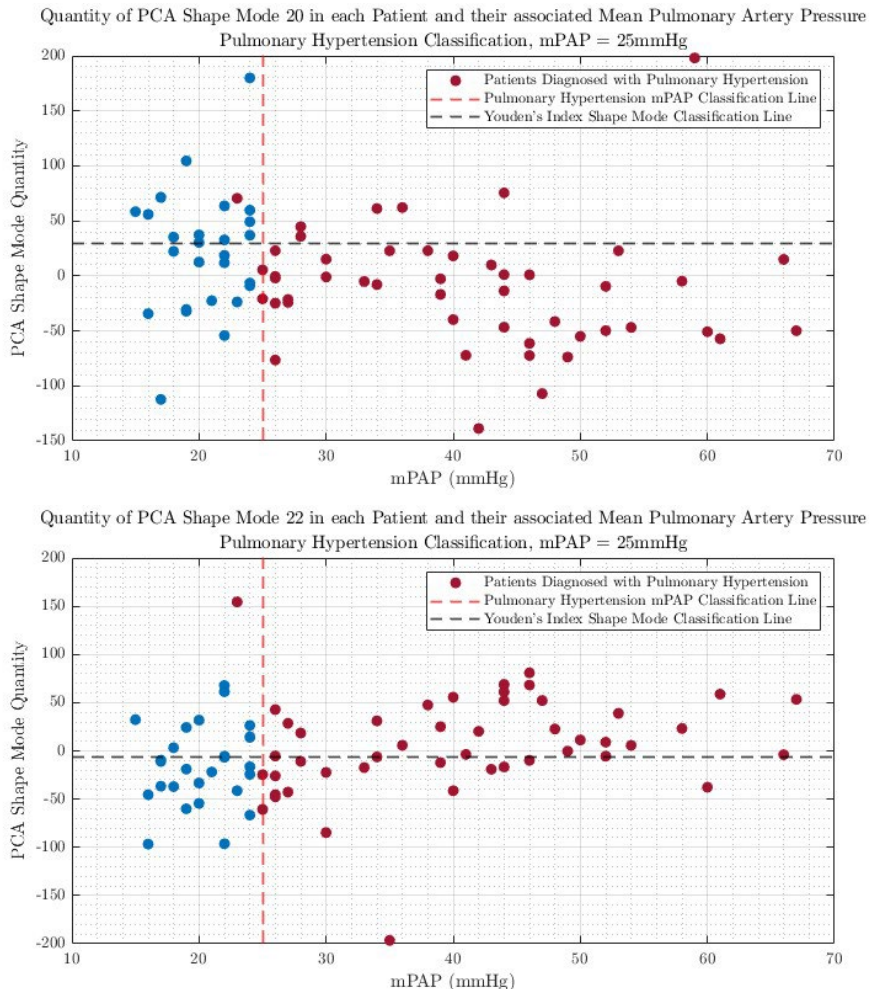


Figure 39. ROC curves for PCA Shape Modes 20 (top) and 22 (bottom) and their representative Youden Index Values, the red dashed line. The black dashed line is the random classifier line.

The ROC curve for Mode 20, as shown in Figure 39, rises steeply above the random classifier line at higher levels of specificity, indicating relatively good performance. Whereas the ROC curve for Mode 22, rises less prominently above the random classifier line to Mode 20. The Youden's Index for both modes, the dashed red line, is marked at a balanced point between sensitivity and specificity, with Mode 20 exhibiting slightly better balance. Mode 20 shows a steeper initial ascent, indicating better sensitivity at low false-positive rates. In contrast, the ROC curve for Mode 22 is more gradual, indicating a lesser ability to distinguish true positives from false positives at lower false-positive rates. Graphical indications of Youden's Index classification threshold are shown for each shape mode in Figure 40.



*Figure 40. The quantity of PCA Shape Modes 20 (top) and 22 (bottom) in each subject within the dataset was plotted against each subject's associated mPAP. The red dashed is the mPAP definition for PH and the black dashed line is the shape mode quantity threshold for classifying PH, defined by Youden's Index.*

*Table 18. The AUCROC values for PCA Shape Modes 20 and 22. And the classification success rate of the shapen modes at the Youden's Index threshold.*

PCA Shape Mode No.	AUCROC Value	Youden's Index Classification Rate
20	0.711	73.33%
22	0.621	61.33%

As seen in Table 18, Mode 20 has a higher AUCROC than Mode 22, indicating a better overall performance in distinguishing between the classes. Mode 20 demonstrates acceptable discriminatory power, with Mode 22 performing worse with poor discriminative power (Zweig and Campbell, 1993). Mode 20 also displays a much better

classification rate than Mode 22 at this threshold, indicating Mode 20 would perform better in real-world classification scenarios. Initially, this seems surprising given their relatively similar correlation magnitudes, however, Mode 20's correlation coefficient would be much greater if it was not for the presence of a very large outlier, as seen in Figure 38 at approximately  $mPAP = 60\text{mmHg}$ . Mode 22's poor performance, can be attributed to its lack of correlation, which can be seen by the fairly flat spread across the range of  $mPAP$  values in Figure 40. Mode 20 captures more variance related to the ability to distinguish patients diagnosed with PH.

#### 4.4.3 Precision-Recall Curve (PRC)

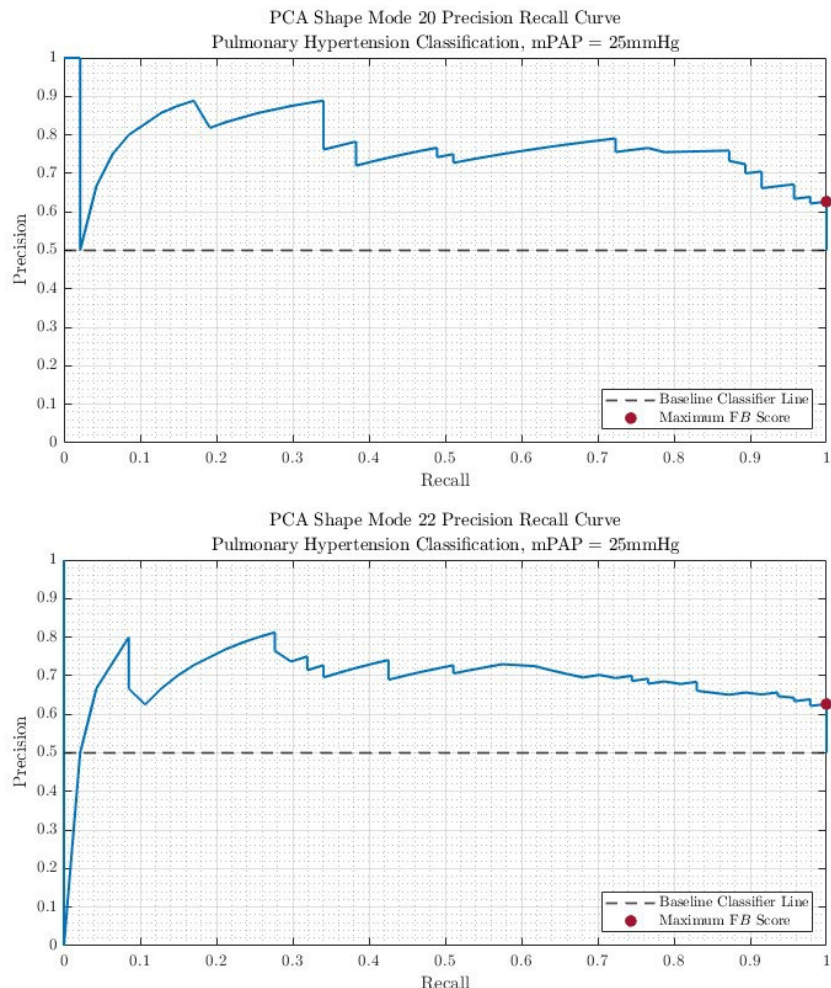
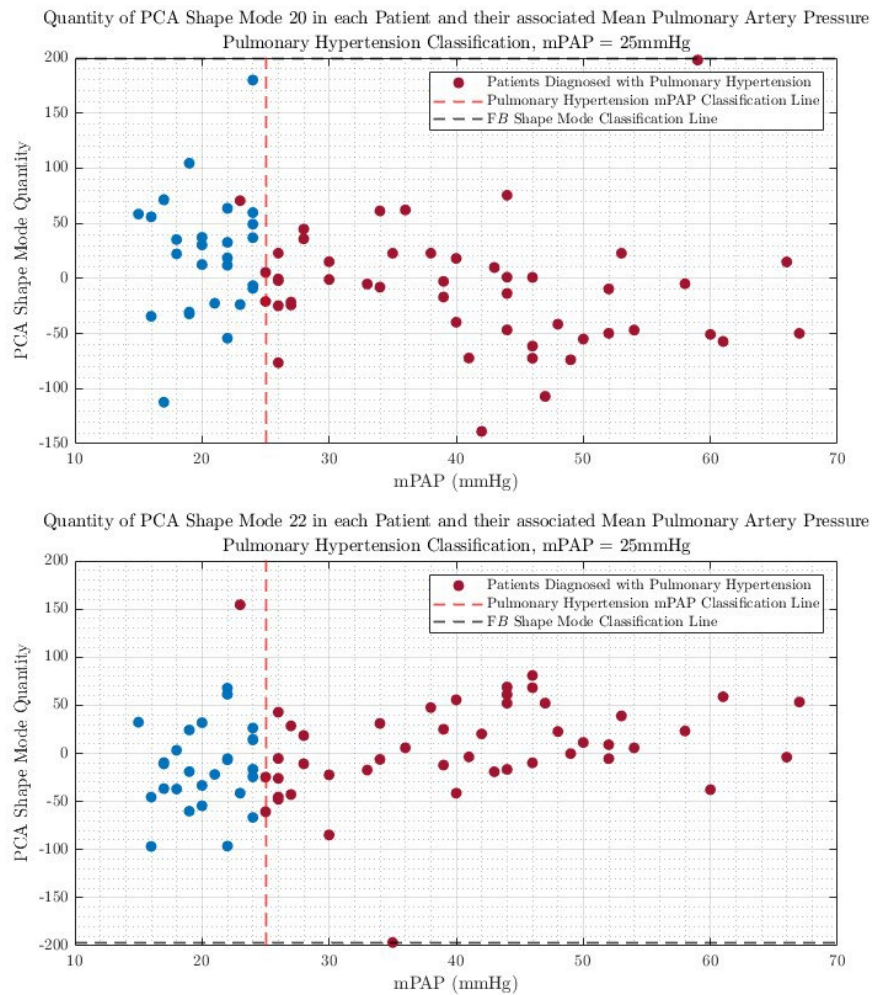


Figure 41. PRC curves for PCA Shape Modes 20 (top) and 22 (bottom) and their representative Maximum  $F\beta$  Score, the red dot. The black dashed line is the baseline classifier line.

Analysing Figure 41, similarly to in 4.2.3, Mode 20's precision takes a sharp decline at initial recall values before steeply rising at slightly higher recall values. From then on, the precision gradually declines for the remaining recall values. Mode 22's PRC acts in a very similar manner but takes an even sharper decline initially. These characteristics represent weak performance, across the range of recall values. Both modes exhibit inconsistent trade-offs between precision and recall across different thresholds. Graphical indications of the  $F\beta$  Score classification threshold can be seen for each mode in Figure 42.



*Figure 42. The quantity of PCA Shape Modes 20 (top) and 22 (bottom) in each subject within the dataset was plotted against each subject's associated mPAP. The red dashed is the mPAP definition for PH, and the black dashed line is the shape mode quantity threshold for classifying PH, defined by the Maximum  $F\beta$  Score.*

*Table 19. The AUCROC values for PCA Shape Modes 20 and 22. The classification success rate of the shapen modes at the Maximum F $\beta$  Score threshold.*

PCA Shape Mode No.	AUC – PRC Value	F $\beta$ Score Classification Rate
20	0.772	62.67%
22	0.621	62.67%

Mode 20 has a much higher AUC – PRC value compared to Mode 22, as seen in Table 19. Mode 20, therefore, can be interpreted as having a better overall performance in terms of maintaining high precision across various recall levels, with a good performance level in general (Saito and Rehmsmeier, 2015). F $\beta$  Scores sensitivity to outliers is alluded to in 4.2.3, and Figure 42 shows that both F $\beta$  Score classification thresholds have been severely influenced by outliers, making reviewing the classification rates redundant. The presence of the outliers is also the likely cause of the strange sharp initial declines in precision for both modes, shown in Figure 41.

Mode 20's good AUC—PRC values compared to Mode 22's indicate that the mode possesses stronger discriminative behaviour related to classifying patients with PH. Moreover, the slightly higher AUC—PRC value for Mode 20 compared to the AUCROC value suggests that the model's ability to maintain high precision at various recall levels is marginally better than its overall discriminative ability.

#### 4.4.4 Defined PH Classification Threshold

Similarly to 4.2.4 the defined classification thresholds for each mode was set as a compromise between the Youden's Index and  $F\beta$  Score classification thresholds. The defined classification thresholds can be visualised for each mode in Figure 43.

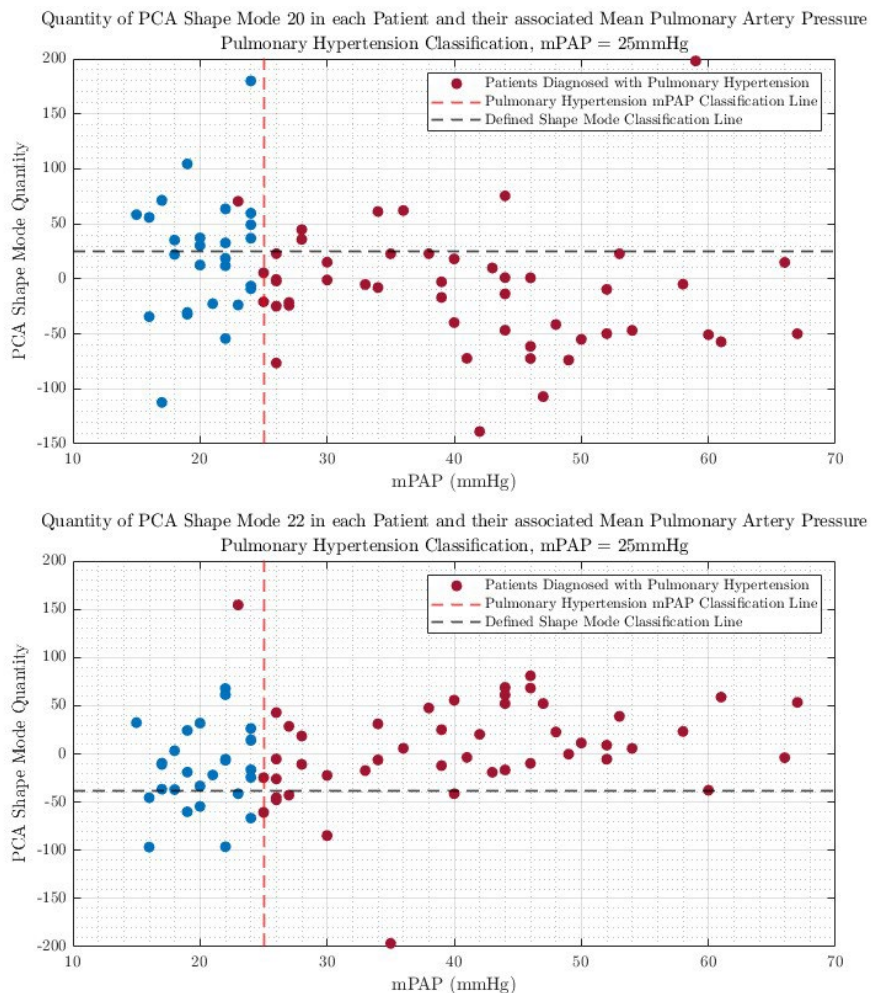


*Figure 43. The quantity of PCA Shape Modes 20 (top) and 22 (bottom) in each subject within the dataset was plotted against each subject's associated mPAP. The red dashed is the mPAP definition for PH and the black dashed line is the shape mode quantity threshold for classifying PH, defined by the optimal value at a compromise between the two thresholds.*

*Table 20. The sensitivity, specificity, and classification success rate of the shape modes at the defined optimal threshold for PCA Shape Modes 20 and 22.*

PCA Shape Mode No.	Sensitivity	Specificity	Classification Rate
20	0.872	0.536	73.33%
22	0.851	0.250	62.67%

The performance metrics for each mode can be seen in Table 20 and show that Mode 20 has a slightly higher sensitivity but much greater specificity compared to Mode 22. This means Mode 20 is better at detecting PH patients and healthy patients than Mode 22. Mode 20 also has a much greater classification rate than Shape Mode 22, likely accounting for its much better correlation if the outlier was to be removed and much better specificity. Moreover, the metrics validated the location of the thresholds, as the classification rates did not decrease while improving specificity for Mode 20 and sensitivity for Mode 22. Mode 20's balanced threshold makes it a reasonable choice for classification cases where it is crucial to identify PH patients due to its high sensitivity whilst retaining a fair, true negative classification rate due to its acceptable specificity. However, Mode 22 will be removed from consideration as a viable shape mode relating to the presence of PH, due to its poor performance metrics.

## 4.5 Validation

This section will discuss the results governing the unseen data validation of the significant shape modes to be used as a diagnosis strategy for PH.

### 4.5.1 Main Pulmonary Artery (MPA)

*Table 21. The unseen data validation study performance metrics for each significant shape mode related to the main pulmonary artery.*

Shape Mode No.	Sensitivity	Specificity	Classification Rate
PCA 1	0.90	0.50	78.57%
PCA 6	0.90	0.25	71.43%
PLS 1	0.80	0.50	71.43%

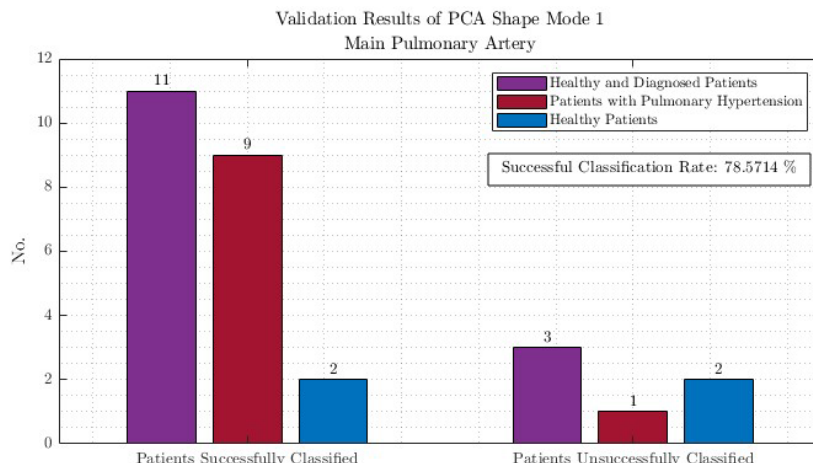


*Figure 44. Bar chart of PCA Shape Mode 1's unseen data validation study results and its successful classification rate. Successful classifications are on the left, and incorrect classifications are on the right. The chart also shows the split of healthy patients to patients with PH.*

PCA Shape Mode 1 achieved greater sensitivity and classification rates, but slightly lower specificity in the unseen data validation study, as seen in Table 21 and Table 9. Since the values are not drastically different, it is logical to conclude that the predicted sensitivity, specificity, and classification rate of the model from the training data are accurate. However, the 0.1 difference in specificity could suggest that the model is slightly overfitted in this aspect. The similarity to the predicted values also indicates that the model generalises well to unseen data and is well-calibrated.

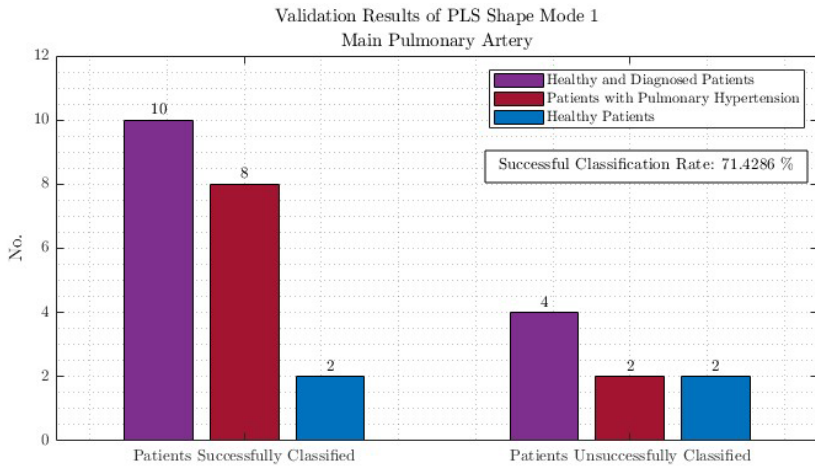


*Figure 45. Bar chart of PLS Shape Mode 1's unseen data validation study results and its successful classification rate. Successful classifications are on the left, and incorrect classifications are on the right. The chart also shows the split of healthy patients to patients with PH.*

PLS Shape Mode 1 achieved similar sensitivity and classification rates, with much greater specificity in the unseen data validation study, as displayed in Table 21 and Table 14. Thus, the lack of significantly worse metrics indicates that the performance metrics attained from the training data are accurate and valid. Moreover, it suggests the model is void of any overfitting, high variance, underfitting, or high bias. The similarity to the predicted values, also indicates that the model generalises well to unseen data and is well-calibrated.

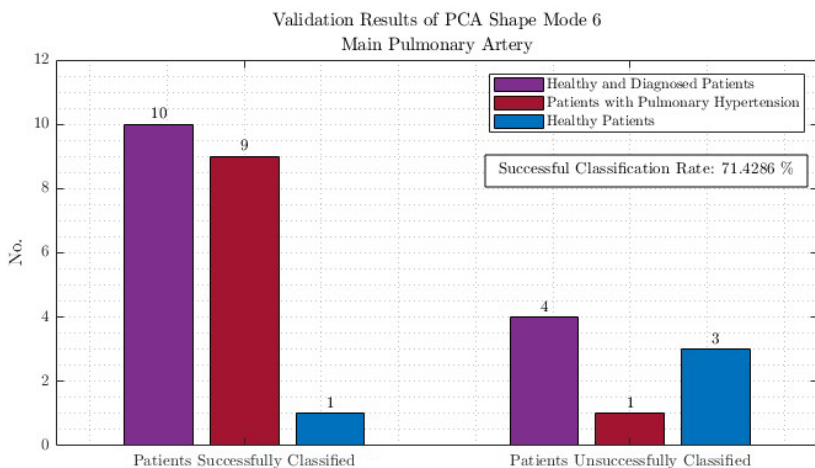


*Figure 46. Bar chart of PCA Shape Mode 6's unseen data validation study results and its successful classification rate. Successful classifications are on the left, and incorrect classifications are on the right. The chart also shows the split of healthy patients to patients with PH.*

PCA Shape Mode 6 achieved similar metrics in sensitivity, specificity and classification rate in the unseen data validation study, as shown in Table 21 and Table 9. Given the similarity, it is logical to conclude that the predicted sensitivity, specificity, and classification rate of the model from the training data are accurate and void of overfitting and underfitting. The similarity to the predicted values also indicates that the model generalises well to unseen data and is well-calibrated.

#### 4.5.2 Aorta

*Table 22. The unseen data validation study performance metrics for each significant shape mode related to the aorta.*

Shape Mode No.	Sensitivity	Specificity	Classification Rate
PCA 20	0.60	0.83	68.75%

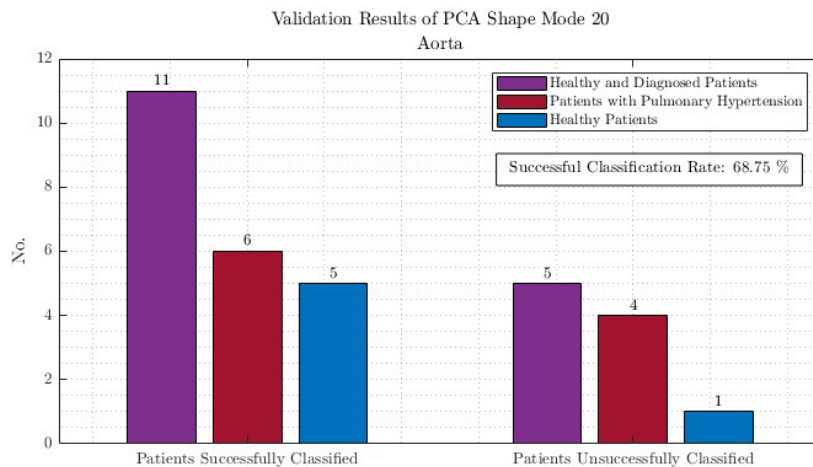


*Figure 47. Bar chart of PCA Shape Mode 20's unseen data validation study results and its successful classification rate. Successful classifications are on the left, and incorrect classifications are on the right. The chart also shows the split of healthy patients to patients with PH.*

PCA Shape Mode 20 achieved considerably less sensitivity and much greater specificity despite the similar classification rate, as seen in Table 22 and Table 20, in the unseen data validation study. Given that the specificity and sensitivity are demonstrating extensive differences, it is reasonable to suggest that the model produced is invalid, due to these inconsistencies. This means both significant shape modes from the clinical aorta datasets have become invalid, confirming the theory in 4.4.1. Interpreting this, one would conclude that shape variation within the aorta anatomy has no correlation to the presence of PH, especially considering that the PLS regression also found significant modes in its supervised learning statistical model.

## 4.6 Current Diagnostic Methods Performance

This section will detail the results governing the comparison between current diagnostic strategy performance metrics and the defined classification threshold performance metrics for the remaining significant shape modes. Correlative graphs and the performance metrics for Pulmonary Artery Artery Ratio (PAA) and Pulmonary Vascular Resistance (PVR) will be investigated. The performance metrics were obtained through effective ROC curves and PRC, which can be found in Appendix 9.14 and 9.15 for PVR and PAA, respectively. The data used was from the same patients, as in the clinical datasets, to ensure consistency, but PAA was in a smaller subsection due to data availability.

### 4.6.1 Pulmonary Artery to Aorta Ratio (PA:A)

Patients Pulmonary Artery : Aorta Diameters Ratio (PA:A) and their Mean Pulmonary Artery Pressure (mPAP)  
Pulmonary Hypertension Classification, mPAP = 25mmHg

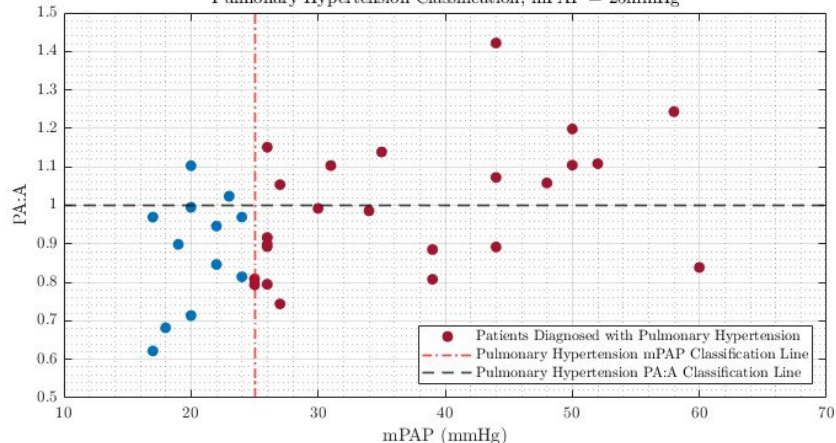


*Figure 48. The PA:A ratio for each subject within the dataset plotted against each subject's associated mPAP. The red dashed is the mPAP definition for PH, and the black dashed line is the PA:A current classification for a patient suspected of having PH, 1.*

*Table 23. The effective AUCROC and AUC – PRC and sensitivity and specificity for the PA:A classification threshold.*

AUCROC	AUC – PRC	Sensitivity	Specificity
0.668	0.830	0.458	0.833

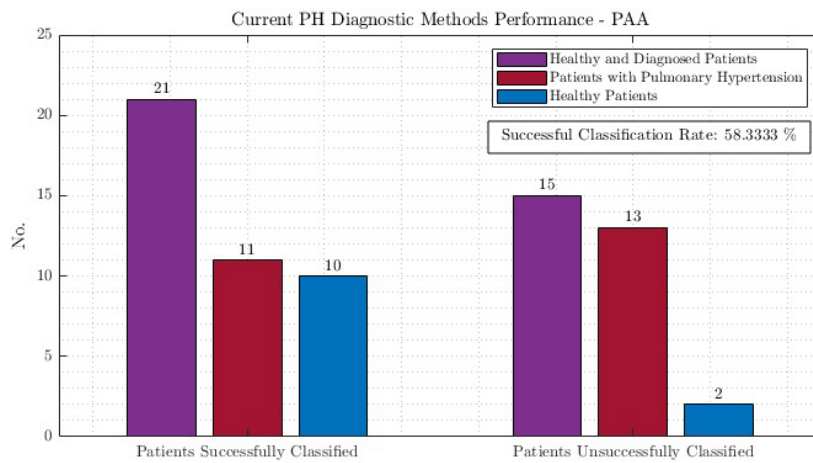


*Figure 49. Bar chart of PA:A's classification results and its successful classification rate. Successful classifications are on the left, and incorrect classifications are on the right. The chart also shows the split of healthy patients to patients with PH.*

The PAA metric generally elicits a much worse sensitivity and classification rate compared to the shape modes, but a much better specificity, as seen in Table 23. This would indicate that the use of PAA to identify patients suspected of having PH would, despite correctly classifying many healthy patients, classify a large proportion of patients with PH incorrectly. The AUCROC value is less than PCA and PLS Modes 1, but similar to PCA Mode 6, exhibiting poor discriminative behaviour. On the other hand, the AUC – PRC values are comparable to values obtained by the significant shape modes, indicating the classifier performs well in identifying the positive class, However, this is predominantly down to the lack of false positives, as seen in Figure 48, and I would theorise that it would be worse for a larger dataset. Overall, the shape mode classifiers perform better than PAA as a classifier, especially considering the emphasis on reducing the number of false negatives so that as many people with PH are captured.

#### 4.6.2 Pulmonary Vascular Resistance (PVR)

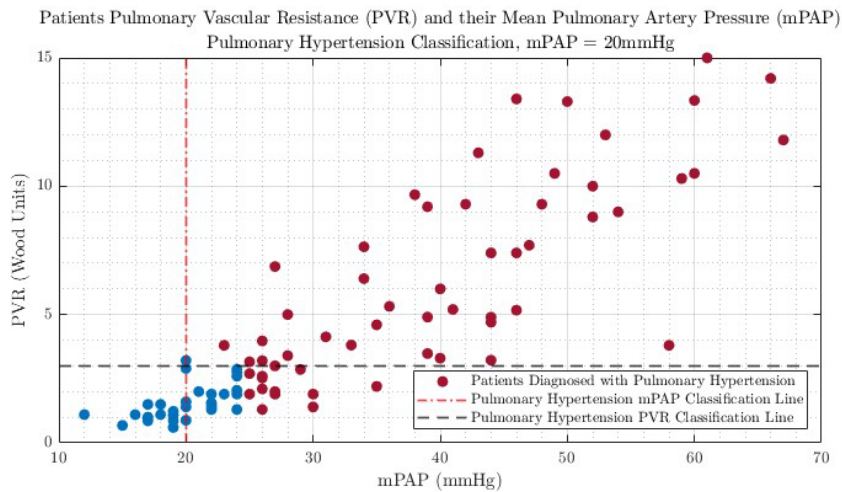


*Figure 50. The PVR quantity for each subject within the dataset was plotted against each subject's associated mPAP. The red dashed is the mPAP definition for PH and the black dashed line is the PVR current classification for a patient suspected of having PH, 3.*

*Table 24. The effective AUCROC and AUC – PRC and sensitivity and specificity for the PVR classification threshold.*

AUCROC	AUC – PRC	Sensitivity	Specificity
0.979	0.996	0.605	1.000

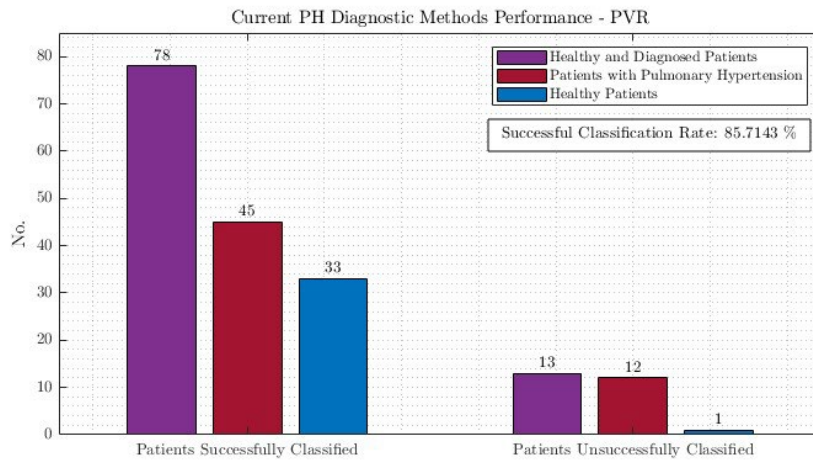


*Figure 51. Bar chart of PVR's classification results and its successful classification rate. Successful classifications are on the left, and incorrect classifications are on the right. The chart also shows the split of healthy patients to patients with PH.*

The PVR metric produces much better specificity and classification rate, but a much worse sensitivity compared to the shape modes, as seen in Table 24. Although, the classification rate is higher than the shape mode classifiers, almost all the incorrect classifications were patients with PH. Thus, this suggests that despite being an excellent general classifier, the PVR metric is worse than the shape mode classifiers at classifying patients with PH. The AUCROC and AUC-PRC values are both extensively better than the shape mode classifiers, affirming the fact that the PVR metric is a convincing overall classifier, especially for healthy patients with exceptional discriminative behaviour. Overall, the shape mode classifiers are better at classifying patients with PH. However, PVR is a better overall classifier and confirms why it is being added to the clinical definition of PH. However, there are flaws in the PVR metric, which potentially could be alleviated by combining it with one of the shape mode classifiers.

#### 4.7 Comparing New & Old PH Definitions

This section will detail the results governing the comparison between the proposed new PH definition and the current PH definition to see if the shape mode classifiers offer a stable classifying solution by also being able to perform at the new definition. It was assumed that all patients with an mPAP  $\geq 20\text{mmHg}$  now had PH. All the ROC curves and PRC used to determine the performance characteristics at PH definition, mPAP = 20mmHg, are displayed in the Appendix's 9.10, 9.11 and 9.12.

*Table 25. The performance characteristics at the new PH definition of mPAP = 20mmHg for the remaining dominant shape modes, with an association with the presence of PH,*

Shape Mode		Classification			
No.	AUCROC	AUC – PRC	Sensitivity	Specificity	Rate
MPA PCA 1	0.720	0.939	0.661	0.700	66.67%
MPA PCA 6	0.671	0.929	0.881	0.200	78.26%
MPA PLS 1	0.740	0.942	0.814	0.500	76.81%

Firstly, comparing the AUCROC values, it can be seen from the values in Table 25 that all the AUCROC values remained similar to their mPAP = 25mmHg counterparts, varying minutely. Therefore, PCA Mode 6 maintained poor discriminative behaviour, and PCA and PLS Modes 1 remained acceptable. They likely remain similar, as analysing Figure 33 and Figure 38, the number of subjects below and above the shape mode quantity classification threshold between mPAP = 20mmHg and 25mmHg is relatively similar. Therefore, the same numbers are being added to the true positives and false negatives. Thus, the true positive rate and sensitivity remain similar. Now, reviewing the AUC – PRC values, each shape mode classifier increased for the new PH definition, suggesting that the shape mode classifier models not only perform better but also excellently at distinguishing the positive class. This indicates that classifiers can greatly reduce the number of patients with PH missed at the new PH definition compared to the old one. This could be attributed to the fact that the number of true positives is dominant in the calculation for AUC – PRC, and by shifting the PH definition, automatically, more true positives are formed, thus increasing the AUC – PRC values.

For PCA Mode 1, the classification rate and sensitivity decrease, with sensitivity reducing more prominently. However, specificity has increased prominently. Consequently, the mode now elicits a more balanced classification performance, although its ability to classify patients with PH correctly has diminished. This is because, as seen in Figure 33, there is a marginally greater number of false negatives produced compared to the number of true positives made by moving the mPAP classification line. With PCA Mode 6, the classification rate increases massively despite both its sensitivity and specificity decreasing. This indicates that the increase in classification success is not representative of the model's performance improving at the new PH definition but indicative of the majority of subjects between mPAP = 20mmHg and 25mmHg being false positives originally and now true positives at the new PH definition. Finally, PLS Mode 1 displays a much greater classification percentage and specificity, with a very marginal decrease in sensitivity at the new PH definition. This suggests the mode is

stable and now has a more balanced classification performance, with no significant reduction in the ability to classify patients with PH. This is likely a result of the fact that there is a greater number of false positives than true negatives between the PH definitions, as seen in Figure 38.

Overall, it appears that at the new PH definition, the PLS Shape Mode 1 performed better than the current PH definition, exhibiting a more balanced classifying model. Whereas the PCA shape modes tended to perform worse or less stably. The fact that the PLS mode was derived from a supervised learning analysis involving the mPAP data, may have played a contributing factor in this outcome. It also, potentially suggests that the PCA shape modes may be slightly overfitted towards the current PH definition.

## 5 Discussion

### 5.1 Project Evaluation

The aim of this study was to assess the feasibility of SSM as a methodology to detect PH. The results indicate that the methodology has great potential to act as a classifier for PH. However, further refinement of the method or combination with other metrics is required. This is because, although the results achieved for the shape mode classifiers were deemed valid and acceptable, with relatively good performance characteristics, this was treating them as general binary classifiers. However, the study is for a medical application; therefore, to be accepted at the industry level, the requirements to be met are extensively stricter. Acceptable binary classifiers in medical applications tend to require sensitivity and specificity levels greater than 0.9 in combination with AUCROC values greater than 0.7, which this study has not met (Akobeng, 2007). AUC – PRC and classification rate required values tend to be more based on the specific disease in the study, and whether reducing false positives or false negatives is more critical. Despite no studies being undertaken on this specific topic, similar studies related to disease classification, like Susinesiaputra et al.'s achieved results of AUCROC = 0.996, sensitivity = 0.97, specificity = 0.99 and accuracy = 0.98 for myocardial infarct classification, demonstrating the typical results required to be achieved (Suinesiaputra et al., 2018).

PLS Shape Mode 1 classifier at the new PH classification was closest to meeting the criteria, although still considerably under the requirements, with an AUCROC = 0.74, AUC – PRC = 0.942, sensitivity = 0.814, specificity = 0.5 and classification accuracy = 0.77. Given previous studies' successful results, it is conclusive to suggest that the SSM framework performed worse than expected. However, I believe this is largely due to a fundamental flaw in the data used, rather than with the SSM methodology. This is the fact that the dataset utilised was heavily biased towards patients with PH, as can be seen from the scatter graph figures, as it came from a hospital, whose data is more representative of an unhealthy population. This became further emphasised when the new PH definition was used, as there were even fewer healthy patients in the dataset. As a result, the mean estimated templates derived from the atlases were of a shape with moderate to severe PH, rather than of a shape which represented the global mean population. This, I theorise, skewed the results, resulting in very poor specificity across all the shape mode classifiers, as it influenced the model's ability to detect healthy patients. If repeated with a balanced dataset, I believe the feasibility results of SSM to detect PH would be extremely positive.

## 5.2 Project Uncertainty

The bias within the clinical dataset was not the only uncertainty which affected the results of the study, another being the fact that general shape variability due to height, gender, weight and age, among other factors, was not considered, as the data was not scaled accordingly. The bias in the dataset also, meant there was developed uncertainty in the ROC and classification rates, making them potentially misleading, as they are sensitive to imbalanced datasets (Muschelli, 2020). Additionally, the manual alignment of the data was extremely likely to not be perfect, and therefore, some rotation and positional variability was likely captured in the atlases as part of the shape variability. This causes greater uncertainty, considering the study attempts to focus purely on anatomical shape variation. Furthermore, given that the clinical data came from CT scans, which are layered 3mm thick, hence the “steps” in the mesh generated, as seen in 3.1.2, it is likely that shape features may have been lost. Moreover, these meshes required smoothing, which likely further removed potential feature variability. Another uncertainty is the size of the dataset. Although 95 subjects are greater than other studies on PH, a dataset larger than 1000, like in other successful studies, would produce more reproducible results. Finally, there would have been general associative uncertainties related to the statistical approaches and shape reconstructure within Deformetrica. All of these were considered when analysing the results.

## 5.3 Project Limitations

There are a few limitations which this particular methodology for the study faced, one of which is the relatively small biased dataset discussed previously, which risks the model potentially overfitting. The manual alignment and atlas construction were incredibly time-consuming, with atlas constructions requiring the computer to perform deformations for over 13 hours for a single atlas. Additionally, time constraints meant that atlas parameter optimisation was limited. Therefore, the accuracy of the atlas was visually judged rather than analytically and using a combination of shape modes or shape mode and other metrics could not be explored. Furthermore, if a larger dataset was used, either a very powerful computer would be required, or the dataset meshes would require decimation, where potential shape features would be lost. Also, given the complex nature of PH diagnosis, mPAP is not the only indicator, hence why an attempt was made to use the whole capillary network to incorporate the PVR. However, this was too computationally intensive to create a robust atlas. At the level of decimation required for the model to run, discreet shape features were all but removed.

## 6 Future Directions

If there was more time available, as indicated previously, an atlas parameterisation study would have been undertaken to determine the optimal parameters, plus an analytical approach developed for reviewing the outputs from the atlas construction. Additionally, an algorithm would have been developed to automate the alignment and scaling of the dataset so that no rotation and positional elements were present in the shape variability. As well as a study to determine the optimal Laplacian and Taubin parameters to minimise any potential feature loss. A couple of future directions related to the findings from the study are to repeat the study on a larger balanced dataset for the pulmonary artery, as previously alluded to, and the pulmonary arteries' individual branches, given the shape variability found specifically on one or the other branch. Finally, I would repeat the study but use the shape modes capturing 90% of the dataset shape variance, firstly to increase the dataset size if necessary, but more importantly to combine different modes together and see if they possess any associative qualities to PH, as done in previous literature for other similar applications.

## 7 Conclusion

The investigation into the feasibility of using SSM to detect PH has demonstrated significant potential for improving the diagnostic process for this complex condition. By developing and validating SSMs based on the geometric variations of the pulmonary artery and aorta, the study has highlighted the ability of SSM to capture critical shape features associated with PH.

Key findings from the study include the identification of specific shape modes within the pulmonary artery that correlate with the presence of PH. Notably, PCA Shape Mode 1 and PLS Shape Mode 1 accounted for 24% and 29% of the shape variability in the dataset, respectively. PCA Mode 1 demonstrated a moderate negative correlation with mPAP, and PLS Mode 1 displayed a strong positive correlation, both suggesting that an enlarged pulmonary artery diameter is indicative of PH.

The application of ROC and PRC provided valuable insights into the diagnostic performance of these shape modes. PCA Mode 1 and PLS Mode 1 attained AUCROC values of 0.718 and 0.734, respectively, exhibiting acceptable discriminative power, while their Precision-Recall curves indicated robust performance in maintaining high precision across various recall levels. These metrics underscore the model's capability to relatively accurately classify patients with PH, with sensitivities of 0.744 and 0.837, but also their inability to consistently classify healthy patients correctly, with specificities of 0.615 and 0.346.

The significant shape mode classifiers were validated in an unseen data study, of which three were valid. The classifiers' performance was also compared against current PH diagnostic strategies and their performance at a PH definition of mPAP = 20mmHg. The classifiers performed better against the PA:A metric but worse against the PVR. Furthermore, at the new PH definition, the significant PCA mode's performance diminished, while the PLS mode's performance improved.

In conclusion, the research has successfully demonstrated that SSM has the potential feasibility to serve as a reliable and efficient tool for detecting PH. However, more refinement is required, like the use of a balanced dataset in the model. By leveraging the geometric variations in medical imaging data, this approach offers a promising avenue for reducing diagnostic intervals and improving the accuracy of PH diagnoses.

## 8 Bibliography

- 3D Slicer, n.d.
- Abdi, H., Williams, L.J., 2010. Principal component analysis. *WIREs Comput. Stat.* 2, 433–459. <https://doi.org/10.1002/wics.101>
- Addetia, K., Maffessanti, F., Yamat, M., Weinert, L., Narang, A., Freed, B.H., Mor-Avi, V., Lang, R.M., 2016. Three-dimensional echocardiography-based analysis of right ventricular shape in pulmonary arterial hypertension. *Eur. Heart J. Cardiovasc. Imaging* 17, 564–575. <https://doi.org/10.1093/ehjci/jev171>
- Agyei-Ntim, F., n.d. Statistical Shape Modeling of the Right Ventricle in Pediatric Pulmonary Hypertension (Ph.D.). University of Colorado at Denver, United States -- Colorado.
- Akobeng, A.K., 2007. Understanding diagnostic tests 1: sensitivity, specificity and predictive values. *Acta Paediatr.* 96, 338–341. <https://doi.org/10.1111/j.1651-2227.2006.00180.x>
- Akoglu, H., 2018. User's guide to correlation coefficients. *Turk. J. Emerg. Med.* 18, 91–93. <https://doi.org/10.1016/j.tjem.2018.08.001>
- Ambellan, F., Lamecker, H., von Tycowicz, C., Zachow, S., 2019. Statistical Shape Models: Understanding and Mastering Variation in Anatomy, in: Rea, P.M. (Ed.), *Biomedical Visualisation : Volume 3*. Springer International Publishing, Cham, pp. 67–84. [https://doi.org/10.1007/978-3-030-19385-0\\_5](https://doi.org/10.1007/978-3-030-19385-0_5)
- Beg, M.F., Miller, M.I., Trouvé, A., Younes, L., 2005. Computing Large Deformation Metric Mappings via Geodesic Flows of Diffeomorphisms. *Int. J. Comput. Vis.* 61, 139–157. <https://doi.org/10.1023/B:VISI.0000043755.93987.aa>
- bhf-cvd-statistics-uk-factsheet.pdf, n.d.
- Biglino, G., Capelli, C., Bruse, J., Bosi, G.M., Taylor, A.M., Schievano, S., 2017. Computational modelling for congenital heart disease: how far are we from clinical translation? *Heart* 103, 98–103. <https://doi.org/10.1136/heartjnl-2016-310423>
- Bonaretti, S., n.d. STATISTICAL SHAPE MODELS (SSM).
- Bône, A., Louis, M., Martin, B., Durrleman, S., 2018. Deformetrica 4: An Open-Source Software for Statistical Shape Analysis, in: Reuter, M., Wachinger, C., Lombaert, H., Paniagua, B., Lüthi, M., Egger, B. (Eds.), *Shape in Medical Imaging*. Springer International Publishing, Cham, pp. 3–13. [https://doi.org/10.1007/978-3-030-04747-4\\_1](https://doi.org/10.1007/978-3-030-04747-4_1)
- Bruse, J.L., 2017. Shape and function in congenital heart disease: a translational study using image, statistical and computational analyses (Doctoral). Dr. Thesis UCL Univ. Coll. Lond. Presented at the University College London, UCL (University College London).
- Bruse, J.L., McLeod, K., Biglino, G., Ntsinjana, H.N., Capelli, C., Hsia, T.-Y., Sermesant, M., Pennec, X., Taylor, A.M., Schievano, S., Taylor, A., Giardini, A., Khambadkone, S., Schievano, S., de Leval, M., Hsia, T.Y., Bove, E., Dorfman, A., Baker, G.H., Hlavacek, A., Migliavacca, F., Pennati, G., Dubini, G., Marsden, A., Feinstein, J., Vignon-Clementel, I., Figliola, R., McGregor, J., for the Modeling of Congenital Hearts Alliance (MOCHA) Collaborative Group, 2016. A statistical shape modelling framework to extract 3D shape biomarkers from medical imaging data: assessing arch morphology of repaired coarctation of the aorta. *BMC Med. Imaging* 16, 40. <https://doi.org/10.1186/s12880-016-0142-z>

- Cardiovascular diseases (CVDs) [WWW Document], n.d. URL [https://www.who.int/news-room/fact-sheets/detail/cardiovascular-diseases-\(cvds\)](https://www.who.int/news-room/fact-sheets/detail/cardiovascular-diseases-(cvds)) (accessed 5.6.24).
- Chin, W., Marcoulides, G., 1998. The Partial Least Squares Approach to Structural Equation Modeling. *Mod. Methods Bus. Res.* 8.
- Cootes, T.F., Taylor, C.J., Cooper, D.H., Graham, J., 1995. Active Shape Models-Their Training and Application. *Comput. Vis. Image Underst.* 61, 38–59. <https://doi.org/10.1006/cviu.1995.1004>
- Cosentino, F., Raffa, G.M., Gentile, G., Agnese, V., Bellavia, D., Pilato, M., Pasta, S., 2020. Statistical Shape Analysis of Ascending Thoracic Aortic Aneurysm: Correlation between Shape and Biomechanical Descriptors. *J. Pers. Med.* 10, 28. <https://doi.org/10.3390/jpm10020028>
- Cutugno, S., Ingrassia, T., Nigrelli, V., Pasta, S., 2021. On the Left Ventricular Remodeling of Patients with Stenotic Aortic Valve: A Statistical Shape Analysis. *Bioengineering* 8, 66. <https://doi.org/10.3390/bioengineering8050066>
- Da Fontoura Costa, L., Cesar Jr., R.M., 2010. Shape Analysis and Classification: Theory and Practice, 0 ed. CRC Press. <https://doi.org/10.1201/9781420037555>
- Dahdouh, S., Varsier, N., Serrurier, A., Plata, J.-P., Anquez, J., Angelini, E., Wiart, J., Bloch, I., 2014. A comprehensive tool for image-based generation of fetus and pregnant women mesh models for numerical dosimetry studies. *Phys. Med. Biol.* 59, 4583. <https://doi.org/10.1088/0031-9155/59/16/4583>
- Davies, R., Twining, C., Taylor, C., 2008. Statistical Models of Shape: Optimisation and Evaluation. Springer Science & Business Media.
- Davies, R.H., Cootes, T.F., Twining, C.J., Taylor, C.J., 2001. An Information Theoretic Approach to Statistical Shape Modelling, in: Proceedings of the British Machine Vision Conference 2001. Presented at the British Machine Vision Conference 2001, British Machine Vision Association, Manchester, p. 2.1-2.10. <https://doi.org/10.5244/C.15.2>
- Davis, J., Goadrich, M., 2006. The relationship between Precision-Recall and ROC curves, in: Proceedings of the 23rd International Conference on Machine Learning, ICML '06. Association for Computing Machinery, New York, NY, USA, pp. 233–240. <https://doi.org/10.1145/1143844.1143874>
- Dawes, T.J.W., de Marvao, A., Shi, W., Fletcher, T., Watson, G.M.J., Wharton, J., Rhodes, C.J., Howard, L.S.G.E., Gibbs, J.S.R., Rueckert, D., Cook, S.A., Wilkins, M.R., O'Regan, D.P., 2017. Machine Learning of Three-dimensional Right Ventricular Motion Enables Outcome Prediction in Pulmonary Hypertension: A Cardiac MR Imaging Study. *Radiology* 283, 381–390. <https://doi.org/10.1148/radiol.2016161315>
- Di Folco, M., Clarysse, P., Moceri, P., Duchateau, N., 2020. Learning Interactions Between Cardiac Shape and Deformation: Application to Pulmonary Hypertension, in: Pop, M., Sermesant, M., Camara, O., Zhuang, X., Li, S., Young, A., Mansi, T., Suinesiaputra, A. (Eds.), Lecture Notes in Computer Science. Springer International Publishing, Cham, pp. 119–127. [https://doi.org/10.1007/978-3-030-39074-7\\_13](https://doi.org/10.1007/978-3-030-39074-7_13)
- Dryden-Mardia-Slides-04.pdf, n.d.
- Durrleman, S., 2010. Statistical models of currents for measuring the variability of anatomical curves, surfaces and their evolution - TEL - Thèses en ligne [WWW Document]. URL <https://theses.hal.science/tel-00631382/> (accessed 5.9.24).
- Durrleman, S., Prastawa, M., Charon, N., Korenberg, J.R., Joshi, S., Gerig, G., Trouvé, A., 2014. Morphometry of anatomical shape complexes with dense

- deformations and sparse parameters. *NeuroImage* 101, 35–49. <https://doi.org/10.1016/j.neuroimage.2014.06.043>
- Fluss, R., Faraggi, D., Reiser, B., 2005. Estimation of the Youden Index and its associated cutoff point. *Biom. J. Biom. Z.* 47, 458–472. <https://doi.org/10.1002/bimj.200410135>
- Freed, B.H., Collins, J.D., François, C.J., Barker, A.J., Cuttica, M.J., Chesler, N.C., Markl, M., Shah, S.J., 2016. MR and CT Imaging for the Evaluation of Pulmonary Hypertension. *JACC Cardiovasc. Imaging* 9, 715–732. <https://doi.org/10.1016/j.jcmg.2015.12.015>
- Frost, A., Badesch, D., Gibbs, J.S.R., Gopalan, D., Khanna, D., Manes, A., Oudiz, R., Satoh, T., Torres, F., Torbicki, A., 2019. Diagnosis of pulmonary hypertension. *Eur. Respir. J.* 53. <https://doi.org/10.1183/13993003.01904-2018>
- Galie, N., Hoeper, M.M., Humbert, M., Torbicki, A., Vachiery, J.-L., Barbera, J.A., Beghetti, M., Corris, P., Gaine, S., Gibbs, J.S., Gomez-Sanchez, M.A., Jondeau, G., Klepetko, W., Opitz, C., Peacock, A., Rubin, L., Zellweger, M., Simonneau, G., ESC Committee for Practice Guidelines (CPG), Vahanian, A., Auricchio, A., Bax, J., Ceconi, C., Dean, V., Filippatos, G., Funck-Brentano, C., Hobbs, R., Kearney, P., McDonagh, T., McGregor, K., Popescu, B.A., Reiner, Z., Sechtem, U., Sirnes, P.A., Tendera, M., Vardas, P., Widimsky, P., Document Reviewers, Sechtem, U., Al Attar, N., Andreotti, F., Aschermann, M., Asteggiano, R., Benza, R., Berger, R., Bonnet, D., Delcroix, M., Howard, L., Kitsiou, A.N., Lang, I., Maggioni, A., Nielsen-Kudsk, J.E., Park, M., Perrone-Filardi, P., Price, S., Domenech, M.T.S., Vonk-Noordegraaf, A., Zamorano, J.L., 2009. Guidelines for the diagnosis and treatment of pulmonary hypertension: The Task Force for the Diagnosis and Treatment of Pulmonary Hypertension of the European Society of Cardiology (ESC) and the European Respiratory Society (ERS), endorsed by the International Society of Heart and Lung Transplantation (ISHLT). *Eur. Heart J.* 30, 2493–2537. <https://doi.org/10.1093/eurheartj/ehp297>
- Galiè, N., McLaughlin, V.V., Rubin, L.J., Simonneau, G., 2019. An overview of the 6th World Symposium on Pulmonary Hypertension. *Eur. Respir. J.* 53, 1802148. <https://doi.org/10.1183/13993003.02148-2018>
- Harris, M.D., Datar, M., Whitaker, R.T., Jurrus, E.R., Peters, C.L., Anderson, A.E., 2013. Statistical shape modeling of cam femoroacetabular impingement. *J. Orthop. Res.* 31, 1620–1626. <https://doi.org/10.1002/jor.22389>
- Heimann, T., Meinzer, H.-P., 2009. Statistical shape models for 3D medical image segmentation: a review. *Med. Image Anal.* 13, 543–563. <https://doi.org/10.1016/j.media.2009.05.004>
- Hoeper, M.M., Bogaard, H.J., Condliffe, R., Frantz, R., Khanna, D., Kurzyna, M., Langleben, D., Manes, A., Satoh, T., Torres, F., Wilkins, M.R., Badesch, D.B., 2013. Definitions and Diagnosis of Pulmonary Hypertension. *J. Am. Coll. Cardiol.* 62, D42–D50. <https://doi.org/10.1016/j.jacc.2013.10.032>
- Hoeper, M.M., Humbert, M., Souza, R., Idrees, M., Kawut, S.M., Sliwa-Hahnle, K., Jing, Z.-C., Gibbs, J.S.R., 2016. A global view of pulmonary hypertension. *Lancet Respir. Med.* 4, 306–322. [https://doi.org/10.1016/S2213-2600\(15\)00543-3](https://doi.org/10.1016/S2213-2600(15)00543-3)
- Hollenbeck, J.F.M., Cain, C.M., Fattor, J.A., Rullkoetter, P.J., Laz, P.J., 2018. Statistical shape modeling characterizes three-dimensional shape and alignment variability in the lumbar spine. *J. Biomech.* 69, 146–155. <https://doi.org/10.1016/j.jbiomech.2018.01.020>

- Humbert, M., Kovacs, G., Hooper, M.M., Badagliacca, R., Berger, R.M.F., Brida, M., Carlsen, J., Coats, A.J.S., Escribano-Subias, P., Ferrari, P., Ferreira, D.S., Ghofrani, H.A., Giannakoulas, G., Kiely, D.G., Mayer, E., Meszaros, G., Nagavci, B., Olsson, K.M., Pepke-Zaba, J., Quint, J.K., Rådegran, G., Simonneau, G., Sitbon, O., Tonia, T., Toshner, M., Vachiery, J.-L., Noordgraaf, A.V., Delcroix, M., Rosenkranz, S., Group, the E.S.D., 2022. 2022 ESC/ERS Guidelines for the diagnosis and treatment of pulmonary hypertension. *Eur. Respir. J.* <https://doi.org/10.1183/13993003.00879-2022>
- Izenman, A.J., 2008. Modern Multivariate Statistical Techniques, Springer Texts in Statistics. Springer New York, New York, NY. <https://doi.org/10.1007/978-0-387-78189-1>
- James, G., Witten, D., Hastie, T., Tibshirani, R., 2022. An introduction to statistical learning with applications in R. *Stat. Theory Relat. Fields* 6, 87–87. <https://doi.org/10.1080/24754269.2021.1980261>
- Khou, V., Anderson, J.J., Strange, G., Corrigan, C., Collins, N., Celermajer, D.S., Dwyer, N., Feenstra, J., Horrigan, M., Keating, D., Kotlyar, E., Lavender, M., McWilliams, T.J., Steele, P., Weintraub, R., Whitford, H., Whyte, K., Williams, T.J., Wrobel, J.P., Keogh, A., Lau, E.M., 2020. Diagnostic delay in pulmonary arterial hypertension: Insights from the Australian and New Zealand pulmonary hypertension registry. *Respirology* 25, 863–871. <https://doi.org/10.1111/resp.13768>
- Klingenberg, C., 2015. Analyzing Fluctuating Asymmetry with Geometric Morphometrics: Concepts, Methods, and Applications.
- Mandras, S.A., Ventura, H.O., Corris, P.A., 2016. Breaking Down the Barriers: Why the Delay in Referral for Pulmonary Arterial Hypertension? 16.
- Mansi, T., 2010. Image-based physiological and statistical models of the heart: application to tetralogy of Fallot (phdthesis). École Nationale Supérieure des Mines de Paris.
- Mansi, T., Voigt, I., Leonardi, B., Pennec, X., Durrleman, S., Sermesant, M., Delingette, H., Taylor, A.M., Boudjemline, Y., Pongiglione, G., Ayache, N., 2011. A statistical model for quantification and prediction of cardiac remodelling: application to tetralogy of Fallot. *IEEE Trans. Med. Imaging* 30, 1605–1616. <https://doi.org/10.1109/TMI.2011.2135375>
- Medrano-Gracia, P., Cowan, B.R., Ambale-Venkatesh, B., Bluemke, D.A., Eng, J., Finn, J.P., Fonseca, C.G., Lima, J.A.C., Suinesiaputra, A., Young, A.A., 2014. Left ventricular shape variation in asymptomatic populations: the Multi-Ethnic Study of Atherosclerosis. *J. Cardiovasc. Magn. Reson. Off. J. Soc. Cardiovasc. Magn. Reson.* 16, 56. <https://doi.org/10.1186/s12968-014-0056-2>
- Melzig, C., Wörz, S., Egenlauf, B., Partovi, S., Rohr, K., Grünig, E., Kauczor, H.-U., Heussel, C.P., Rengier, F., 2019. Combined automated 3D volumetry by pulmonary CT angiography and echocardiography for detection of pulmonary hypertension. *Eur. Radiol.* 29, 6059–6068. <https://doi.org/10.1007/s00330-019-06188-7>
- Mesh Smoothing.pdf, n.d.
- Muschelli, J., 2020. ROC and AUC with a Binary Predictor: a Potentially Misleading Metric. *J. Classif.* 37, 696–708. <https://doi.org/10.1007/s00357-019-09345-1>
- Nahm, F.S., 2022. Receiver operating characteristic curve: overview and practical use for clinicians. *Korean J. Anesthesiol.* 75, 25–36. <https://doi.org/10.4097/kja.21209>
- Paraview, n.d.

- Pesapane, F., Codari, M., Sardanelli, F., 2018. Artificial intelligence in medical imaging: threat or opportunity? Radiologists again at the forefront of innovation in medicine. *Eur. Radiol. Exp.* 2, 35. <https://doi.org/10.1186/s41747-018-0061-6>
- Powers, D., 2008. Evaluation: From Precision, Recall and F-Factor to ROC, Informedness, Markedness & Correlation. *Mach Learn Technol* 2.
- Precision-Recall [WWW Document], n.d. . Scikit-Learn. URL [https://scikit-learn/stable/auto\\_examples/model\\_selection/plot\\_precision\\_recall.html](https://scikit-learn/stable/auto_examples/model_selection/plot_precision_recall.html) (accessed 5.8.24).
- Pulmonary circulation | Definition, Function, Diagram, & Facts | Britannica [WWW Document], 2024. URL <https://www.britannica.com/science/pulmonary-circulation> (accessed 5.6.24).
- Pulmonary hypertension: patients in the UK 2004-2022 [WWW Document], n.d. . Statista. URL <https://www.statista.com/statistics/571912/patients-with-pulmonary-hypertension-in-the-united-kingdom-uk/> (accessed 5.6.24).
- Rajagopal, S., Ruetzler, K., Ghadimi, K., Horn, E.M., Kelava, M., Kudelko, K.T., Moreno-Duarte, I., Preston, I., Rose Bovino, L.L., Smilowitz, N.R., Vaidya, A., null, null, 2023. Evaluation and Management of Pulmonary Hypertension in Noncardiac Surgery: A Scientific Statement From the American Heart Association. *Circulation* 147, 1317–1343. <https://doi.org/10.1161/CIR.0000000000001136>
- Rangayyan, R.M., n.d. Biomedical Image Analysis. *Image Anal.*
- Ratner, B., 2009. The correlation coefficient: Its values range between +1/-1, or do they? *J. Target. Meas. Anal. Mark.* 17, 139–142. <https://doi.org/10.1057/jt.2009.5>
- Rigaud, B., Simon, A., Gobeli, M., Leseur, J., Duvergé, L., Williaume, D., Castelli, J., Lafond, C., Acosta, O., Haigron, P., De Crevoisier, R., 2019. Statistical Shape Model to Generate a Planning Library for Cervical Adaptive Radiotherapy. *IEEE Trans. Med. Imaging* 38, 406–416. <https://doi.org/10.1109/TMI.2018.2865547>
- Rosipal, R., Krämer, N., 2006. Overview and Recent Advances in Partial Least Squares, in: Saunders, C., Grobelnik, M., Gunn, S., Shawe-Taylor, J. (Eds.), Subspace, Latent Structure and Feature Selection. Springer, Berlin, Heidelberg, pp. 34–51. [https://doi.org/10.1007/11752790\\_2](https://doi.org/10.1007/11752790_2)
- Sabry, M., Hermida, U., Hassan, A., Nagy, M., Stojanovski, D., Samuel, I., Locas, J., Yacoub, M.H., De Vecchi, A., Lamata, P., 2024. Exploring the Relationship Between Pulmonary Artery Shape and Pressure in Pulmonary Hypertension: A Statistical Shape Analysis Study, in: Statistical Atlases and Computational Models of the Heart. Regular and CMRxRecon Challenge Papers. Presented at the International Workshop on Statistical Atlases and Computational Models of the Heart, Springer, Cham, pp. 186–195. [https://doi.org/10.1007/978-3-031-52448-6\\_18](https://doi.org/10.1007/978-3-031-52448-6_18)
- Saito, T., Rehmsmeier, M., 2015. The precision-recall plot is more informative than the ROC plot when evaluating binary classifiers on imbalanced datasets. *PloS One* 10, e0118432. <https://doi.org/10.1371/journal.pone.0118432>
- Schneider, P.J., Eberly, D.H., 2003. Geometric tools for computer graphics, The Morgan Kaufmann series in computer graphics and geometric modeling. Boston Morgan Kaufmann Publishers, Amsterdam.
- Schober, P., Boer, C., Schwarte, L.A., 2018. Correlation Coefficients: Appropriate Use and Interpretation. *Anesth. Analg.* 126, 1763. <https://doi.org/10.1213/ANE.0000000000002864>
- Shreffler, J., Huecker, M.R., 2024. Hypothesis Testing, P Values, Confidence Intervals, and Significance, in: StatPearls. StatPearls Publishing, Treasure Island (FL).

- Simonneau, G., Montani, D., Celermajer, D.S., Denton, C.P., Gatzoulis, M.A., Krowka, M., Williams, P.G., Souza, R., 2019. Haemodynamic definitions and updated clinical classification of pulmonary hypertension. *Eur. Respir. J.* 53, 1801913. <https://doi.org/10.1183/13993003.01913-2018>
- Sokolova, M., Lapalme, G., 2009. A systematic analysis of performance measures for classification tasks. *Inf. Process. Manag.* 45, 427–437. <https://doi.org/10.1016/j.ipm.2009.03.002>
- Sophocleous, F., Bône, A., Shearn, A.I.U., Forte, M.N.V., Bruse, J.L., Caputo, M., Biglino, G., 2022. Feasibility of a longitudinal statistical atlas model to study aortic growth in congenital heart disease. *Comput. Biol. Med.* 144, 105326. <https://doi.org/10.1016/j.compbioemed.2022.105326>
- Styner, M.A., Rajamani, K.T., Nolte, L.-P., Zsemlye, G., Székely, G., Taylor, C.J., Davies, R.H., 2003. Evaluation of 3D Correspondence Methods for Model Building, in: Taylor, C., Noble, J.A. (Eds.), *Information Processing in Medical Imaging*. Springer, Berlin, Heidelberg, pp. 63–75. [https://doi.org/10.1007/978-3-540-45087-0\\_6](https://doi.org/10.1007/978-3-540-45087-0_6)
- Suinesiaputra, A., Ablin, P., Albà, X., Alessandrini, M., Allen, J., Bai, W., Çimen, S., Claes, P., Cowan, B.R., D'hooge, J., Duchateau, N., Ehrhardt, J., Frangi, A.F., Gooya, A., Grau, V., Lekadir, K., Lu, A., Mukhopadhyay, A., Oksuz, I., Parajuli, N., Pennec, X., Pereañez, M., Pinto, C., Piras, P., Rohé, M.-M., Rueckert, D., Säring, D., Sermesant, M., Siddiqi, K., Tabassian, M., Teresi, L., Tsaftaris, S.A., Wilms, M., Young, A.A., Zhang, X., Medrano-Gracia, P., 2018. Statistical shape modeling of the left ventricle: myocardial infarct classification challenge. *IEEE J. Biomed. Health Inform.* 22, 503–515. <https://doi.org/10.1109/JBHI.2017.2652449>
- Taubin, G., Zhang, T., Golub, G., 1996. Optimal Surface Smoothing as Filter Design, *Lecture Notes in Computer Science*. <https://doi.org/10.1007/BFb0015544>
- Ujj, B. (CDC/DDPHSS/CSELS/DLS), 2022. Diagnostic Sensitivity and Specificity for Clinical Laboratory Testing.
- VTK File Formats - VTK documentation [WWW Document], n.d. URL [https://docs.vtk.org/en/latest/design\\_documents/VTKFileFormats.html](https://docs.vtk.org/en/latest/design_documents/VTKFileFormats.html) (accessed 5.8.24).
- What is A Confusion Matrix in Machine Learning? The Model Evaluation Tool Explained [WWW Document], n.d. URL <https://www.datacamp.com/tutorial/what-is-a-confusion-matrix-in-machine-learning> (accessed 5.8.24).
- Xu, T., Wang, J., Fang, Y., 2014. A model-free estimation for the covariate-adjusted Youden index and its associated cut-point. *Stat. Med.* 33. <https://doi.org/10.1002/sim.6290>
- Youden, W.J., 1950. Index for rating diagnostic tests. *Cancer* 3, 32–35. [https://doi.org/10.1002/1097-0142\(1950\)3:1<32::aid-cncr2820030106>3.0.co;2-3](https://doi.org/10.1002/1097-0142(1950)3:1<32::aid-cncr2820030106>3.0.co;2-3)
- Young, A.A., Frangi, A.F., 2009. Computational cardiac atlases: from patient to population and back. *Exp. Physiol.* 94, 578–596. <https://doi.org/10.1113/expphysiol.2008.044081>
- Zhang, M., Wells, W.M., Golland, P., 2017. Probabilistic modeling of anatomical variability using a low dimensional parameterization of diffeomorphisms. *Med. Image Anal.*, Special Issue on the 2016 Conference on Medical Image Computing and Computer Assisted Intervention (Analog to MICCAI 2015) 41, 55–62. <https://doi.org/10.1016/j.media.2017.06.013>

- Zhang, X., Medrano-Gracia, P., Ambale-Venkatesh, B., Bluemke, D.A., Cowan, B.R., Finn, J.P., Kadish, A.H., Lee, D.C., Lima, J.A.C., Young, A.A., Suinesiaputra, A., 2017. Orthogonal decomposition of left ventricular remodeling in myocardial infarction. *GigaScience* 6, 1–15.  
<https://doi.org/10.1093/gigascience/gix005>
- Zweig, M.H., Campbell, G., 1993. Receiver-operating characteristic (ROC) plots: a fundamental evaluation tool in clinical medicine. *Clin. Chem.* 39, 561–577.

## 9 Appendix

### 9.1 Appendix A – Dataset

ID	Study ID	Pressure (mPAP)	PA:A Ratio	PVR (WU)
1	S46	25	0.808667737	1.9
2	S45	23	1.023756163	1.9
3	S44	18	0.682037372	1.1
4	S43			
5	S42	20	0.713773314	1.4
6	S41	27	0.744151319	6.87
7	S40	27	1.0537985	2
8	S39	29		2.86
9	S38	35		2.2
10	S37	60	0.838828968	10.5
11	S36	20	1.10310219	1.6
12	S35	24	0.969563476	2.6
13	S34			
14	S33	22	0.946165414	1.5
15	S32	39	0.885208452	3.48
16	S31	31	1.103412969	4.13
17	S30	20		2.9
18	S29	26	0.898554999	1.3
19	S28	50	1.198542805	13.3
20	S27	44	0.891909385	4.7
21	S26	44	1.421783235	4.9
22	S25	44	1.0726082	3.22
23	S24	22	0.846401404	1.4
24	S23	43		11.3
25	S22			
26	S20	48	1.058245852	9.3
27	S19	19	0.898737577	1.08
28	S18	26	0.795072115	2.1
29	S17	52	1.108374384	8.8
30	S16	30	0.9921875	1.9
31	S15	26	1.151027703	2.6
32	S14	34	0.985833077	6.4
33	S13	25	0.793650794	3.16
34	S12	20	0.994974874	3.21

35	S11	24	0.814565826	2.05
36	S10	58	1.243325706	3.8
37	S9	35	1.138654041	4.6
38	S8	39	0.807936989	9.2
39	S5	26	0.893002915	2.53
40	S4	26	0.916508539	3.2
41	S3	50	1.104622111	
42	S2	17	0.969604863	0.86
43	S1	17	0.621965056	0.97
44	Imbio1	59		10.3
45	Imbio2	27		3
46	Imbio3	53		12
47	Imbio5	40		6
48	Imbio6	25		2.7
49	Imbio7	38		9.67
50	Imbio8	33		3.81
51	Imbio9	28		5
52	Imbio10	54		9
53	Imbio11	42		9.3
54	Imbio12	46		7.4
55	Imbio15	28		3.4
56	Imbio16	46		13.4
57	Imbio17	16		1.1
58	Imbio18	19		1.23
59	Imbio19	19		0.6
60	Imbio20	22		1.9
61	Imbio21	15		0.68
62	Imbio22	20		0.88
63	Imbio23	18		1.5
64	Imbio24	18		1.1
65	Imbio25	23		3.8
66	Imbio26	21		2
67	Imbio29	67		11.8

68	Imbio30	40		3.3
69	Imbio31	26		3.97
70	Imbio32	60		13.34
71	Imbio33	34		7.64
72	Imbio34	47		7.7
73	Imbio36	66		14.2
74	Imbio37	46		5.17
75	Imbio38	61		15
76	Imbio39	36		5.32
77	Imbio40	44		7.4
78	Imbio41	41		5.2
79	Imbio43	52		10
80	Imbio44	27		1.9
81	Imbio45	49		10.5
82	Imbio46	39		4.9
83	Imbio47	24		2.87
84	Imbio48	30		1.4
85	Imbio49	22		1.3
86	Imbio50	24		1.9
87	Imbio51	24		1.3
88	Imbio52	24		1.9
89	Imbio53	22		1.56
90	Imbio54	17		1.5
91	Imbio55	16		1.1
92	Imbio56	24		2.76
93	Imbio57	12		1.1
94	Imbio58	19		0.86
95	Imbio59	17		1

## 9.2 Appendix B – Normality Test MATLAB File

```
% Import Pressure Data
fileID2 = fopen('mPAP_Data.txt','r');
formatspec2 = '%f';
B = fscanf(fileID2,formatspec2); % numerical vector of mPaP data
data = B;

% Anderson-Darling Test for normality
h1 = adtest(data);

% Lilliefors Test for normality
h2 = lillietest(data);

% Shapiro-Wilk Test for normality
h3 = swtest(data);

% Kolmogorov-Smirnov Test for normality
M = mean(data);
S = std(data);
KSmPAP = (data-M)/S;
h4 = kstest(data);

% Create a table of all normality test results
NormalityTest = ["Anderson-Darling Test"; "Lilliefors
Test"; "Shapiro-Wilk Test"; "Kolmogorov-Smirnov Test"];
NormalityTestResults = [h1;h2;h3;h4];
NormalityTestTable = table(NormalityTest,NormalityTestResults)
```

### 9.3 Appendix C – PCA MATLAB File

```
clear
clc

%% Importing Data
% Read momenta vectors from text file
fileID =
fopen('DeterministicAtlas__EstimatedParameters__Momenta.txt','r');
formatSpec = '%f';
A = fscanf(fileID,formatSpec);

subjects = A(1); % Number of subject shapes used in deformetrica
model
controlPoints = A(2); % Number of control points used in
deformetrica model
dimensions = A(3); % Shape dimension (i.e. 2D or 3D)

% Initialise and populate a 2D momenta vector
momenta2D = zeros(controlPoints*dimensions,subjects);

for i = 1:subjects
    offset = (i-1)*controlPoints*3;
    momenta2D(1:controlPoints*3,i) =
A(4+offset:3+controlPoints*3+offset);
end

% Import Pressure Data
fileID2 = fopen('PAmPAP__Data.txt','r');
formatSpec2 = '%f';
B = fscanf(fileID2,formatSpec2); % numerical vector of mPaP data
mPAP = B;

% Import Pulmonary Hypertension Classification Data
fileID3 = fopen('PAph__Data.txt','r');
formatSpec3 = '%f';
C = fscanf(fileID3,formatSpec3); % numerical vector of mPaP data
phClass = C;

% Remove template from mPAP and PH data
% Create user input for defining template data ID
prompt = {'Define Template ID:'};
dlgtitle = 'UI';
fieldsize = [1 30];
definput = {'52'};
answer = inputdlg(prompt,dlgtitle,fieldsize,definput);
templateID = str2double(answer);

H = height(mPAP); % Define number of data points
h = height(phClass); % Define no. of data points

% Remove template from datasets
```

```

mPAPdata = zeros(H-1,1);
mPAPdata(1:templateID-1,:) = mPAP(1:templateID-1,:);
mPAPdata(templateID,:) = mPAP(templateID+1,:);
mPAPdata(templateID+1:H-1,:) = mPAP(templateID+2:H,:);
mPAP = mPAPdata; % Set new data

phData = zeros(h-1,1);
phData(1:templateID-1,:) = phClass(1:templateID-1,:);
phData(templateID,:) = phClass(templateID+1,:);
phData(templateID+1:H-1,:) = phClass(templateID+2:H,:);
PHclass = phData; % Set new data

% Removed samples S43, S34, and S22, prior to deformetrica, because
they have no mPAP value

% Define number of modes
numModes = subjects;

%% Statistical Analysis - Find eigenvalues and eigenvectors
% Calculate the covariance matrix
covarianceMatrix = cov(momenta2D);

% Calculate the eigenvalues (D) and eigenvectors (V)
[V,D] = eig(covarianceMatrix);

%% Calculate shape mode percentage of variation and accumulated
variation
% Convert eigenvalues matrix to vector in descending order
[eigVals,ind] = sort(diag(D),'descend');
Dd = D(ind,ind); % New Eigenvalue matrix in descending order
D = Dd;
Vd = V(:,ind); % Changes Eigenvectors to descending order
V = Vd;

eigSum = sum(eigVals); % Sum eigenvalues

% Obtain eigenvalue percentages and cumulative percentage vector
eigPercent = 100 * (eigVals/eigSum); % Eigenvalue Percentages
eigCumPercent = cumsum(eigPercent); % Cumulative Percentages

SMcumPercent = eigCumPercent;
SMs = (1:1:numModes)';

SMsP(2:numModes+1,1) = SMs;
SMsP(1,1) = 0;
SMcumPercentP(2:numModes+1,1) = SMcumPercent;
SMcumPercentP(1,1) = 0;

% Interpolate for 90% Variance
[~,SM90s]= min(abs(SMcumPercent - 90));
SM90 = max(SM90s);
if SMcumPercent(SM90) < 90
    SM90 = SM90 + 1;

```

```

end

P90 = spline(SMcumPercentP,SMsP,90);
PVD90x = [0;P90];
PVD90y = [90;90];
PVDx = [P90;P90];
PVDy = [0;90];

% Plot cumulative shape mode percentage
figure(1)
plot(SMsP,SMcumPercentP,'MarkerFaceColor',[0 0.4470
0.7410],'LineWidth',1.25)
hold on
plot(PVD90x,PVD90y,'k--',PVDx,PVDy,'k--','LineWidth',1.25)
scatter(P90,90,'k','filled','LineWidth',1.25)
box on
grid, grid minor
title("Cumulative Amount of Dataset Shape Variance Captured by PCA
Shape Modes",'interpreter','latex')
xlabel("No. of PCA Shape Modes",'interpreter','latex')
ylabel("Dataset Shape Variance Captured
(\%)",'interpreter','latex')
xlim([0 69])
ylim([0 100])
set(gca,'TickLabelInterpreter','latex')
set(gcf,'Position',[600 400 800 400])
str = {"90% of the Dataset Shape Variance is
Captured",strjoin(["by the first ",num2str(SM90)," PCA Shape
Modes."])};
annotation('textbox',[0.65 0.19 0.1
0.1],'Interpreter','latex','String',str,'BackgroundColor','w','FitB
oxToText','on','HorizontalAlignment','center')

% Create tables of each individual and cumulative shape mode
variance
SMpercentT = table(SMs,eigPercent);
SMpercentT.Properties.VariableNames = ["Shape Mode No.", "Percentage
Variance of the Dataset (%)"];

% Do the sum of the dot product between V and momenta2D to create
the shape modes
shape_modes = zeros(controlPoints*3,numModes);

for m = 1:numModes
    for j = 1:subjects
        shape_modes(:,m) = shape_modes(:,m) + V(j,m) * momenta2D(:,j);
    end
end

SMpca_S08 = shape_modes;
writematrix(SMpca_S08)

```

```

% Set t for number of standard deviations and m for which shape
mode
for m = 1:numModes
    for t = -2:4:2

        output = t*sqrt(D(m,m)).*shape_modes(:,m);

        % Save the output to a .txt file
        % Create the positive file name
        name1 = strcat('PCA_Momenta_mode_',num2str(m));
        name2 = strcat('__nSD__',num2str(t(:,1)));
        name = strcat(name1,name2);
        filename = strcat(name,'.txt');

        % The first three lines are 1 A(2) and A(3)
        header1 = '1'; % number of subjects per file
        header2 = num2str(A(2)); % number of control points
        header3 = num2str(A(3)); % number of dimensions

        % Create a file ID
        fid = fopen(filename,'w');

        % Put the header info into the text file
        fprintf(fid, [ header1 ' ']);
        fprintf(fid, [ header2 ' ']);
        fprintf(fid, [ header3 '\n']);

        % Print the data to a text file
        reshapeOutput = ones(controlPoints,dimensions);

        for i = 1:controlPoints
            a = num2str(output((i-1)*3+1));
            b = num2str(output((i-1)*3+2));
            c = num2str(output((i-1)*3+3));
            fprintf(fid, ['\n' a ' ' b ' ' c ]);
        end
    end
end

% Calculate how much of each shape mode is present in each patient
% Save the output to a .txt file
% Create the file name
filename = 'PCA_AmountOfEachMode.txt';

% Create a file ID
fid = fopen(filename,'w');

scores = zeros(subjects,numModes);

for subject = 1:subjects
    for mode = 1:numModes

        subject_n = momenta2D(:,subject);

```

```

    mode_m = shape_modes(:,mode);

    score = dot(subject_n,mode_m);

    % Create an array where each row represents all the scores
    % for one subject from mode 1 to 69
    scores(subject,mode) = score;

    % Print the data to a text file
    a = num2str(score);

    text1 = strcat('Subject: ',num2str(subject));
    text2 = strcat('; Mode: ',num2str(mode));
    text = strcat(text1, text2);

    fprintf(fid, ['\n' text ]);
    fprintf(fid, ['\n' a ]);

end
end

%% Widely Accepted pulmonary hypertension (PH) classification
% Define mPAP PH classification
PHmPAP = 25; % mmHg

% Obtain graphical results and display AUCROC table
[AUC25,YI25,R25,PVD25,SRCC25,csr25] =
ScatPlotsPCA(numModes,mPAP,scores,PHmPAP,eigPercent,PHclass);
disp(PVD25)
disp(SRCC25)
disp(AUC25)
disp(YI25)
disp(R25)
disp(csr25)

%% New pulmonary hypertension (PH) classification
% Define new mPAP PH classification
newPHmPAP = 20; % mmHg

% Obtain graphical results and display AUCROC table
[AUC20,YI20,R20,PVD20,SRCC20,csr20] =
ScatPlotsPCA(numModes,mPAP,scores,newPHmPAP,eigPercent,PHclass);
disp(AUC20)
disp(YI20)
disp(R20)
disp(csr20)

```

#### 9.4 Appendix D – PLS MATLAB File

```
clear
clc

%% Importing Data
% Read momenta vectors from text file
fileID =
fopen('DeterministicAtlas__EstimatedParameters__Momenta.txt','r');
formatSpec = '%f';
A = fscanf(fileID,formatSpec);

subjects = A(1); % Number of subject shapes used in deformetrica
model
controlPoints = A(2); % Number of control points used in
deformetrica model
dimensions = A(3); % Shape dimension (i.e. 2D or 3D)

% Initialise and populate a 2D momenta vector
momenta2D = zeros(controlPoints*dimensions,subjects);

for i = 1:subjects
    offset = (i-1)*controlPoints*3;
    momenta2D(1:controlPoints*3,i) =
A(4+offset:3+controlPoints*3+offset);
end

% Import Pressure Data
fileID2 = fopen('PAmPAP__Data.txt','r');
formatSpec2 = '%f';
B = fscanf(fileID2,formatSpec2); % numerical vector of mPaP data
mPAP = B;

% Import Pulmonary Hypertension Classification Data
fileID3 = fopen('PAph__Data.txt','r');
formatSpec3 = '%f';
C = fscanf(fileID3,formatSpec3); % numerical vector of mPaP data
phClass = C;

% Remove template from mPAP and PH data
% Create user input for defining template data ID
prompt = {'Define Template ID:'};
dlgtitle = 'UI';
fieldsize = [1 30];
definput = {'52'};
answer = inputdlg(prompt,dlgtitle,fieldsize,definput);
templateID = str2double(answer);

H = height(mPAP); % Define number of data points
h = height(phClass); % Define no. of data points

% Remove template from dataset
```

```

mPAPdata = zeros(H-1,1);
mPAPdata(1:templateID-1,:) = mPAP(1:templateID-1,:);
mPAPdata(templateID,:) = mPAP(templateID+1,:);
mPAPdata(templateID+1:H-1,:) = mPAP(templateID+2:H,:);
mPAP = mPAPdata; % Set new data

phData = zeros(h-1,1);
phData(1:templateID-1,:) = phClass(1:templateID-1,:);
phData(templateID,:) = phClass(templateID+1,:);
phData(templateID+1:H-1,:) = phClass(templateID+2:H,:);
PHclass = phData; % Set new data

% Removed samples S43, S34, and S22, prior to deformetrica, because
they have no mPAP value

% Define number of modes
numModes = subjects-1;

%% Statistical Analysis
% Prep data for PLS
X = transpose(momenta2D);
Y = mPAP;

% Carry out PLS regression
[XL,YL,XS,YS,BETA,PCTVAR,MSE,stats] = plsregress(X,Y,numModes);

%% Calculate shape mode percentage of variation and accumulated
variation
% Obtain vector of percentages in descending order
smPCTVAR = 100 * PCTVAR(2,:)';
SMpctvar = sort(smPCTVAR,'descend');

% Obtain Cumulative Percentage Vector
SMcumPercent = cumsum(SMpctvar);
SMs = (1:1:numModes)';

SMsP(2:numModes+1,1) = SMs;
SMsP(1,1) = 0;
SMcumPercentP(2:numModes+1,1) = SMcumPercent;
SMcumPercentP(1,1) = 0;

% Interpolate for 90% Variance
[~,SM90s]= min(abs(SMcumPercent - 90));
SM90 = max(SM90s);
if SMcumPercent(SM90) < 90
    SM90 = SM90 + 1;
end

P90 = spline(SMcumPercentP(1:30,:),SMsP(1:30,:),90);
PVD90x = [0;P90];
PVD90y = [90;90];
PVDx = [P90;P90];
PVDy = [0;90];

```

```

% Plot cumulative shape mode percentage
figure(1)
plot(SMsP,SMcumPercentP,'MarkerFaceColor',[0 0.4470
0.7410],'LineWidth',1.25)
hold on
plot(PVD90x,PVD90y,'k--',PVDx,PVDy,'k--','LineWidth',1.25)
scatter(P90,90,'k','filled','LineWidth',1.25)
box on
grid, grid minor
title("Cumulative Amount of Dataset Shape Variance Captured by PLS
Shape Modes",'interpreter','latex')
xlabel("No. of PLS Shape Modes",'interpreter','latex')
ylabel("Dataset Shape Variance Captured
(\%)",'interpreter','latex')
xlim([0 69])
ylim([0 100])
set(gca,'TickLabelInterpreter','latex')
set(gcf,'Position',[600 400 800 400])
str = {"90\% of the Dataset Shape Variance is
Captured",strjoin(["by the first ",num2str(SM90)," PLS Shape
Modes."])};
annotation('textbox',[0.65 0.19 0.1
0.1],'Interpreter','latex','String',str,'BackgroundColor','w','FitB
oxToText','on','HorizontalAlignment','center')

% Create tables of each individual shape mode variance of the
dataset
SMpercentT = table(SMs,smPCTVAR);
SMpercentT.Properties.VariableNames = ["Shape Mode No.", "Percentage
Variance of the Dataset (%)"];

SMpls_S08 = XL;
writematrix(SMpls_S08)

% Set t for number of standard deviations and m for which shape
mode
for m = 1:numModes
    for t = -2:4:2
        output = t*XL(:,m);

        % Save the output to a .txt file
        % Create the file name
        name1 = strcat('PLS__Momenta__mode__',num2str(m));
        name2 = strcat('__nSD__',num2str(t));
        name = strcat(name1,name2);

        filename = strcat(name,'.txt');

        % The first three lines are 1 A(2) and A(3)
        header1 = '1'; % number of subjects per file
        header2 = num2str(A(2)); % number of control points
        header3 = num2str(A(3)); % number of dimensions

```

```

% Create a file ID
fid = fopen(filename, 'w');

% Put the header info into the text file
fprintf(fid, [ header1 ' ' ]);
fprintf(fid, [ header2 ' ' ]);
fprintf(fid, [ header3 '\n']);

% Print the data to a text file
reshapeOutput = ones(controlPoints,dimensions);

for i = 1:controlPoints

    a = num2str(output((i-1)*3+1));
    b = num2str(output((i-1)*3+2));
    c = num2str(output((i-1)*3+3));

    fprintf(fid, ['\n' a ' ' b ' ' c ]);
end
end
end

% Calculate how much of each shape mode is present in each patient
% Save the output to a .txt file
% Create the file name
filename = 'PLS_AmountOfEachMode.txt';

% Create a file ID
fid = fopen(filename, 'w');

scores = zeros(subjects,numModes);

for subject = 1:subjects
    for mode = 1:numModes

        subject_n = momenta2D(:,subject);
        mode_m = XL(:,mode);
        score = dot(subject_n,mode_m);

        % Create an array where each row represents all the scores
        % for one subject from mode 1 to 69
        scores(subject,mode) = score;

    % Print the data to a text file
    a = num2str(score);

    text1 = strcat('Subject: ',num2str(subject));
    text2 = strcat('; Mode: ',num2str(mode));
    text = strcat(text1, text2);

    fprintf(fid, ['\n' text ]);
    fprintf(fid, ['\n' a ]);


```

```

        end
    end

%% Widely Accepted pulmonary hypertension (PH) classification
% Define mPAP PH classification
PHmPAP = 25; % mmHg

% Obtain graphical results and display AUCROC table
[AUC25,YI25,R25,PVD25,SRCC25,csr25] =
ScatPlotsPLS(numModes,mPAP,scores,PHmPAP,smPCTVAR,PHclass);
disp(PVD25)
disp(SRCC25)
disp(AUC25)
disp(YI25)
disp(R25)
disp(csr25)

%% New pulmonary hypertension (PH) classification
% Define new mPAP PH classification
newPHmPAP = 20; % mmHg

% Obtain graphical results and display AUCROC table
[AUC20,YI20,R20,PVD20,SRCC20,csr20] =
ScatPlotsPLS(numModes,mPAP,scores,newPHmPAP,smPCTVAR,PHclass);
disp(AUC20)
disp(YI20)
disp(R20)
disp(csr20)

```

## 9.5 Appendix E – Scatter Plots MATLAB Function File

```
function [AUCROCPRC,YIcsr,Rcsr,PVDt,newSRCC,csr] =
ScatPlotsPLS(numModes,mPAP,scores,mPAPcutoff,PercentVar,PHclass)

% Calculate Spearman's Rank Correlation Coefficient for all modes
for i = 1:numModes

    SRCC(i,1) = i;
    [rho,pval] = corr(mPAP,scores(:,i),'Type','Spearman');
    SRCC(i,2) = rho;
    SRCC(i,3) = pval;

end

% Convert Arrays to a Table
SRCC = array2table(SRCC, 'VariableNames', ["PLS Shape Mode
No.", "Spearman's Rank Correlation Coefficient", "Spearman's P-
Value"]);

%% Indexing for meeting correlation requirements
% Index SRCC table for SRCC >= 0.3 & SRCC <= -0.3
idx = SRCC.("Spearman's Rank Correlation Coefficient") >= 0.3 | 
SRCC.("Spearman's Rank Correlation Coefficient") <= -0.3;
newSRCC = SRCC(idx,:);

% Index new SRCC table for P-Value <=0.05
idx = newSRCC.("Spearman's P-Value") <= 0.05;
newSRCC = newSRCC(idx,:);

% Define number of shape modes which have met the conditions
H = height(newSRCC);

% Error message if no modes are found
if H ==0
    msg = "No significant PLS shape modes were found to correlate
to Pulmonary Hypertension.";
    error(msg)
end

%% Receiver Operating Characteristic mPAP classification = 25mmHg
% Receiver Operating Characteristic
for i = 1:H

    % Index for Shape Mode Number
    SM = table2array(newSRCC(i,1));
    SMn(i,1) = SM;

    L = floor(min(scores(:,SM))); % Finds least Shape Mode Amount
    U = ceil(max(scores(:,SM))); % Finds most Shape Mode Amount
    d = log10((U - L)); % Find the power of 10 magnitude of the
difference between the values
```

```

% Defining increment amount based of shape mode magnitudes
if d >= 2
    e = 1;
else
    e = 0.01;
end

smA = scores(:,SM); % Define shape mode amount vector
T = table(mPAP,smA,PHclass); % Create table of mPAP and SM
amount

% Define Correlation as Positive (1) or Negative (0)
PN = table2array(newSRCC(i,2));
if PN >= 0
    C = 1;
else
    C = 0;
end

%% ROC step function (Vary Shape Mode Classifying Amount)
% Set initial conditions
SMAC(1) = L;
MpapC = mPAPcutoff;

[Spec(1,:),Sens(1,:),J(1,:),SRa(1,:),SRt(1,:),Prcn(1,:),Recl(1,:),F
b(1,:)] = ROC(T,MpapC,SMAC(1),C);

% Step Variable
n = 1;
while SMAC(n) <= U

    % Increment Input
    SMAC(n+1) = SMAC(n) + e;

    % Apply ROC to extract specificity and sensitivity vector

[Spec(n+1,:),Sens(n+1,:),J(n+1,:),SRa(n+1,:),SRt(n+1,:),Prcn(n+1,:)
,Recl(n+1,:),Fb(n+1,:)] = ROC(T,MpapC,SMAC(n+1),C);

n = n+1;

end

%% Youden's Index Calculations
% Find Youden's Index
j = J(1:n,1);
spec = Spec(1:n,1);
sens = Sens(1:n,1);
prcn = Prcn(1:n,1);
recl = Recl(1:n,1);
fb = Fb(1:n,1);

```

```

cut0 = max(fb);
cutI = find(fb==cut0);

YI = max(j);
YIi = find(j==YI);

if C == 1
    SMAcutoff = min(SMAc(YIi)); % Finds the YI shape mode
amount cutoff
else
    SMAcutoff = max(SMAc(YIi)); % Finds the YI shape mode
amount cutoff
end

smaCut = median(SMAc(cutI));

ROCx = [0;1];
ROCy = [0;1];

% Random Classifier Line
p = polyfit(ROCx,ROCy,1);
RCLx = linspace(0,1,n)';
RCLy = polyval(p,RCLx);
BC = 0.5;

% Data points for vertical line
vl = polyval(p,spec);
YIx = [spec(YIi);spec(YIi)];
YIy = [vl(YIi);sens(YIi)];

% Data points for F1 score
fbx = recl(max(cutI));
fby = prcn(max(cutI));

% PRC vertical line
if C == 1
    recl(2:n+1,:) = recl;
    recl(1,:) = 1;
    prcn(2:n+1,:) = prcn;
    prcn(1,:) = 0.5;
else
    recl(n+1,:) = 1;
    prcn(n+1,:) = 0.5;
end

%% Determine Actual and Theoretical Success Rates
% Actual Success Rate
srA = SRa(1:n,1);
SucRateA(i,1) = 100 * max(srA(YIi));

% Theoretical Success Rate
srT = SRt(1:n,1);
SucRateT(i,1) = 100 * max(srT(YIi));

```

```

%% Indexing for Pulmonary Hypertension Diagnosed Patients
% Indexing for positive PH
idx = T.PHclass == 1;
PosPs = table2array(T(idx,:));

%% Plotting Graphs
if mPAPcutoff == 25
    % Plot Receiver Operating Characterisitc curve graph
    figure(i*25)
    plot(spec,sens,'MarkerFaceColor',[0 0.4470
0.7410],'LineWidth',1.25)
    hold on
    box on
    grid, grid minor
    plot(RCLx,RCLy,'k--','LineWidth',1.25)
    plot(YIx,YIy,'r-.','LineWidth',1.25)
    title(strjoin(["PLS Shape Mode ",num2str(SM)," Receiver
Operating Characteristic Curve"]),'interpreter','latex')
    subtitle("Pulmonary Hypertension Classification, mPAP =
25mmHg",'interpreter','latex')
    xlabel("1 - Specificity",'interpreter','latex')
    ylabel("Sensitivity",'interpreter','latex')
    xlim([0 1])
    ylim([0 1])
    legend("", "Random Classifier Line", "Youden's Index (J
Statistic)",'interpreter','latex','Location','southeast')
    set(gca,'TickLabelInterpreter','latex')
    set(gcf,'Position',[600 400 800 400])

    % Calculate Area Under Curve for ROC curve (AUCROC)
    AUC(i,1) = abs(trapz(spec,sens));

    % Plot Scatter Graphs
    figure(i*250)
    scatter(mPAP,scores(:,SM),'MarkerFaceColor',[0 0.4470
0.7410],'MarkerEdgeColor',[0 0.4470 0.7410])
    hold on
    box on
    grid, grid minor
    scatter(PosPs(:,1),PosPs(:,2),'MarkerFaceColor',[0.6350
0.0780 0.1840],'MarkerEdgeColor',[0.6350 0.0780 0.1840])
    xline(mPAPcutoff,'--r','LineWidth',1.25)
    yline(SMACutoff,'--k','LineWidth',1.25)
    title(strjoin(["Quantity of PLS Shape Mode ",num2str(SM)," in each Patient and their associated Mean Pulmonary Artery
Pressure"]),'interpreter','latex')
    subtitle("Pulmonary Hypertension Classification, mPAP =
25mmHg",'interpreter','latex')
    xlabel("mPAP (mmHg)",'interpreter','latex')
    ylabel("PLS Shape Mode Quantity",'interpreter','latex')
    xlim([10 70])

```

```

    legend("", "Patients Diagnosed with Pulmonary
Hypertension", "Pulmonary Hypertension mPAP Classification
Line", "Youden's Index Shape Mode Classification
Line", 'interpreter', 'latex')
    set(gca, 'TickLabelInterpreter', 'latex')
    set(gcf, 'Position', [600 400 800 400])

else
    % Plot Receiver Operating Characterisitc curve graph
    figure(i*20)
    plot(spec,sens, 'MarkerFaceColor',[0 0.4470
0.7410], 'LineWidth',1.25)
    hold on
    box on
    grid, grid minor
    plot(RCLx,RCLy, 'k--', 'LineWidth',1.25)
    plot(YIx,YIy, 'r-.', 'LineWidth',1.25)
    title(strjoin(["PLS Shape Mode ",num2str(SM)," Receiver
Operating Characteristic Curve"]),'interpreter', 'latex')
    subtitle("Pulmonary Hypertension Classification, mPAP =
20mmHg", 'interpreter', 'latex')
    xlabel("1 - Specificity",'interpreter', 'latex')
    ylabel("Sensitivity",'interpreter', 'latex')
    xlim([0 1])
    ylim([0 1])
    legend("", "Random Classifier Line", "Youden's Index (J
Statistic)", 'interpreter', 'latex', 'Location', 'southeast')
    set(gca, 'TickLabelInterpreter', 'latex')
    set(gcf, 'Position', [600 400 800 400])

    % Calculate Area Under Curve for ROC curve (AUCROC)
    AUC(i,1) = abs(trapz(spec,sens));

    % Plot Scatter Graphs
    figure(i*200)
    scatter(mPAP,smA, 'MarkerFaceColor',[0 0.4470
0.7410], 'MarkerEdgeColor',[0 0.4470 0.7410])
    hold on
    box on
    grid, grid minor
    scatter(PosPs(:,1),PosPs(:,2), 'MarkerFaceColor',[0.6350
0.0780 0.1840], 'MarkerEdgeColor',[0.6350 0.0780 0.1840])
    xline(mPAPcutoff, '--r', 'LineWidth',1.25)
    yline(SMACutoff, '--k', 'LineWidth',1.25)
    title(strjoin(["Quantity of PLS Shape Mode ",num2str(SM)," in each Patient and their associated Mean Pulmonary Artery
Pressure"]),'interpreter', 'latex')
    subtitle("Pulmonary Hypertension Classification, mPAP =
20mmHg", 'interpreter', 'latex')
    xlabel("mPAP (mmHg)",'interpreter', 'latex')
    ylabel("PLS Shape Mode Quantity",'interpreter', 'latex')
    xlim([10 70])

```

```

        legend("", "Patients Diagnosed with Pulmonary
Hypertension", "Pulmonary Hypertension mPAP Classification
Line", "Youden's Index Shape Mode Classification
Line", 'interpreter', 'latex')
        set(gca, 'TickLabelInterpreter', 'latex')
        set(gcf, 'Position', [600 400 800 400])

    end

    %% Move Shape Mode Amount Cutoff and find new Actual and
    %% Successfull Classification Rates
    % Run ROC function to get successful classification rates
    [~,~,~,SCRa,SCRt,~,~,~] = ROC(T,MpapC,smaCut,C);
    scrA(i,1) = SCRa;
    scrT(i,1) = SCRt;

    % Plot PRC graphs
    if mPAPcutoff == 25
        % Plot Receiver Operating Characterisitc curve graph
        figure(i*2500)
        plot(recl,prcn, 'MarkerFaceColor',[0 0.4470
0.7410], 'LineWidth',1.25)
        hold on
        box on
        grid, grid minor
        yline(BC,'--k','LineWidth',1.25)
        scatter(fbx,fby, 'MarkerFaceColor',[0.6350 0.0780
0.1840], 'MarkerEdgeColor',[0.6350 0.0780 0.1840], 'LineWidth',1.25)
        title(strjoin(["PLS Shape Mode ",num2str(SM)," Precision
Recall Curve"]),'interpreter','latex')
        subtitle("Pulmonary Hypertension Classification, mPAP =
25mmHg",'interpreter','latex')
        xlabel("Recall",'interpreter','latex')
        ylabel("Precision",'interpreter','latex')
        xlim([0 1])
        ylim([0 1])
        legend("", "Baseline Classifier Line", "Maximum F$B$ Score",
'interpreter','latex','Location','southeast')
        set(gca, 'TickLabelInterpreter', 'latex')
        set(gcf, 'Position', [600 400 800 400])

    % Calculate Area Under Curve for ROC curve (AUCROC)
    PRC(i,1) = abs(trapz(recl,prcn));

    % Plot Scatter Graphs
    figure(i*2500)
    scatter(mPAP,scores(:,SM), 'MarkerFaceColor',[0 0.4470
0.7410], 'MarkerEdgeColor',[0 0.4470 0.7410])
    hold on
    box on
    grid, grid minor
    scatter(PosPs(:,1),PosPs(:,2), 'MarkerFaceColor',[0.6350
0.0780 0.1840], 'MarkerEdgeColor',[0.6350 0.0780 0.1840])

```

```

xline(mPAPcutoff,'--r','LineWidth',1.25)
yline(smaCut,'--k','LineWidth',1.25)
xlim([10 70])
title(strjoin(["Quantity of PLS Shape Mode ",num2str(SM)," in each Patient and their associated Mean Pulmonary Artery Pressure"]),'interpreter','latex')
subtitle("Pulmonary Hypertension Classification, mPAP = 25mmHg",'interpreter','latex')
xlabel("mPAP (mmHg)",'interpreter','latex')
ylabel("PLS Shape Mode Quantity",'interpreter','latex')
legend("", "Patients Diagnosed with Pulmonary Hypertension", "Pulmonary Hypertension mPAP Classification Line", "F$B$ Shape Mode Classification Line",'interpreter','latex')
set(gca,'TickLabelInterpreter','latex')
set(gcf,'Position',[600 400 800 400])

else
    % Plot Receiver Operating Characterisitc curve graph
    figure(i*2000)
    plot(recl,prcn,'MarkerFaceColor',[0 0.4470 0.7410], 'LineWidth',1.25)
    hold on
    box on
    grid, grid minor
    yline(BC,'--k','LineWidth',1.25)
    scatter(fbx,fby,'MarkerFaceColor',[0.6350 0.0780 0.1840], 'MarkerEdgeColor',[0.6350 0.0780 0.1840], 'LineWidth',1.25)
    title(strjoin(["PLS Shape Mode ",num2str(SM)," Precision Recall Curve"]),'interpreter','latex')
    subtitle("Pulmonary Hypertension Classification, mPAP = 20mmHg",'interpreter','latex')
    xlabel("Recall",'interpreter','latex')
    ylabel("Precision",'interpreter','latex')
    xlim([0 1])
    ylim([0 1])
    legend("", "Baseline Classifier Line", "Maximum F$B$ Score",'interpreter','latex','Location','southeast')
    set(gca,'TickLabelInterpreter','latex')
    set(gcf,'Position',[600 400 800 400])

    % Calculate Area Under Curve for PRC curve (PRC-ROC)
    PRC(i,1) = abs(trapz(recl,prcn));

    % Plot Scatter Graphs
    figure(i*2000)
    scatter(mPAP,smA,'MarkerFaceColor',[0 0.4470 0.7410], 'MarkerEdgeColor',[0 0.4470 0.7410])
    hold on
    box on
    grid, grid minor
    scatter(PosPs(:,1),PosPs(:,2), 'MarkerFaceColor',[0.6350 0.0780 0.1840], 'MarkerEdgeColor',[0.6350 0.0780 0.1840])
    xline(mPAPcutoff,'--r','LineWidth',1.25)

```

```

yline(smaCut,'--k','LineWidth',1.25)
xlim([10 70])
title(strjoin(["Quantity of PLS Shape Mode ",num2str(SM)," in each Patient and their associated Mean Pulmonary Artery Pressure"]),'interpreter','latex')
subtitle("Pulmonary Hypertension Classification, mPAP = 20mmHg",'interpreter','latex')
xlabel("mPAP (mmHg)",'interpreter','latex')
ylabel("PLS Shape Mode Quantity",'interpreter','latex')
legend("", "Patients Diagnosed with Pulmonary Hypertension", "Pulmonary Hypertension mPAP Classification Line", "F$B$ Shape Mode Classification Line",'interpreter','latex')
set(gca,'TickLabelInterpreter','latex')
set(gcf,'Position',[600 400 800 400])

end

%% Plot defined classification line
smAcut = -2000;
% Run ROC function to get successful classification rates
[specD,sensD,~,SCRa,SCRt,~,~,~] = ROC(T,MpapC,smAcut,C);
sucRaA(i,1) = SCRa;
sucRaT(i,1) = SCRt;
SpecD(i,1) = 1 - specD;
SensD(i,1) = sensD;

% Plot PRC graphs
if mPAPcutoff == 25
    % Plot Scatter Graphs
    figure(i*250000)
    scatter(mPAP,scores(:,SM),'MarkerFaceColor',[0 0.4470 0.7410], 'MarkerEdgeColor',[0 0.4470 0.7410])
    hold on
    box on
    grid, grid minor
    scatter(PosPs(:,1),PosPs(:,2), 'MarkerFaceColor',[0.6350 0.0780 0.1840], 'MarkerEdgeColor',[0.6350 0.0780 0.1840])
    xline(mPAPcutoff,'--r','LineWidth',1.25)
    yline(smAcut,'--k','LineWidth',1.25)
    xlim([10 70])
    title(strjoin(["Quantity of PLS Shape Mode ",num2str(SM)," in each Patient and their associated Mean Pulmonary Artery Pressure"]),'interpreter','latex')
    subtitle("Pulmonary Hypertension Classification, mPAP = 25mmHg",'interpreter','latex')
    xlabel("mPAP (mmHg)",'interpreter','latex')
    ylabel("PLS Shape Mode Quantity",'interpreter','latex')
    legend("", "Patients Diagnosed with Pulmonary Hypertension", "Pulmonary Hypertension mPAP Classification Line", "Defined Shape Mode Classification Line",'interpreter','latex')
    set(gca,'TickLabelInterpreter','latex')
    set(gcf,'Position',[600 400 800 400])

```

```

    else
        % Plot Scatter Graphs
        figure(i*200000)
        scatter(mPAP,smA, 'MarkerFaceColor',[0 0.4470
0.7410], 'MarkerEdgeColor',[0 0.4470 0.7410])
        hold on
        box on
        grid, grid minor
        scatter(PosPs(:,1),PosPs(:,2), 'MarkerFaceColor',[0.6350
0.0780 0.1840], 'MarkerEdgeColor',[0.6350 0.0780 0.1840])
        xline(mPAPcutoff,'--r','LineWidth',1.25)
        yline(smAcut,'--k','LineWidth',1.25)
        xlim([10 70])
        title(strjoin(["Quantity of PLS Shape Mode ",num2str(SM)," in each Patient and their associated Mean Pulmonary Artery Pressure"]),'interpreter','latex')
        subtitle("Pulmonary Hypertension Classification, mPAP = 20mmHg",'interpreter','latex')
        xlabel("mPAP (mmHg)",'interpreter','latex')
        ylabel("PLS Shape Mode Quantity",'interpreter','latex')
        legend("", "Patients Diagnosed with Pulmonary Hypertension", "Pulmonary Hypertension mPAP Classification Line", "Defined Shape Mode Classification Line",'interpreter','latex')
        set(gca,'TickLabelInterpreter','latex')
        set(gcf,'Position',[600 400 800 400])
    end
end

% Filter for Shape Modes Percentage Variances of the Dataset
o = height(SMn);
for i = 1:o
    PVD(i,1) = PercentVar(SMn(i));
end

%% Create tables of results
% Create table of PVD and their representative shape mode numbers
PVDt = table(SMn,PVD);
PVDt.Properties.VariableNames = ["PLS Shape Mode No.", "Percentage Variance of the Dataset (%)"];

% Create table of AUCROC and AUC-PRC data and their representative shape mode numbers
AUCROCPRC = table(SMn,AUC,PRC);
AUCROCPRC.Properties.VariableNames = ["PLS Shape Mode No.", "AUCROC Value", "AUC-PRC Value"];

% Create table of Youden Index classification success rates and their representative shape mode numbers
YIcsr = table(SMn,SucRateA,SucRateT);

```

```

YIcsr.Properties.VariableNames = ["PLS Shape Mode No.", " Actual
Successful Classification Rate (%)", " Theoretical Successful
Classification Rate (%)];

% Create table of refined classification success rates and their
representative shape mode numbers
Rcsr = table(SMn,scrA,scrt);
Rcsr.Properties.VariableNames = ["PLS Shape Mode No.", " Actual
Successful Classification Rate (%)", " Theoretical Successful
Classification Rate (%)];

% Create table of refined classification success rates and their
representative shape mode numbers
csr = table(SMn,sucRaA,sucRaT,SensD,SpecD);
csr.Properties.VariableNames = ["PLS Shape Mode No.", " Actual
Successful Classification Rate (%)", " Theoretical Successful
Classification Rate (%)","Sensitivity","Specificity"];

```

## 9.6 Appendix F – ROC & PRC MATLAB Function File

```
function [FPR,TPR,J,srA,srT,Prcn,Recl,Fbeta] =
ROC(T,mPAPco,SMACo,c)

%% If statement for positive or negative correlation
if c==1 % Positive Correlation

    %% Index table for the different conditions
    % True Positive
    idx1 = T.mPAP >= mPAPco & T.smA >= SMACo;
    T1 = T(idx1,:);
    TP = height(T1);

    % False Negative
    idx2 = T.mPAP >= mPAPco & T.smA < SMACo;
    T2 = T(idx2,:);
    FN = height(T2);

    % False Positive
    idx3 = T.mPAP < mPAPco & T.smA >= SMACo;
    T3 = T(idx3,:);
    FP = height(T3);

    % True Negative
    idx4 = T.mPAP < mPAPco & T.smA < SMACo;
    T4 = T(idx4,:);
    TN = height(T4);

    %% Actual Successful Classifications
    idx5 = T.mPAP >= mPAPco & T.smA >= SMACo & T.PHclass == 1;
    T5 = T(idx5,:);
    idx6 = T.mPAP < mPAPco & T.smA < SMACo & T.PHclass == 0;
    T6 = T(idx6,:);
    SucClass = height(T5) + height(T6);

elseif c==0 % Negative Correlation

    %% Index table for the different conditions
    % True Positive
    idx1 = T.mPAP >= mPAPco & T.smA <= SMACo;
    T1 = T(idx1,:);
    TP = height(T1);

    % False Negative
    idx2 = T.mPAP >= mPAPco & T.smA > SMACo;
    T2 = T(idx2,:);
    FN = height(T2);

    % False Positive
    idx3 = T.mPAP < mPAPco & T.smA <= SMACo;
    T3 = T(idx3,:);
```

```

FP = height(T3);

% True Negative
idx4 = T.mPAP < mPAPco & T.smA > SMaco;
T4 = T(idx4,:);
TN = height(T4);

% Actual Successful Classifications
idx5 = T.mPAP >= mPAPco & T.smA <= SMaco & T.PHclass == 1;
T5 = T(idx5,:);
idx6 = T.mPAP < mPAPco & T.smA > SMaco & T.PHclass == 0;
T6 = T(idx6,:);
SucClass = height(T5) + height(T6);

else
    msg = 'Error occured defining correlation type.';
    error(msg)
end

%% Calculate specificity and sensitivity
% 1-Specificity - False Positive Rate
FPR = FP / (FP + TN);

% Sensitivity - True Positive Rate
TPR = TP / (TP + FN);

% Youden's Index (J Statistics)
J = TPR - FPR;

%% Calculate actual and theoretical classifying success rates
% Actual Success Rate
sRA = (SucClass) / (TP + TN + FP + FN);

% Theoretical Success Rate
srT = (TP + TN) / (TP + TN + FP + FN);

%% Precision-Recall
% Precision
if (TP + FP) == 0
    Prcn = 1;
else
    Prcn = TP / (TP + FP);
end

% Recall
Recl = TPR;

% Beta
beta = 2;

% Fbeta Score

```

```
Fbeta = ((1+(beta^2)) * Prcn * Recl)/(((beta^2) * Prcn) + Recl);
```

## 9.8 Appendix G – Current Diagnostic Methods Performance MATLAB File

```
clear
clc

%% Importing Data
% Import Pulmonary Artery to Aorta Ratio (PA:A) data
fileID = fopen('PAA_Data.txt','r');
formatSpec = '%f';
PAA = fscanf(fileID,formatSpec);

% Import mPAP data for PA:A
fileID2 = fopen('PAAmPAP_Data.txt','r');
formatSpec2 = '%f';
PAAmPAP = fscanf(fileID2,formatSpec2); % numerical vector of mPaP
data

% Import Pulmonary Hypertension classification for PA:A
fileID3 = fopen('PAAph_Data.txt','r');
formatSpec3 = '%f';
PAAph = fscanf(fileID3,formatSpec3); % numerical vector of mPaP
data

% Import Wood Resistance PVR data
fileID4 = fopen('PVR_Data.txt','r');
formatSpec4 = '%f';
PVR = fscanf(fileID4,formatSpec4);

% Import mPAP data for PVR
fileID5 = fopen('PVRmPAP_Data.txt','r');
formatSpec5 = '%f';
PVRmPAP = fscanf(fileID5,formatSpec5); % numerical vector of mPaP
data

% Import Pulmonary Hypertension classification for PVR
fileID6 = fopen('PVRph_Data.txt','r');
formatSpec6 = '%f';
PVRph = fscanf(fileID6,formatSpec6); % numerical vector of mPaP
data

%% Indexing Data
% Create tables of the data
PAAt = table(PAA,PAAmPAP,PAAph);
PAAt.Properties.VariableNames = ["PA:A","mPAP","PH Index"];

PVRT = table(PVR,PVRmPAP,PVRph);
PVRT.Properties.VariableNames = ["PVR","mPAP","PH Index"];

% Indexing for Postive PH
idx = PAAt."PH Index" == 1;
posPAA = table2array(PAAt(idx,:));
```

```

idx = PVrt.("PH_Index") == 1;
posPVR = table2array(PVrt(idx,:));

% Indexing for actual correctly classified patients
idx = PAAt.("PH_Index") == 1 & PAAt.("PA:A") >= 1 & PAAt.("mPAP")
>= 25;
PASucPPAt25 = PAAt(idx,:);

idx = PAAt.("PH_Index") == 0 & PAAt.("PA:A") < 1 & PAAt.("mPAP") <
25;
NASucPPAt25 = PAAt(idx,:);

idx = PAAt.("PH_Index") == 1 & PAAt.("PA:A") >= 1 & PAAt.("mPAP")
>= 20;
PASucPPAt20 = PAAt(idx,:);

idx = PAAt.("PH_Index") == 0 & PAAt.("PA:A") < 1 & PAAt.("mPAP") <
20;
NASucPPAt20 = PAAt(idx,:);

idx = PVrt.("PH_Index") == 1 & PVrt.("PVR") >= 3 & PVrt.("mPAP") >=
20;
PASucPVrt = PVrt(idx,:);

idx = PVrt.("PH_Index") == 0 & PVrt.("PVR") < 3 & PVrt.("mPAP") <
20;
NASucPVrt = PVrt(idx,:);

% Indexing for theoretically correctly classified patients
idx = PAAt.("PA:A") >= 1 & PAAt.("mPAP") >= 25;
PTSucPPAt25 = PAAt(idx,:);

idx = PAAt.("PA:A") < 1 & PAAt.("mPAP") < 25;
NTSucPPAt25 = PAAt(idx,:);

idx = PAAt.("PA:A") >= 1 & PAAt.("mPAP") >= 20;
PTSucPPAt20 = PAAt(idx,:);

idx = PAAt.("PA:A") < 1 & PAAt.("mPAP") < 20;
NTSucPPAt20 = PAAt(idx,:);

idx = PVrt.("PVR") >= 3 & PVrt.("mPAP") >= 20;
PTSucPVrt = PVrt(idx,:);

idx = PVrt.("PVR") < 3 & PVrt.("mPAP") < 20;
NTSucPVrt = PVrt(idx,:);

%% Calculating actual and theoretical classifying success rates
% Obtain total number of patients
PPAnumPatients = height(PAAt);
PVRnumPatients = height(PVrt);

% Obtain number actual successful classifications

```

```

PPAsucA25 = height(PAsucPPAt25) + height(NAsucPPAt25);
PPAsucA20 = height(PAsucPPAt20) + height(NAsucPPAt20);
PVRsucA = height(PAsucPVRT) + height(NAsucPVRT);

% Obtain number of theoretical successful classifications
PPAsucT25 = height(PTsucPPAt25) + height(NTsucPPAt25);
PPAsucT20 = height(PTsucPPAt20) + height(NTsucPPAt20);
PVRsucT = height(PTsucPVRT) + height(NTsucPVRT);

% Calculate actual successful classification percentages
PPApercentA25 = 100 * (PPAsucA25 / PPAnumPatients);
PPApercentA20 = 100 * (PPAsucA20 / PPAnumPatients);
PVRpercentA = 100 * (PVRsucA / PVRnumPatients);

% Calculate theoretical successful classification percentages
PPApercentT25 = 100 * (PPAsucT25 / PPAnumPatients);
PPApercentT20 = 100 * (PPAsucT20 / PPAnumPatients);
PVRpercentT = 100 * (PVRsucT / PVRnumPatients);

% Create table
cPHc = ["PA:A @ mPAP = 25mmHg"; "PA:A @ mPAP = 20mmHg"; "Pulmonary Vascular Resistance"];
percentagesA = [PPApercentA25;PPApercentA20;PVRpercentA];
percentagesT = [PPApercentT25;PPApercentT20;PVRpercentT];
T = table(cPHc,percentagesA,percentagesT);
T.Properties.VariableNames = ["Current PH Classifying Methods", "Actual Successful Classification Rate (%)", "Theoretical Successful Classification Rate (%)"];

% Bar Chart Calcs
idx = PAAt.("PH Index") == 1 & PAAt.("PA:A") >= 1;
PAA25TP = height(PAAt(idx,:));

idx = PAAt.("PH Index") == 0 & PAAt.("PA:A") < 1;
PAA25TN = height(PAAt(idx,:));

idx = PAAt.("PH Index") == 0 & PAAt.("PA:A") >= 1;
PAA25FP = height(PAAt(idx,:));

idx = PAAt.("PH Index") == 1 & PAAt.("PA:A") < 1;
PAA25FN = height(PAAt(idx,:));

PAA25suc = PAA25TP + PAA25TN;
PAA25unsuc = PAA25FP + PAA25FN;
PAA25sucP = 100 * (PAA25suc/PPAnumPatients);

PAA25sens = PAA25TP / (PAA25TP + PAA25FN);
PAA25spec = PAA25TN / (PAA25TN + PAA25FP);

idx = PVRT.("PH Index") == 1 & PVRT.("PVR") >= 3;
PVR25TP = height(PVRT(idx,:));

idx = PVRT.("PH Index") == 0 & PVRT.("PVR") < 3;

```

```

PVR25TN = height(PVRt(idx,:));

idx = PVRt.( "PH Index" ) == 0 & PVRt.( "PVR" ) >= 3;
PVR25FP = height(PVRt(idx,:));

idx = PVRt.( "PH Index" ) == 1 & PVRt.( "PVR" ) < 3;
PVR25FN = height(PVRt(idx,:));

PVR25suc = PVR25TP + PVR25TN;
PVR25unsuc = PVR25FP + PVR25FN;
PVR25sucP = 100 * (PVR25suc/PVRnumPatients);

PVR25sens = PVR25TP / (PVR25TP + PVR25FN);
PVR25spec = PVR25TN / (PVR25TN + PVR25FP);

%% Plot scatter graphs
% Define PH classifiers
mPAPcutoff = [25;20];
PAAcutoff = 1;
PVRCutoff = 3;

% PA:A
% PA:A Ratio @ mPAP = 25mmHg
figure(1)
scatter(PAAmPAP,PAA, 'MarkerFaceColor',[0 0.4470
0.7410], 'MarkerEdgeColor',[0 0.4470 0.7410])
hold on
box on
grid, grid minor
scatter(posPAA(:,2),posPAA(:,1), 'MarkerFaceColor',[0.6350 0.0780
0.1840], 'MarkerEdgeColor',[0.6350 0.0780 0.1840])
xline(mPAPcutoff(1),'r-','LineWidth',1.25)
yline(PAAcutoff,'k--','LineWidth',1.25)
title("Patients Pulmonary Artery : Aorta Diameters Ratio (PA:A) and
their Mean Pulmonary Artery Pressure (mPAP)",'interpreter','latex')
subtitle("Pulmonary Hypertension Classification, mPAP =
25mmHg",'interpreter','latex')
xlabel("mPAP (mmHg)",'interpreter','latex')
ylabel("PA:A",'interpreter','latex')
xlim([10 70])
ylim([0.5 1.5])
legend("", "Patients Diagnosed with Pulmonary
Hypertension", "Pulmonary Hypertension mPAP Classification
Line", "Pulmonary Hypertension PA:A Classification
Line", 'interpreter','latex', 'Location', 'southeast')
set(gca, 'TickLabelInterpreter', 'latex')
set(gcf, 'Position', [600 400 800 400])

% PA:A Ratio @ mPAP = 20mmHg
figure(2)
scatter(PAAmPAP,PAA, 'MarkerFaceColor',[0 0.4470
0.7410], 'MarkerEdgeColor',[0 0.4470 0.7410])
hold on

```

```

box on
grid, grid minor
scatter(posPAA(:,2),posPAA(:,1), 'MarkerFaceColor',[0.6350 0.0780
0.1840], 'MarkerEdgeColor',[0.6350 0.0780 0.1840])
xline(mPAPcutoff(2),'r-.', 'LineWidth',1.25)
yline(PAAcutoff,'k--','LineWidth',1.25)
title("Patients Pulmonary Artery : Aorta Diameters Ratio (PA:A) and
their Mean Pulmonary Artery Pressure (mPAP)",'interpreter','latex')
subtitle("Pulmonary Hypertension Classification, mPAP =
20mmHg",'interpreter','latex')
xlabel("mPAP (mmHg)",'interpreter','latex')
ylabel("PA:A",'interpreter','latex')
xlim([10 70])
ylim([0.5 1.5])
legend("", "Patients Diagnosed with Pulmonary
Hypertension", "Pulmonary Hypertension mPAP Classification
Line", "Pulmonary Hypertension PA:A Classification
Line", 'interpreter','lateX','Location','southeast')
set(gca, 'TickLabelInterpreter', 'lateX')
set(gcf, 'Position', [600 400 800 400])

% PVR
figure(3)
scatter(PVRmPAP,PVR, 'MarkerFaceColor',[0 0.4470
0.7410], 'MarkerEdgeColor',[0 0.4470 0.7410])
hold on
box on
grid, grid minor
scatter(posPVR(:,2),posPVR(:,1), 'MarkerFaceColor',[0.6350 0.0780
0.1840], 'MarkerEdgeColor',[0.6350 0.0780 0.1840])
xline(mPAPcutoff(2),'r-.', 'LineWidth',1.25)
yline(PVRcutoff,'k--','LineWidth',1.25)
title("Patients Pulmonary Vascular Resistance (PVR) and their Mean
Pulmonary Artery Pressure (mPAP)",'interpreter','lateX')
subtitle("Pulmonary Hypertension Classification, mPAP =
20mmHg",'interpreter','lateX')
xlabel("mPAP (mmHg)",'interpreter','lateX')
ylabel("PVR (Wood Units)",'interpreter','lateX')
xlim([10 70])
ylim([0 15])
legend("", "Patients Diagnosed with Pulmonary
Hypertension", "Pulmonary Hypertension mPAP Classification
Line", "Pulmonary Hypertension PVR Classification
Line", 'interpreter','lateX','Location','southeast')
set(gca, 'TickLabelInterpreter', 'lateX')
set(gcf, 'Position', [600 400 800 400])

%% Effective AUCROC Values
% Define new tables of the data
paaT = table(PAAmPAP,PAA);
paaT.Properties.VariableNames = ["mPAP", "Amount"];

pvrT = table(PVRmPAP,PVR);

```

```

pvrT.Properties.VariableNames = ["mPAP", "Amount"];

% Find min and max PA:A and PVR values in Data
lPAA = floor(min(PAA));
uPAA = ceil(max(PAA));

lPVR = floor(min(PVR));
uPVR = ceil(max(PVR));

% PA:A
for mPAPc = 20:5:25

    % Set initial conditons
    PAAc(1) = lPAA;
    [SpecPAA(1,:),SensPAA(1,:),PrcnPAA(1,:),ReclPAA(1,:)] =
    ROCcdm(paaT,mPAPc,PAAc(1));

    % Step Variable
    n = 1;
    while PAAc(n) <= uPAA

        % Increment Input
        PAAc(n+1) = PAAc(n) + 0.01;

        % Apply ROC to extract specificity and sensitivity vector
        [SpecPAA(n+1,:),SensPAA(n+1,:),PrcnPAA(n+1,:),ReclPAA(n+1,:)] =
        ROCcdm(paaT,mPAPc,PAAc(n+1));

        n = n+1;

    end

    PAAspec = SpecPAA(1:n,1);
    PAA sens = SensPAA(1:n,1);
    PAAprcn = PrcnPAA(1:n,1);
    PAArec1 = ReclPAA(1:n,1);
    BC = 0.5;

    % Plot graphs
    figure(mPAPc)
    plot(PAAspec,PAA sens, 'MarkerFaceColor',[0 0.4470
    0.7410], 'LineWidth',1.25)
    hold on
    plot([0;1],[0;1], '--k', 'LineWidth',1.25)
    box on
    grid, grid minor
    title("PA:A Effective Receiver Operating Characteristic
    Curve", 'interpreter','latex')
    subtitle(strjoin(["Pulmonary Hypertension Classification, mPAP
    = ", num2str(mPAPc), "mmHg"]], 'interpreter', 'latex')
    xlabel("1 - Specificity", 'interpreter', 'latex')
    ylabel("Sensitivity", 'interpreter', 'latex')

```

```

    legend("", "Random Classification
Line", 'interpreter', 'latex', 'Location', 'southeast')
    xlim([0 1])
    ylim([0 1])
    set(gca, 'TickLabelInterpreter', 'latex')
    set(gcf, 'Position', [600 400 800 400])

    figure(mPAPc*10)
    plot(PAArecl,PAAprcn, 'MarkerFaceColor', [0 0.4470
0.7410], 'LineWidth',1.25)
        hold on
        box on
        grid, grid minor
        yline(BC, '--k', 'LineWidth',1.25)
        title("PA:A Effective Precision Recall
Curve", 'interpreter', 'latex')
        subtitle(strjoin(["Pulmonary Hypertension Classification,
mPAP = ", num2str(mPAPc), "mmHg"]),'interpreter', 'latex')
        xlabel("Recall", 'interpreter', 'latex')
        ylabel("Precision", 'interpreter', 'latex')
        xlim([0 1])
        ylim([0 1])
        legend("", "Baseline Classifier
Line", 'interpreter', 'latex', 'Location', 'southeast')
        set(gca, 'TickLabelInterpreter', 'latex')
        set(gcf, 'Position', [600 400 800 400])

% Calculate Area Under Curve for ROC curve (AUCROC)
AUC(mPAPc,1) = abs(trapz(PAAspec,PAAsens));

% Calculate Area Under Curve for ROC curve (AUCROC)
PRC(mPAPc,1) = abs(trapz(PAArecl,PAAprcn));

end

% PVR
% Set initial conditions
PVRc(1) = 1PVR;
mPAPc = 20;
[SpecPVR(1,:),SensPVR(1,:),PrvnPVR(1,:),ReclPVR(1,:)] =
ROCCdm(pvrT,mPAPc,PVRc(1));

% Step Variable
n = 1;
while PVRc(n) <= uPVR

    % Increment Input
    PVRc(n+1) = PVRc(n) + 0.01;

    % Apply ROC to extract specificity and sensitivity vector
    [SpecPVR(n+1,:),SensPVR(n+1,:),PrvnPVR(n+1,:),ReclPVR(n+1,:)] =
ROCCdm(pvrT,mPAPc,PVRc(n+1));

```

```

n = n+1;

end

PVRspec = SpecPVR;
PVRsens = SensPVR;
PVRprcn = PrcnPVR;
PVRrecl = ReclPVR;

% Plot graphs
figure(4)
plot(PVRspec,PVRsens,'MarkerFaceColor',[0 0.4470
0.7410],'LineWidth',1.25)
hold on
plot([0;1],[0;1], '--k','LineWidth',1.25)
box on
grid, grid minor
title("PVR Effective Receiver Operating Characteristic
Curve",'interpreter','latex')
subtitle("Pulmonary Hypertension Classification, mPAP =
20mmHg",'interpreter','latex')
xlabel("1 - Specificity",'interpreter','latex')
ylabel("Sensitivity",'interpreter','latex')
legend("", "Random Classification
Line",'interpreter','latex','Location','southeast')
xlim([0 1])
ylim([0 1])
set(gca,'TickLabelInterpreter','latex')
set(gcf,'Position',[600 400 800 400])

figure(5)
plot(PVRrecl,PVRprcn,'MarkerFaceColor',[0 0.4470
0.7410],'LineWidth',1.25)
hold on
box on
grid, grid minor
yline(BC,'--k','LineWidth',1.25)
title("PVR Effective Precision Recall
Curve",'interpreter','latex')
subtitle("Pulmonary Hypertension Classification, mPAP =
20mmHg",'interpreter','latex')
xlabel("Recall",'interpreter','latex')
ylabel("Precision",'interpreter','latex')
xlim([0 1])
ylim([0 1])
legend("", "Baseline Classifier
Line",'interpreter','latex','Location','southeast')
set(gca,'TickLabelInterpreter','latex')
set(gcf,'Position',[600 400 800 400])

% Calculate Area Under Curve for ROC curve (AUCROC)
AUC(3,1) = abs(trapz(PVRspec,PVRsens));

```

```

% Calculate Area Under Curve for ROC curve (AUCROC)
PRC(3,1) = abs(trapz(PVRrec1,PVRprcn));

% Add AUC-PRC-AUCROC data to table
AUCROC = [AUC(25,1);AUC(20,1);AUC(3,1)];
T.("AUCROC Value") = AUCROC;

AUCPRC = [PRC(25,1);PRC(20,1);PRC(3,1)];
T.("AUC-PRC Value") = AUCPRC;

% Add Sensitivity and Specificity
[SpecPAAAd,SensPAAAd,~,~] = ROCCdm(paaT,25,1);
[SpecPVRd,SensPVRd,~,~] = ROCCdm(pvrT,20,3);

Sensitivity = [SensPAAAd;0;SensPVRd];
T.("Sensitivity") = Sensitivity;

Specificity = [1-SpecPAAAd;0;1-SpecPVRd];
T.("Specificity") = Specificity;

disp(T)

%% Bar Charts
x = {'Patients Successfully Classified' 'Patients Unsuccessfully
Classified'};
% PAA mPAP=25
figure(6)
barPAA25 = [PAA25suc PAA25TP PAA25TN; PAA25unsuc PAA25FN PAA25FP];
b1 = bar(barPAA25,'FaceColor','flat');
b1(1).FaceColor = [0.4940 0.1840 0.5560];
b1(2).FaceColor = [0.6350 0.0780 0.1840];
b1(3).FaceColor = [0 0.4470 0.7410];
box on
grid minor
xticklabels(x)
ylabel("No.",'interpreter','latex')
ylim([0 25])
title("Current PH Diagnostic Methods Performance -
PAA",'interpreter','latex')
legend("Healthy and Diagnosed Patients","Patients with Pulmonary
Hypertension","Healthy Patients",'interpreter','latex')
set(gca,'TickLabelInterpreter','latex')
set(gcf,'Position',[600 400 800 400])
str = {strjoin(["Successful Classification Rate:
",num2str(PAA25sucP),"\%"]);}
annotation('textbox',[0.68 0.65 0.1
0.1],'Interpreter','latex','String',str,'BackgroundColor','w','FitB
oxToText','on','HorizontalAlignment','center')

xtips1 = b1(1).XEndPoints;
ytips1 = b1(1).YEndPoints;
labels1 = string(b1(1).YData);

```

```

text(xtips1,ytips1,labels1,'HorizontalAlignment','center','Vertical
Alignment','bottom','Interpreter','latex')

xtips2 = b1(2).XEndPoints;
ytips2 = b1(2).YEndPoints;
labels2 = string(b1(2).YData);
text(xtips2,ytips2,labels2,'HorizontalAlignment','center','Vertical
Alignment','bottom','Interpreter','latex')

xtips3 = b1(3).XEndPoints;
ytips3 = b1(3).YEndPoints;
labels3 = string(b1(3).YData);
text(xtips3,ytips3,labels3,'HorizontalAlignment','center','Vertical
Alignment','bottom','Interpreter','latex')

% PVR
figure(7)
barPVR25 = [PVR25suc PVR25TP PVR25TN; PVR25unsuc PVR25FN PVR25FP];
b1 = bar(barPVR25,'FaceColor','flat');
b1(1).FaceColor = [0.4940 0.1840 0.5560];
b1(2).FaceColor = [0.6350 0.0780 0.1840];
b1(3).FaceColor = [0 0.4470 0.7410];
box on
grid minor
xticklabels(x)
ylabel("No.",'interpreter','latex')
ylim([0 85])
title("Current PH Diagnostic Methods Performance -
PVR",'interpreter','latex')
legend("Healthy and Diagnosed Patients","Patients with Pulmonary
Hypertension","Healthy Patients",'interpreter','latex')
set(gca,'TickLabelInterpreter','latex')
set(gcf,'Position',[600 400 800 400])
str = {strjoin(["Successful Classification Rate:
",num2str(PVR25sucP),"\%"])};
annotation('textbox',[0.68 0.65 0.1
0.1],'Interpreter','latex','String',str,'BackgroundColor','w','FitB
oxToText','on','HorizontalAlignment','center')

xtips1 = b1(1).XEndPoints;
ytips1 = b1(1).YEndPoints;
labels1 = string(b1(1).YData);
text(xtips1,ytips1,labels1,'HorizontalAlignment','center','Vertical
Alignment','bottom','Interpreter','latex')

xtips2 = b1(2).XEndPoints;
ytips2 = b1(2).YEndPoints;
labels2 = string(b1(2).YData);
text(xtips2,ytips2,labels2,'HorizontalAlignment','center','Vertical
Alignment','bottom','Interpreter','latex')

xtips3 = b1(3).XEndPoints;
ytips3 = b1(3).YEndPoints;

```

```
labels3 = string(b1(3).YData);
text(xtips3,ytips3,labels3,'HorizontalAlignment','center','Vertical
Alignment','bottom','Interpreter','latex')
```

## 9.9 Appendix H – Validation MATLAB File

```
clear
clc

%% Aorta
noAoval = [57,58,59,28,29,30,31,32,36,37,38,39,40,41,44,46];

% Read shape_modes from PCA for Imbio 47
A0pcaSM = readmatrix('SMpca_Imbio47.txt');

% Read shape_modes from PLS for Imbio 47
A0plsSM = readmatrix('SMpls_Imbio47.txt');

for i = 1:3

    no = noAoval(i);

    id = {[ 'AO_Imbio' ,num2str(no), '_Momenta.txt' ]};
    str = strjoin(id);

    %% Importing Data
    % Read momenta vectors from text file
    fileID = fopen(str,'r');
    formatspec = '%f';
    A = fscanf(fileID,formatspec);

    subjects = A(1); % Number of subject shapes used in
deformetrica model
    controlPoints = A(2); % Number of control points used in
deformetrica model
    dimensions = A(3); % Shape dimension (i.e. 2D or 3D)

    % Initialise and populate a 2D momenta vector
    A0momenta2D = zeros(controlPoints*dimensions,subjects);

    for j = 1:subjects
        offset = (j-1)*controlPoints*3;
        A0momenta2D(1:controlPoints*3,j) =
A(4+offset:3+controlPoints*3+offset);
    end

    aoMomenta2D = A0momenta2D';

    A0pcaSMs(i,:) = aoMomenta2D * A0pcaSM;
    A0plsSMs(i,:) = aoMomenta2D * A0plsSM;

end

for i = 4:16

    no = noAoval(i);
```

```

id = {[ 'AO_S',num2str(no), '__Momenta.txt' ]};
str = strjoin(id);

%% Importing Data
% Read momenta vectors from text file
fileID = fopen(str,'r');
formatSpec = '%f';
A = fscanf(fileID,formatSpec);

subjects = A(1); % Number of subject shapes used in
deformetrica model
controlPoints = A(2); % Number of control points used in
deformetrica model
dimensions = A(3); % Shape dimension (i.e. 2D or 3D)

% Initialise and populate a 2D momenta vector
A0momenta2D = zeros(controlPoints*dimensions,subjects);

for j = 1:subjects
    offset = (j-1)*controlPoints*3;
    A0momenta2D(1:controlPoints*3,j) =
A(4+offset:3+controlPoints*3+offset);
end

aoMomenta2D = A0momenta2D';

A0pcaSMs(i,:) = aoMomenta2D * A0pcaSM;
A0plsSMs(i,:) = aoMomenta2D * A0plsSM;

end

%% Pulmonary Artery
noPAval = [57,58,59,27,28,29,31,37,38,39,40,41,44,46];

% Read shape_modes from PCA for S08
PApcaSM = readmatrix('SMpca_S08.txt');

% Read shape_modes from PLS for S08
PAplsSM = readmatrix('SMpls_S08.txt');

for i = 1:3

no = noPAval(i);

id = {[ 'PA_Imbio',num2str(no), '__Momenta.txt' ]};
str = strjoin(id);

%% Importing Data
% Read momenta vectors from text file
fileID = fopen(str,'r');
formatSpec = '%f';
A = fscanf(fileID,formatSpec);

```

```

subjects = A(1); % Number of subject shapes used in
deformetrica model
controlPoints = A(2); % Number of control points used in
deformetrica model
dimensions = A(3); % Shape dimension (i.e. 2D or 3D)

% Initialise and populate a 2D momenta vector
PAmomenta2D = zeros(controlPoints*dimensions,subjects);

for j = 1:subjects
    offset = (j-1)*controlPoints*3;
    PAmomenta2D(1:controlPoints*3,j) =
A(4+offset:3+controlPoints*3+offset);
end

paMomenta2D = PAmomenta2D';

PApcasMs(i,:) = paMomenta2D * PApcasM;
PAplsMs(i,:) = paMomenta2D * PAplsSM;

end

for i = 4:14

no = noPaval(i);

id = {[ 'PA_S',num2str(no), '_Momenta.txt' ]};
str = strjoin(id);

%% Importing Data
% Read momenta vectors from text file
fileID = fopen(str,'r');
formatspec = '%f';
A = fscanf(fileID,formatspec);

subjects = A(1); % Number of subject shapes used in
deformetrica model
controlPoints = A(2); % Number of control points used in
deformetrica model
dimensions = A(3); % Shape dimension (i.e. 2D or 3D)

% Initialise and populate a 2D momenta vector
PAmomenta2D = zeros(controlPoints*dimensions,subjects);

for j = 1:subjects
    offset = (j-1)*controlPoints*3;
    PAmomenta2D(1:controlPoints*3,j) =
A(4+offset:3+controlPoints*3+offset);
end

paMomenta2D = PAmomenta2D';

```

```

PApcaSMs(i,:) = paMomenta2D * PApcaSM;
PAplsSMs(i,:) = paMomenta2D * PAplsSM;

end

% Import Pressure Data
fileID2 = fopen('PAval.txt','r');
formatSpec2 = '%f';
B = fscanf(fileID2,formatSpec2); % numerical vector of mPaP data
PAmPAP = B;

fileID2 = fopen('AOval.txt','r');
formatSpec2 = '%f';
C = fscanf(fileID2,formatSpec2); % numerical vector of mPaP data
AOmPAP = C;

% Import PH Data
fileID3 = fopen('PAvalPH.txt','r');
formatSpec3 = '%f';
D = fscanf(fileID3,formatSpec3); % numerical vector of mPaP data
PAph = D;

fileID3 = fopen('AOvalPH.txt','r');
formatSpec3 = '%f';
E = fscanf(fileID3,formatSpec3); % numerical vector of mPaP data
AOph = E;

PAsubject = noPAval';
AOsubject = noAOval';

% Put data into table
PAT = table(PAsubject,PAmPAP,PAph);
AOT = table(AOsubject,AOmPAP,AOph);

%% Index for success rates
x = {'Patients Successfully Classified' 'Patients Unsuccessfully Classified'};
% PA PCA Shape Mode 1
SM = 1;
SMcutoff = 1060;
c = 0;
n = 1;
[SucPrct(n,:),TP(n,:),TN(n,:),FP(n,:),FN(n,:),spec(n,:),sens(n,:))]
= indVal(c,SMcutoff,PAT,PApcaSMs,SM);

figure(1)
bar1 = [(TP(n,:)+TN(n,:)) TP(n,:) TN(n,:); (FN(n,:)+FP(n,:))
FN(n,:) FP(n,:)];
b1 = bar(bar1,'FaceColor','flat');
b1(1).FaceColor = [0.4940 0.1840 0.5560];
b1(2).FaceColor = [0.6350 0.0780 0.1840];
b1(3).FaceColor = [0 0.4470 0.7410];
box on

```

```

grid minor
xticklabels(x)
ylabel("No.",'interpreter','latex')
ylim([0 12])
title("Validation Results of PCA Shape Mode
1",'interpreter','latex')
subtitle("Main Pulmonary Artery",'interpreter','latex')
legend("Healthy and Diagnosed Patients","Patients with Pulmonary
Hypertension","Healthy Patients",'interpreter','latex')
set(gca,'TickLabelInterpreter','latex')
set(gcf,'Position',[600 400 800 400])
str = {strjoin(["Successful Classification Rate:
",num2str(SucPrct(n,:)),"\%"])};
annotation('textbox',[0.68 0.6 0.1
0.1],'Interpreter','latex','String',str,'BackgroundColor','w','FitB
oxToText','on','HorizontalAlignment','center')

xtips1 = b1(1).XEndPoints;
ytips1 = b1(1).YEndPoints;
labels1 = string(b1(1).YData);
text(xtips1,ytips1,labels1,'HorizontalAlignment','center','Vertical
Alignment','bottom','Interpreter','latex')

xtips2 = b1(2).XEndPoints;
ytips2 = b1(2).YEndPoints;
labels2 = string(b1(2).YData);
text(xtips2,ytips2,labels2,'HorizontalAlignment','center','Vertical
Alignment','bottom','Interpreter','latex')

xtips3 = b1(3).XEndPoints;
ytips3 = b1(3).YEndPoints;
labels3 = string(b1(3).YData);
text(xtips3,ytips3,labels3,'HorizontalAlignment','center','Vertical
Alignment','bottom','Interpreter','latex')

% PA PCA Shape Mode 6
SM = 6;
SMcutoff = 250;
c = 0;
n = n + 1;
[SucPrct(n,:),TP(n,:),TN(n,:),FP(n,:),FN(n,:),spec(n,:),sens(n,:)]
= indVal(c,SMcutoff,PAt,PApcaSMs,SM);

figure(2)
bar2 = [(TP(n,:)+TN(n,:)) TP(n,:) TN(n,:); (FN(n,:)+FP(n,:))
FN(n,:) FP(n,:)];
b2 = bar(bar2,'FaceColor','flat');
b2(1).FaceColor = [0.4940 0.1840 0.5560];
b2(2).FaceColor = [0.6350 0.0780 0.1840];
b2(3).FaceColor = [0 0.4470 0.7410];
box on
grid minor
xticklabels(x)

```

```

ylabel("No.",'interpreter','latex')
ylim([0 12])
title("Validation Results of PCA Shape Mode
6",'interpreter','latex')
subtitle("Main Pulmonary Artery",'interpreter','latex')
legend("Healthy and Diagnosed Patients","Patients with Pulmonary
Hypertension","Healthy Patients",'interpreter','latex')
set(gca,'TickLabelInterpreter','latex')
set(gcf,'Position',[600 400 800 400])
str = {strjoin(["Successful Classification Rate:
",num2str(SucPrct(n,:)),"\%"]);}
annotation('textbox',[0.68 0.6 0.1
0.1],'Interpreter','latex','String',str,'BackgroundColor','w','FitB
oxToText','on','HorizontalAlignment','center')

xtips1 = b2(1).XEndPoints;
ytips1 = b2(1).YEndPoints;
labels1 = string(b2(1).YData);
text(xtips1,ytips1,labels1,'HorizontalAlignment','center','Vertical
Alignment','bottom','Interpreter','latex')

xtips2 = b2(2).XEndPoints;
ytips2 = b2(2).YEndPoints;
labels2 = string(b2(2).YData);
text(xtips2,ytips2,labels2,'HorizontalAlignment','center','Vertical
Alignment','bottom','Interpreter','latex')

xtips3 = b2(3).XEndPoints;
ytips3 = b2(3).YEndPoints;
labels3 = string(b2(3).YData);
text(xtips3,ytips3,labels3,'HorizontalAlignment','center','Vertical
Alignment','bottom','Interpreter','latex')

% PA PLS Good Index Shape Mode 1
SM = 1;
SMcutoff = -1000;
c = 1;
n = n + 1;
[SucPrct(n,:),TP(n,:),TN(n,:),FP(n,:),FN(n,:),spec(n,:),sens(n,:)]
= indVal(c,SMcutoff,PAt,PAplsSMS,SM);

figure(3)
bar3 = [(TP(n,:)+TN(n,:)) TP(n,:) TN(n,:); (FN(n,:)+FP(n,:))
FN(n,:) FP(n,:)];
b3 = bar(bar3,'FaceColor','flat');
b3(1).FaceColor = [0.4940 0.1840 0.5560];
b3(2).FaceColor = [0.6350 0.0780 0.1840];
b3(3).FaceColor = [0 0.4470 0.7410];
box on
grid minor
xticklabels(x)
ylabel("No.",'interpreter','latex')
ylim([0 12])

```

```

title("Validation Results of PLS Shape Mode
1",'interpreter','latex')
subtitle("Main Pulmonary Artery",'interpreter','latex')
legend("Healthy and Diagnosed Patients","Patients with Pulmonary
Hypertension","Healthy Patients",'interpreter','latex')
set(gca,'TickLabelInterpreter','latex')
set(gcf,'Position',[600 400 800 400])
str = {strjoin(["Successful Classification Rate:
",num2str(SucPrct(n,:)),"\%"]);}
annotation('textbox',[0.68 0.6 0.1
0.1],'Interpreter','latex','String',str,'BackgroundColor','w','FitB
oxToText','on','HorizontalAlignment','center')

xtips1 = b3(1).XEndPoints;
ytips1 = b3(1).YEndPoints;
labels1 = string(b3(1).YData);
text(xtips1,ytips1,labels1,'HorizontalAlignment','center','Vertical
Alignment','bottom','Interpreter','latex')

xtips2 = b3(2).XEndPoints;
ytips2 = b3(2).YEndPoints;
labels2 = string(b3(2).YData);
text(xtips2,ytips2,labels2,'HorizontalAlignment','center','Vertical
Alignment','bottom','Interpreter','latex')

xtips3 = b3(3).XEndPoints;
ytips3 = b3(3).YEndPoints;
labels3 = string(b3(3).YData);
text(xtips3,ytips3,labels3,'HorizontalAlignment','center','Vertical
Alignment','bottom','Interpreter','latex')

% AO PCA Shape Mode 20
SM = 20;
SMcutoff = 0;
c = 0;
n = n + 1;
[SucPrct(n,:),TP(n,:),TN(n,:),FP(n,:),FN(n,:),spec(n,:),sens(n,:)]
= indVal(c,SMcutoff,A0t,A0pcaSMs,SM);

figure(4)
bar4 = [(TP(n,:)+TN(n,:)) TP(n,:) TN(n,:); (FN(n,:)+FP(n,:))
FN(n,:) FP(n,:)];
b4 = bar(bar4,'FaceColor','flat');
b4(1).FaceColor = [0.4940 0.1840 0.5560];
b4(2).FaceColor = [0.6350 0.0780 0.1840];
b4(3).FaceColor = [0 0.4470 0.7410];
box on
grid minor
xticklabels(x)
ylabel("No.",'interpreter','latex')
ylim([0 12])
title("Validation Results of PCA Shape Mode
20",'interpreter','latex')

```

```

subtitle("Aorta",'interpreter','latex')
legend("Healthy and Diagnosed Patients","Patients with Pulmonary
Hypertension","Healthy Patients",'interpreter','latex')
set(gca,'TickLabelInterpreter','latex')
set(gcf,'Position',[600 400 800 400])
str = {strjoin(["Successful Classification Rate:
",num2str(SucPrct(n,:)),"\%"]);}
annotation('textbox',[0.68 0.6 0.1
0.1], 'Interpreter','latex', 'String',str, 'BackgroundColor', 'w', 'FitB
oxToText', 'on', 'HorizontalAlignment', 'center')

xtips1 = b4(1).XEndPoints;
ytips1 = b4(1).YEndPoints;
labels1 = string(b4(1).YData);
text(xtips1,ytips1,labels1,'HorizontalAlignment','center','Vertical
Alignment','bottom','Interpreter','latex')

xtips2 = b4(2).XEndPoints;
ytips2 = b4(2).YEndPoints;
labels2 = string(b4(2).YData);
text(xtips2,ytips2,labels2,'HorizontalAlignment','center','Vertical
Alignment','bottom','Interpreter','latex')

xtips3 = b4(3).XEndPoints;
ytips3 = b4(3).YEndPoints;
labels3 = string(b4(3).YData);
text(xtips3,ytips3,labels3,'HorizontalAlignment','center','Vertical
Alignment','bottom','Interpreter','latex')

% AO PCA Shape Mode 22
SM = 22;
SMcutoff = -38;
c = 1;
n = n + 1;
[SucPrct(n,:),TP(n,:),TN(n,:),FP(n,:),FN(n,:),spec(n,:),sens(n,:)]
= indVal(c,SMcutoff,A0t,A0pcaSMs,SM);

figure(5)
bar5 = [(TP(n,:)+TN(n,:)) TP(n,:) TN(n,:); (FN(n,:)+FP(n,:))
FN(n,:)] FP(n,:];
b5 = bar(bar5, 'FaceColor', 'flat');
b5(1).FaceColor = [0.4940 0.1840 0.5560];
b5(2).FaceColor = [0.6350 0.0780 0.1840];
b5(3).FaceColor = [0 0.4470 0.7410];
box on
grid minor
xticklabels(x)
ylabel("No.",'interpreter','latex')
ylim([0 12])
title("Validation Results of PCA Shape Mode
22",'interpreter','latex')
subtitle("Aorta",'interpreter','latex')

```

```

legend("Healthy and Diagnosed Patients","Patients with Pulmonary
Hypertension","Healthy
Patients",'interpreter','latex','Location','northwest')
set(gca,'TickLabelInterpreter','latex')
set(gcf,'Position',[600 400 800 400])
str = {strjoin(["Successful Classification Rate:
",num2str(SucPrct(n,:)),"\%"]);}
annotation('textbox',[0.252 0.6 0.1
0.1],'Interpreter','latex','String',str,'BackgroundColor','w','FitB
oxToText','on','HorizontalAlignment','center')

xtips1 = b5(1).XEndPoints;
ytips1 = b5(1).YEndPoints;
labels1 = string(b5(1).YData);
text(xtips1,ytips1,labels1,'HorizontalAlignment','center','Vertical
Alignment','bottom','Interpreter','latex')

xtips2 = b5(2).XEndPoints;
ytips2 = b5(2).YEndPoints;
labels2 = string(b5(2).YData);
text(xtips2,ytips2,labels2,'HorizontalAlignment','center','Vertical
Alignment','bottom','Interpreter','latex')

xtips3 = b5(3).XEndPoints;
ytips3 = b5(3).YEndPoints;
labels3 = string(b5(3).YData);
text(xtips3,ytips3,labels3,'HorizontalAlignment','center','Vertical
Alignment','bottom','Interpreter','latex')

% Specificity from 1-specificity
spec = 1- spec;

% Put into a tablea and display
ValT = table(SucPrct,TP,TN,FN,FP,sens,spec);
disp(ValT)

```

## 9.10 Appendix I – Deformetrica File

```
import os
import deformetrica as dfca
import glob

### EDIT THESE PATHS #####
data_path = '/home/ssgm_uni/deformetrica/fyp/datasets/'
data_base = os.path.join(data_path, 'align/DataPA/')

output_directory = './clinicalPA_output/' #directory where the
outputs will be saved
#####

iteration_status_dictionaries = []

def estimator_callback(status_dict):
    iteration_status_dictionaries.append(status_dict)
    return True

# instantiate a Deformetrica object
deformetrica = dfca.Deformetrica(output_dir=output_directory,
verbosity='INFO')

template_file = os.path.join(data_base, 'S12.vtk') #Define S12
as template file
vtk_files = glob.glob(os.path.join(data_base, '*.vtk')) #Grab
all .vtk files from the data folder
vtk_files.remove(template_file) #Remove the template file

dataset_files = []
subject_ids = []
for i, file_name in enumerate(vtk_files):
    ID = os.path.basename(file_name).split('.vtk')[0] #Get
'ImbioXX' or 'SXX' as a string for subjectID
    tmp = [{'pulmonary artery': file_name}]
    dataset_files.append(tmp)
    subject_ids.append(ID)

dataset_specifications = { 'dataset_filenames' : dataset_files,
'subject_ids' : subject_ids }

template_specifications = {
```

```

    'pulmonary artery': {'deformable_object_type':
'SurfaceMesh',
                    'kernel_type': 'torch', 'kernel_width': 17.0,
#Vary this one
                    'noise_std': 2.0, #Vary this one
                    'filename': template_file,
                    'attachment_type': 'Current',
                    #'kernel_device' : 'cpu'
                    }
}

estimator_options={'optimization_method_type':
'GradientAscent',
                    'initial_step_size': 0.01, #
                    'max_iterations': 500, #
                    'max_line_search_iterations': 10,
                    'convergence_tolerance': 1e-5, #
                    'freeze_template': 'Off',
                    'number_of_processes': 4,
                    'callback': estimator_callback}

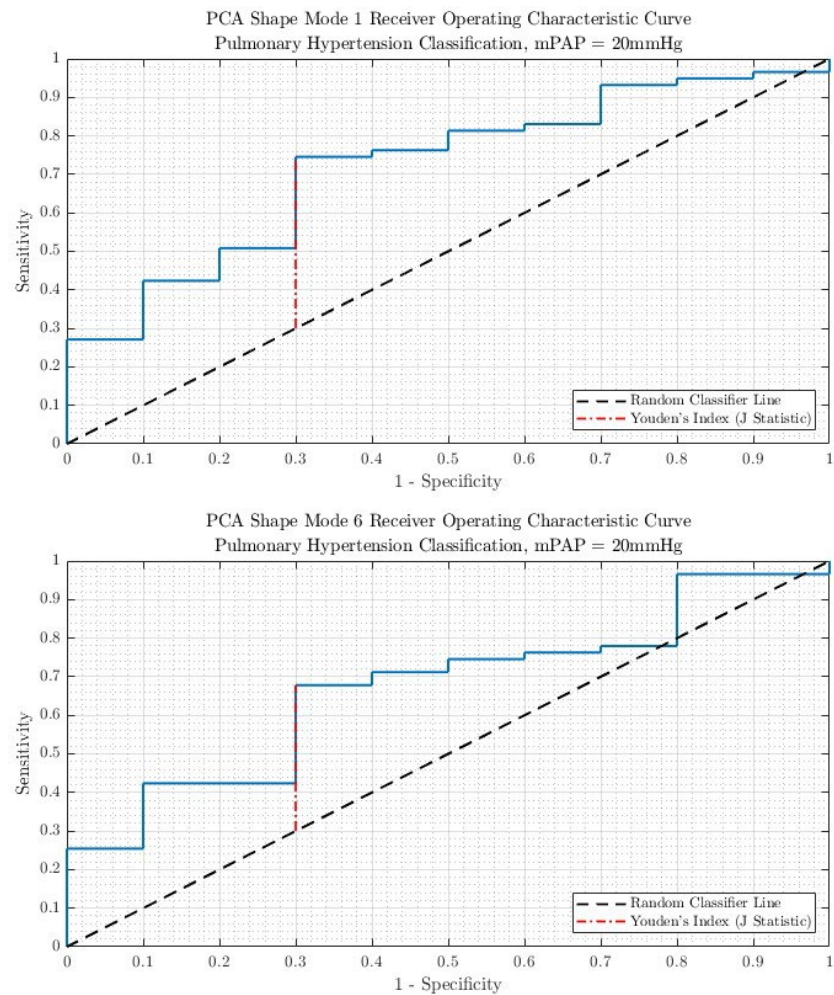
# deformation-parameters
model_options={'deformation_kernel_type': 'torch',
                'deformation_kernel_width': 17.0, #vary this one
                'dtype': 'float32'}
```

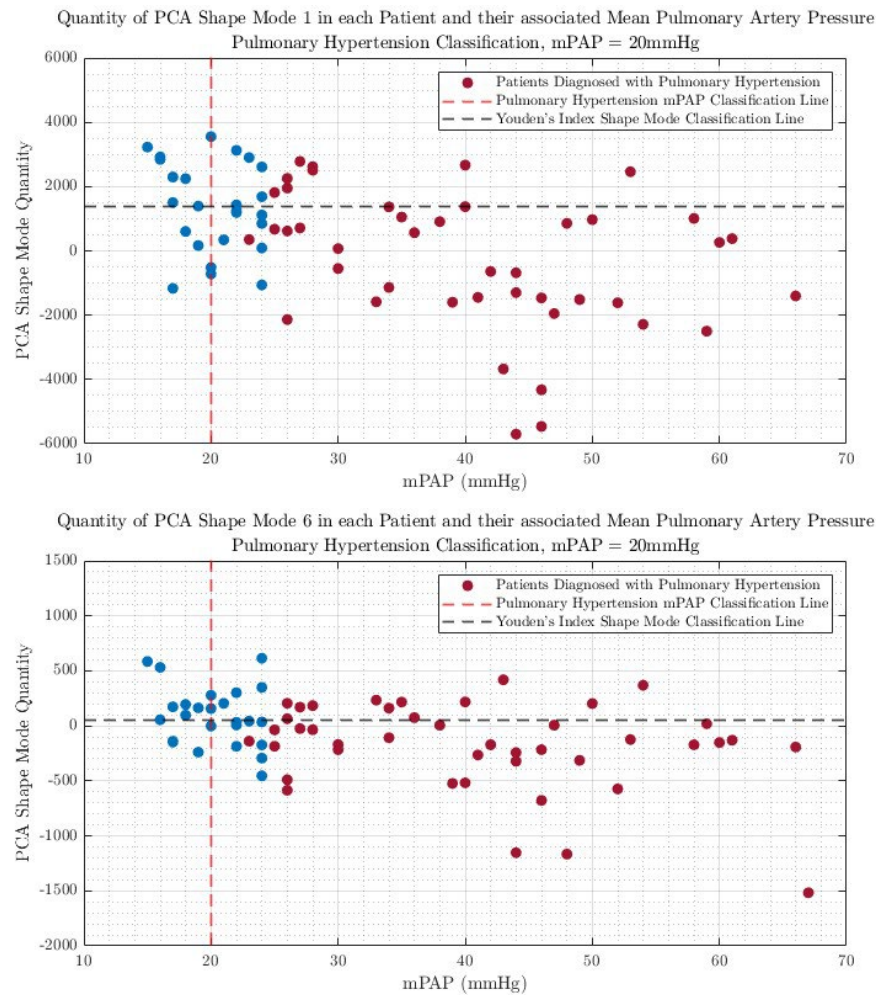
model =

```
deformetrica.estimate_deterministic_atlas(template_specifications, dataset_specifications, estimator_options, model_options=model_options)
```

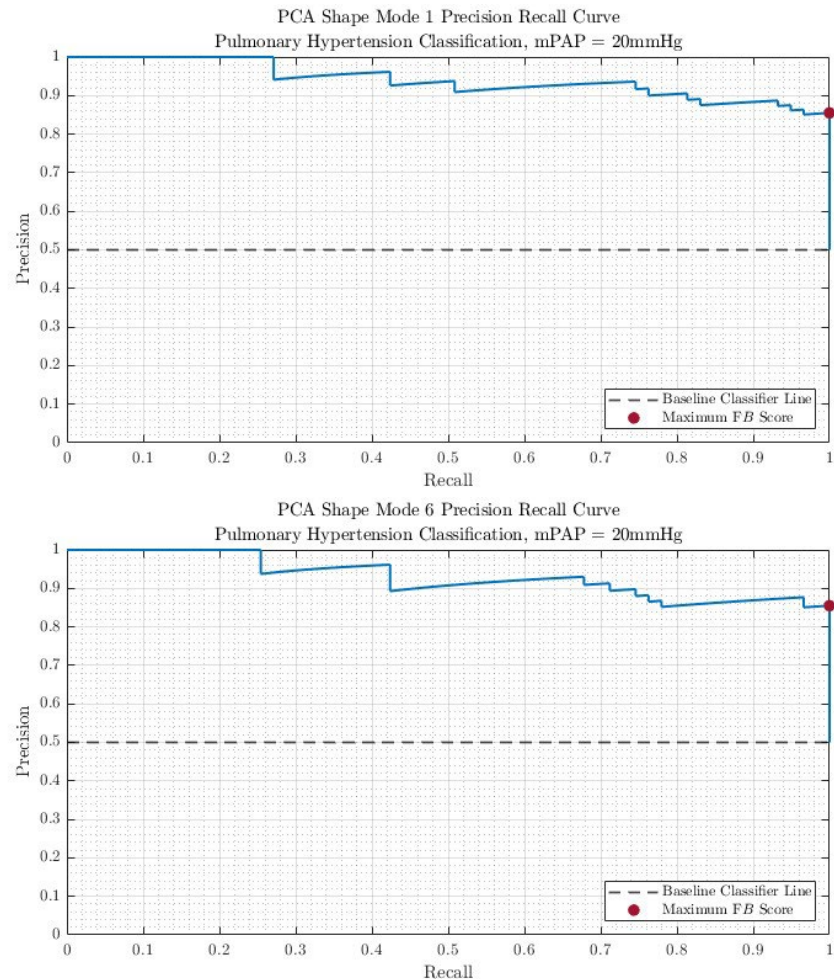
## 9.11 Appendix J – New PH Definition Results - PCA Main Pulmonary Artery

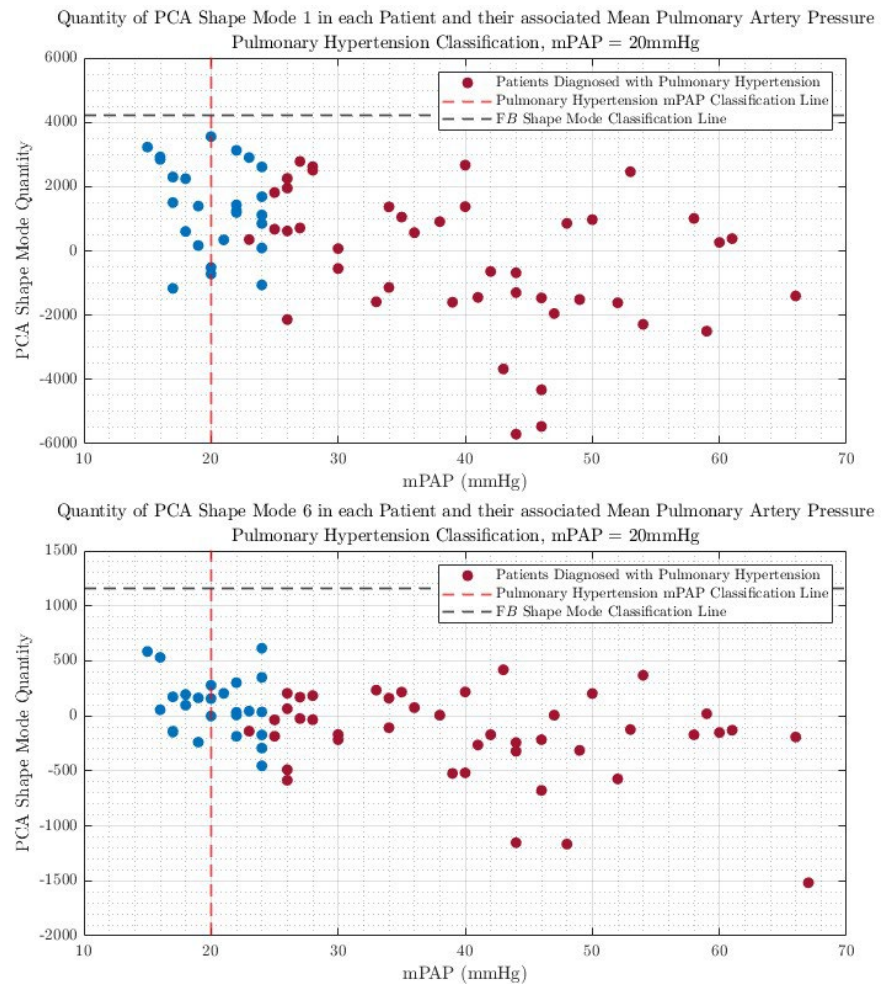
### 9.11.1 Receiver Operating Characteristic (ROC)





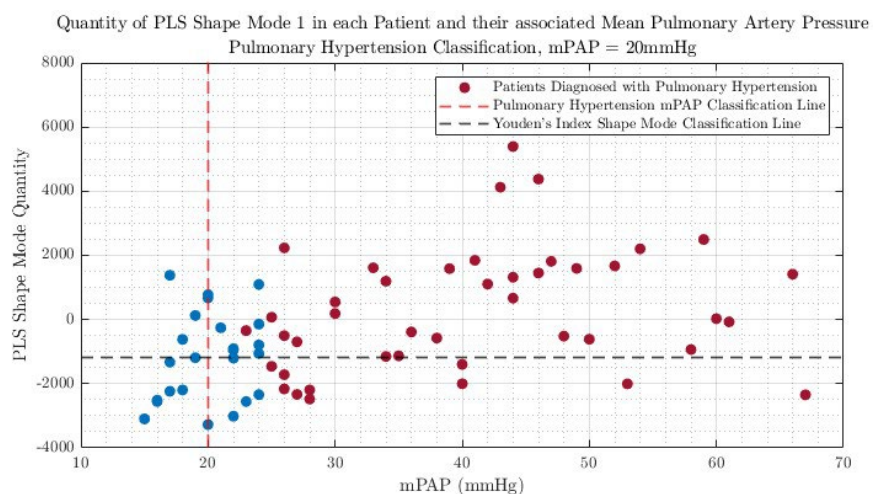
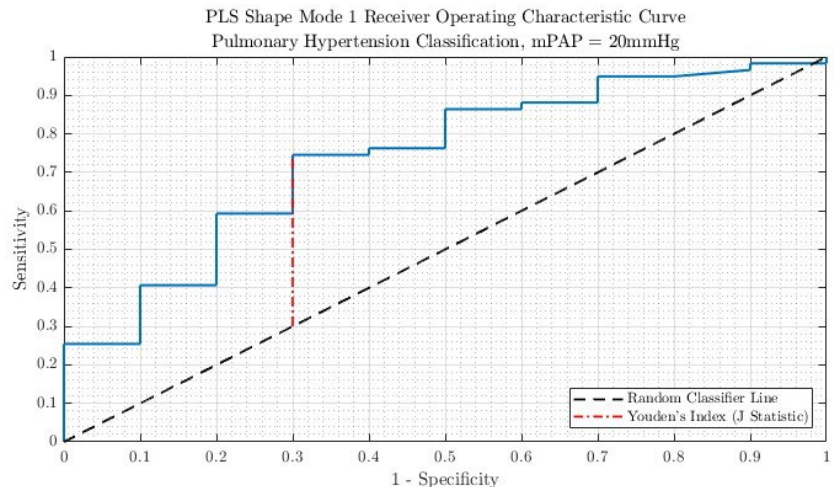
### 9.11.2 Precision Recall Curve (PRC)



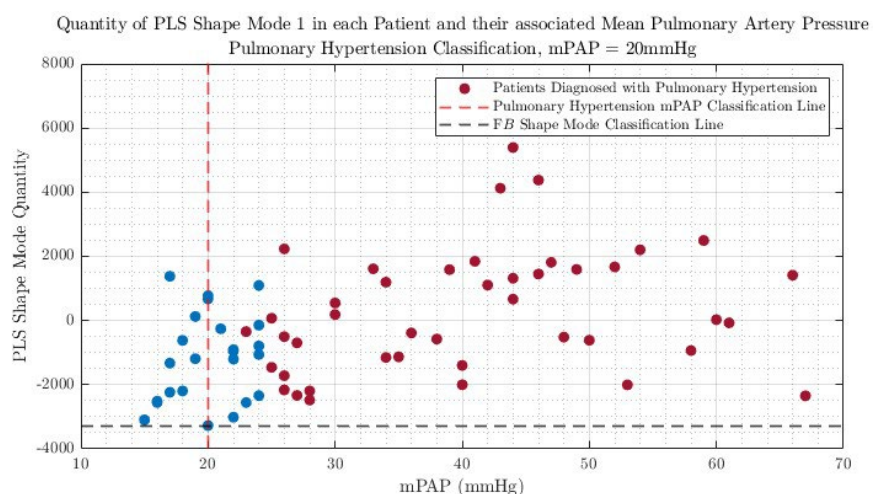
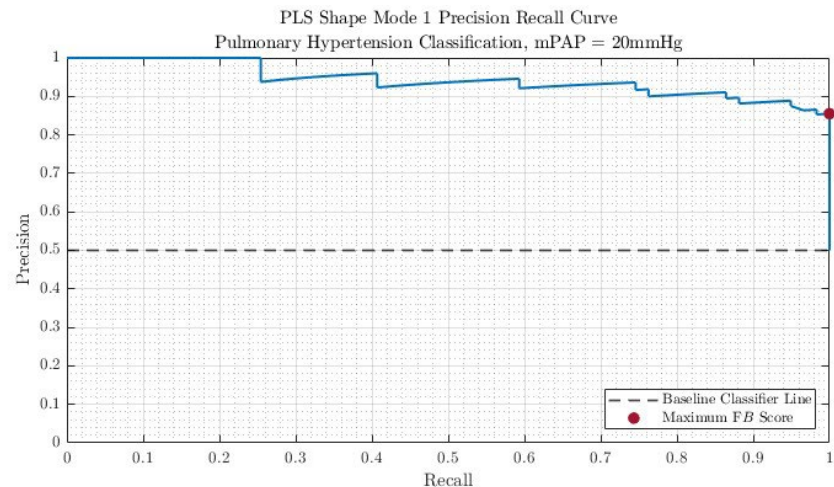


## 9.12 Appendix K – New PH Definition Results - PLS Main Pulmonary Artery

### 9.12.1 Receiver Operating Characteristic (ROC)

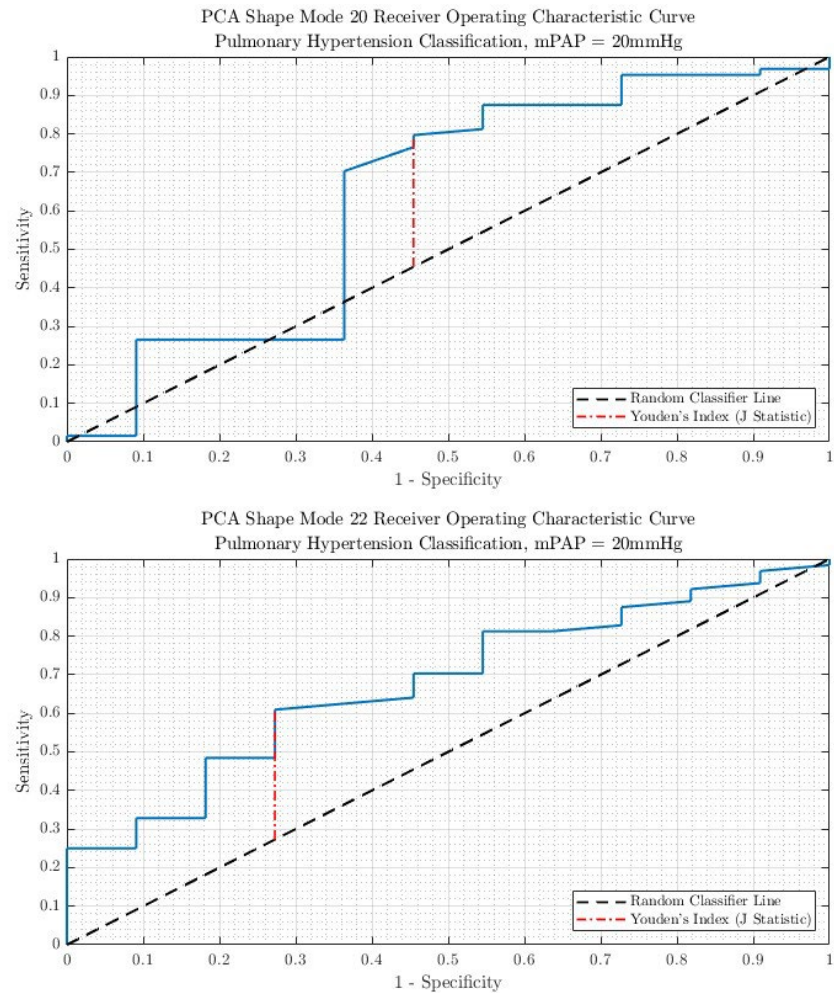


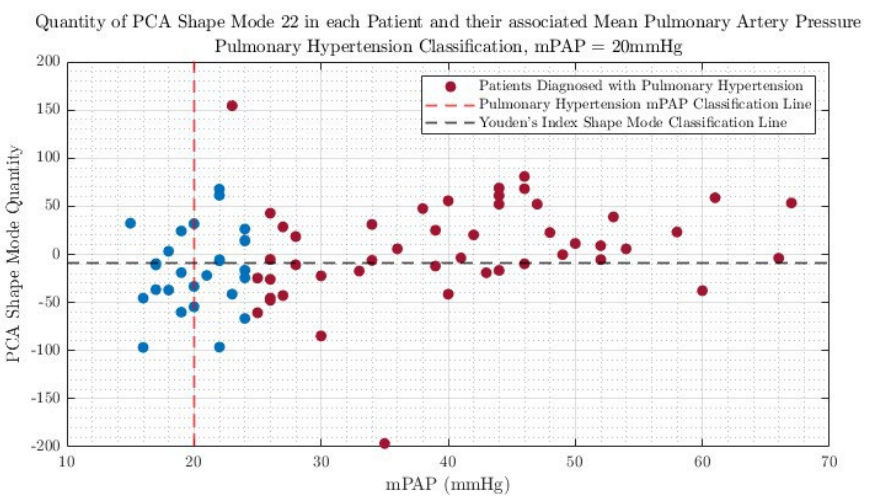
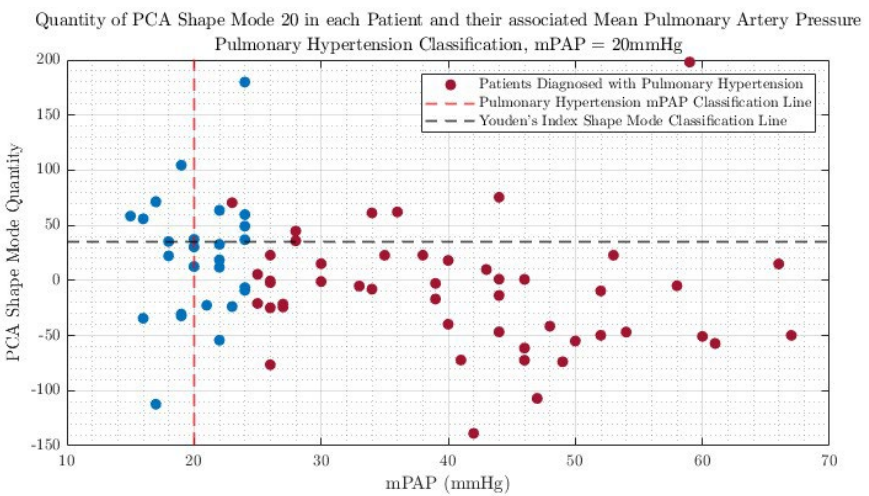
### 9.12.2 Precision Recall Curve (PRC)



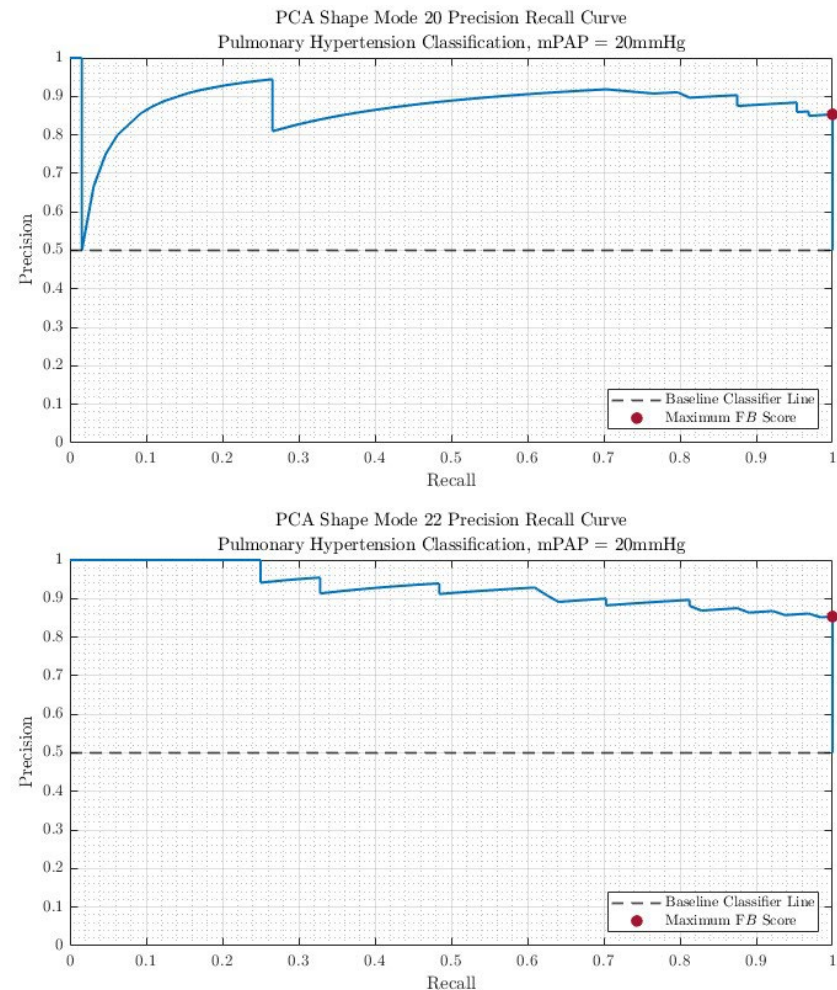
## 9.13 Appendix L – New PH Definition Results - PCA Aorta

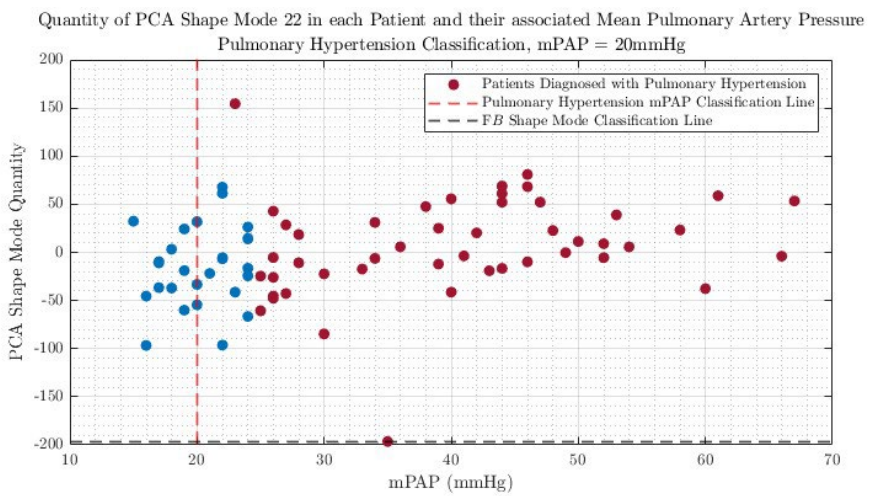
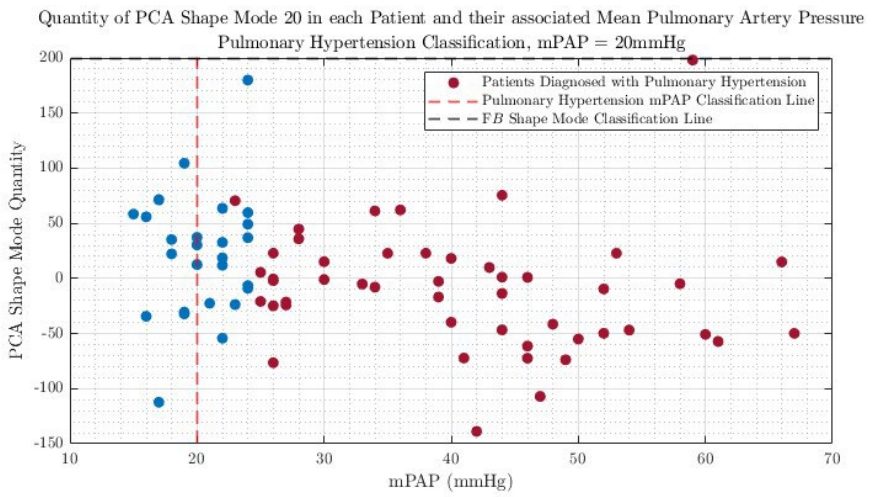
### 9.13.1 Receiver Operating Characteristic (ROC)





### 9.13.2 Precision Recall Curve (PRC)





## 9.14 Appendix M – Extra Information

### 9.14.1 PH Classifications

PH is classified into five groups. Within these classifications, clinical conditions manifesting PH are categorised by pathological, pathophysiological, and therapeutic characteristics. Despite comparable pulmonary arterial pressure (PAP) and PVR elevations across distinct clinical groups, the underlying mechanisms, diagnostic and prognostic approaches, and therapeutic implications are distinctively different (Galie et al., 2009).

These five groups are:

- Pulmonary Arterial Hypertension (PAH) and Idiopathic Pulmonary Arterial Hypertension (IPAH).
- Pulmonary Hypertension due to left heart disease.
- Pulmonary Hypertension due to lung diseases/hypoxia.
- Chronic Thromboembolic Pulmonary Hypertension (CTEPH).
- Pulmonary Hypertension with unclear or multifactorial mechanisms.

Although these classifications hold significant relevance for patient prognosis and treatment, due to time restrictions, this project will concentrate on the broad detection of PH rather than simultaneously attempting to categorise the specific aetiology of the identified PH.

### 9.14.2 Segmentation

Studies with similar investigative aims have tended to begin with the acquisition of high-resolution image data, such as magnetic resonance images (MRI) or computed tomography (CT) scans, capturing the three-dimensional morphology of biological structures (Ambellan et al., 2019). Manual or automated segmentation using machine learning algorithms would be conducted from these. Segmentation is a process which delineates structures of interest from medical images, ensuring accurate shape representation. By isolating relevant anatomical regions, segmentation facilitates the extraction of shape features essential for modelling variability within populations. However, segmentation is not within the scope of the project due to time restrictions and, therefore, will not be conducted. The segmented medical image data for the pulmonary artery and aorta, in neuroimaging informatics technology initiative (NIfTI)

format, was used for the project and was kindly provided by Liam Burrows through a machine learning algorithm he created. The precision and resolution of the provided segmented data will enhance the reliability of the statistical analysis, offering greater opportunities for more discreet variations within the dataset to be captured (Rangayyan, n.d.). An example segmentation from the dataset is shown in Figure 18.

#### 9.14.3 Mesh Generation

In order to conduct SSM, each .NIfTI data file containing the segmented anatomies requires conversion to a surface mesh due to its capability to accurately represent geometric shapes and facilitation of feature extraction whilst offering a lesser computationally intensive method to volumetric data. Surface mesh files in Visualisation Toolkit (VTK) format were selected predominantly for their compatibility with a desired software, which will be later discussed; however, the format also offered a versatile, efficient and standardised geometric data storage solution (“VTK File Formats - VTK documentation,” n.d.).

#### 9.14.4 Bayesian Vs Deterministic Atlases

Deterministic atlases and Bayesian atlases represent two fundamental approaches in SSM, each with distinct characteristics. Deterministic atlases are constructed by computing a mean shape from a set of aligned anatomical structures. They serve as a fixed reference template, providing a standard model against which individual shapes can be compared. This approach offers simplicity and ease of interpretation, making it suitable for situations where the mean shape adequately captures the primary structural variability. However, its rigidity in representing variations can be a drawback when modelling highly variable populations, potentially leading to less accurate predictions (Davies et al., 2008).

On the other hand, Bayesian atlases utilise probabilistic models to represent shape variations. They incorporate prior information about anatomical structures and shape variability, allowing for a more flexible and accurate representation of diverse structures. This probabilistic framework can handle uncertainty and variability better, offering improved robustness in modelling complex anatomical changes. Nevertheless, the complexity of Bayesian methods can lead to increased computational demands and require careful tuning of prior distributions to prevent overfitting or underfitting (M.

Zhang et al., 2017) Consequently, the simplicity of the deterministic atlas is more suitable for the purposes of this project.

#### 9.14.5 Large Deformation Diffeomorphic Metric Mapping (LDDMM)

The core of this methodology lies in the deformation model, which creates a deformation field to map every point in the mean template to corresponding points in the target subject shape. This mapping process utilises transformation models such as Large Deformation Diffeomorphic Metric Mapping (LDDMM) transformations to account for global changes and non-linear transformations to capture local shape deformations (Beg et al., 2005). LDDMM models the transformations as a flow of vector fields. Specifically, it considers a time-dependent vector field,  $v$ , such that the diffeomorphism,  $\phi$ , evolves according to:

$$\frac{d\phi}{dt} = v(\phi)$$

With  $\phi_0$  being the identity map (Durrleman, 2010). LDDMM fundamentally solves a variational problem to find the optimal vector field,  $v_t$ . The solution to this issue provides a geodesic flow in the space of diffeomorphisms. The path,  $\phi_t$ , traced out by the optimal vector field,  $v_t$ , represents the shortest path between the source and target shapes.

#### 9.14.6 Laplacian and Taubin Filtering

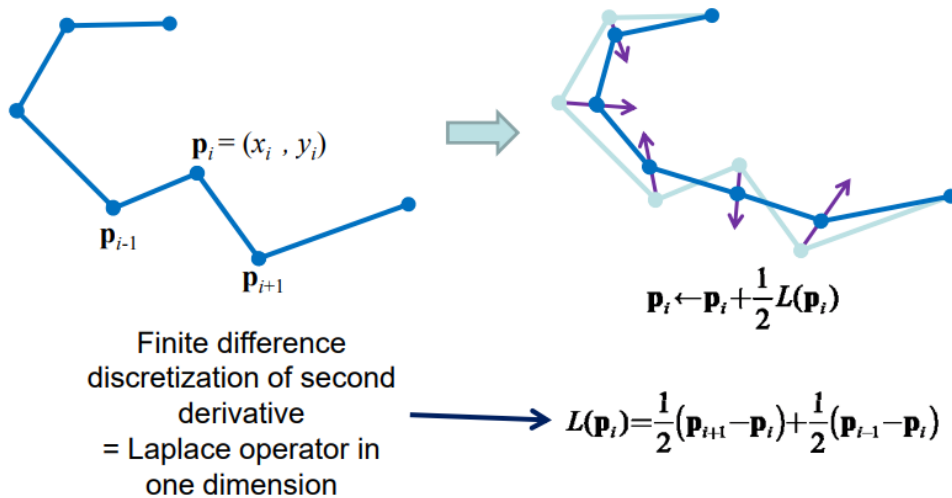
In previous similar studies, the main smoothing and denoising techniques used have been Taubin, Laplacian and Gaussian methodologies (Rigaud et al., 2019). Gaussian methods, although possessing a greater capability of preserving detailed features, are extremely sensitive and, therefore, difficult to use and time-consuming. As a result, it is more appropriate for larger anatomies like bone structures rather than blood vessels, as in this project. Hence, despite the method's iterative nature and tendency to shrink its subjects, Taubin and Laplcien seem more appropriate for the project (Schneider and Eberly, 2003).

Laplacian filtering, used for both denoising and smoothing, works by adjusting each vertex in the mesh to the average position of its adjacent vertices, effectively reducing local variations, as seen below. The update for each vertex,  $P_i = (x_i, y_i, z_i)$ , in the mesh can be described by the equation ("Mesh Smoothing.pdf," n.d.):

$$P'_i = P_i + \lambda \Delta P_i$$

Where:

- $P'_i$  is the new position of the vertex.
- $\lambda$  is a smoothing factor, usually  $0 < \lambda < 1$ .
- $\Delta P_i$  is the Laplacian vector at vertex  $P_i$ , defined as  $\Delta P_i = \frac{1}{N_i} \sum_{j \in N(i)} (P_j - P_i)$ .
- $N(i)$  represents the set of vertices adjacent to  $P_i$ , and  $N_i$  is the number of such vertices.
- This is repeated for  $m$  iterations.



Taubin smoothing was proposed to counteract the shrinkage problem inherent in Laplacian smoothing, consisting of an alternating shrinking step, similar to Laplacian and an inflating step moving vertices outwards. Taubin filtering is primarily used for smoothing rather than denoising, effectively reducing high-frequency noise while preserving the overall subject shape ((Taubin et al., 1996)). The two passes involved:

- First Shrinking Pass:  $P'_i = P_i + \lambda \Delta P_i$
- Next Inflating Pass:  $P''_i = P_i - \mu \Delta P'_i$

Where:

- $P''_i$  is the final position of the vertex after the second pass.
- $\mu$  is a factor usually set to a value slightly larger than  $\lambda$  but negative, chosen to counteract the shrinkage from the first pass.

In order for Taubin to be effective, these parameters require careful tuning, such that the inflation pass acts as a correction rather than an excessive expansion of the mesh.

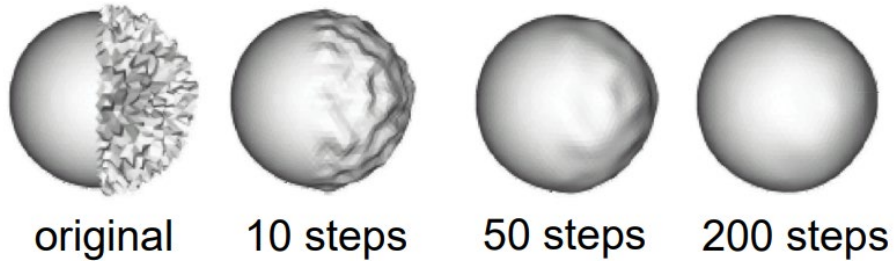
The Taubin filtering process is illustrated below.

**Iterate:**

$$\mathbf{p}_i \leftarrow \mathbf{p}_i + \lambda \Delta \mathbf{p}_i \quad \text{Shrink}$$

$$\mathbf{p}_i \leftarrow \mathbf{p}_i + \mu \Delta \mathbf{p}_i \quad \text{Inflate}$$

with  $\lambda > 0$  and  $\mu < 0$



#### 9.14.7 Kernel Width

The template kernel width defines the curvature of the shape space. Intuitively, this hyper-parameter controls the spatial resolution of the geometric changes that can be encoded in the progression pattern and should be chosen in relation to the size of the 3D surface mesh subjects (Sphocleous et al., 2022). Similarly, the model kernel width defines the curvature of an auxiliary shape space that allows the residuals to be computed between meshes that are not in point-to-point correspondence. Intuitively, this hyper-parameter controls the targeted level of detail when registering the longitudinal model to the observations; it should be set in relation to the size of the 3D surface mesh subjects (Sphocleous et al., 2022).

#### 9.14.8 Deformetrica

There are various tools which can be exploited in order to construct atlases for statistical shape analysis. A popular option in the literature is the visualisation toolkit (VTK) software (Sabry et al., 2024), which offers a broad visualisation library with a comprehensive set of visualisation and computational tools but lacks specialised features for SSM. On the other hand, Deformetrica is a specialised software toolkit designed for statistical analysis of 2D and 3D shapes, providing a suite of tools geared towards processing anatomical data. Its capabilities allow for detailed morphometric studies like in Bruse et al. study, with emphasis on the interpretation and visualisation of biological and medical data (Bruse et al., 2016). Although Deformetrica has yet to be used on the main pulmonary artery or the pulmonary artery capillary network in

previous studies, given that it has been used on other blood vessels like in the Bruse et al. study, it is logical to believe it will be successful in applying the software to these other blood vessel applications.

#### 9.14.9 Correlation Coefficients

In order to determine the classifying performance from the model, the shape mode variations which correlate the most to correctly classify whether a patient has PH or not need to be identified (Cutugno et al., 2021). Other studies have done this by plotting a scatter graph of shape mode amount for every subject on the y-axis and the diagnostic variable, the subjects' respective mPAP in our study, on the x-axis for each shape mode and determining which shape modes are exhibiting a correlation (Hollenbeck et al., 2018). Studies have tended to use a Pearson's Correlation Coefficient (PCC) however, PCC can only be used under certain conditions, which all need to be met (Schober et al., 2018):

- Linear Relationship – The two variables have a linear relationship, as one increases, the other increases or decreases by a constant amount.
- Continuous Data – PCC is most suited for continuous data and not recommended for categorical or ordinal data.
- Approximately Normally Distributed – Data must exhibit normality.
- No Outliers – There must be no significant outliers, as PCC is sensitive to outliers.

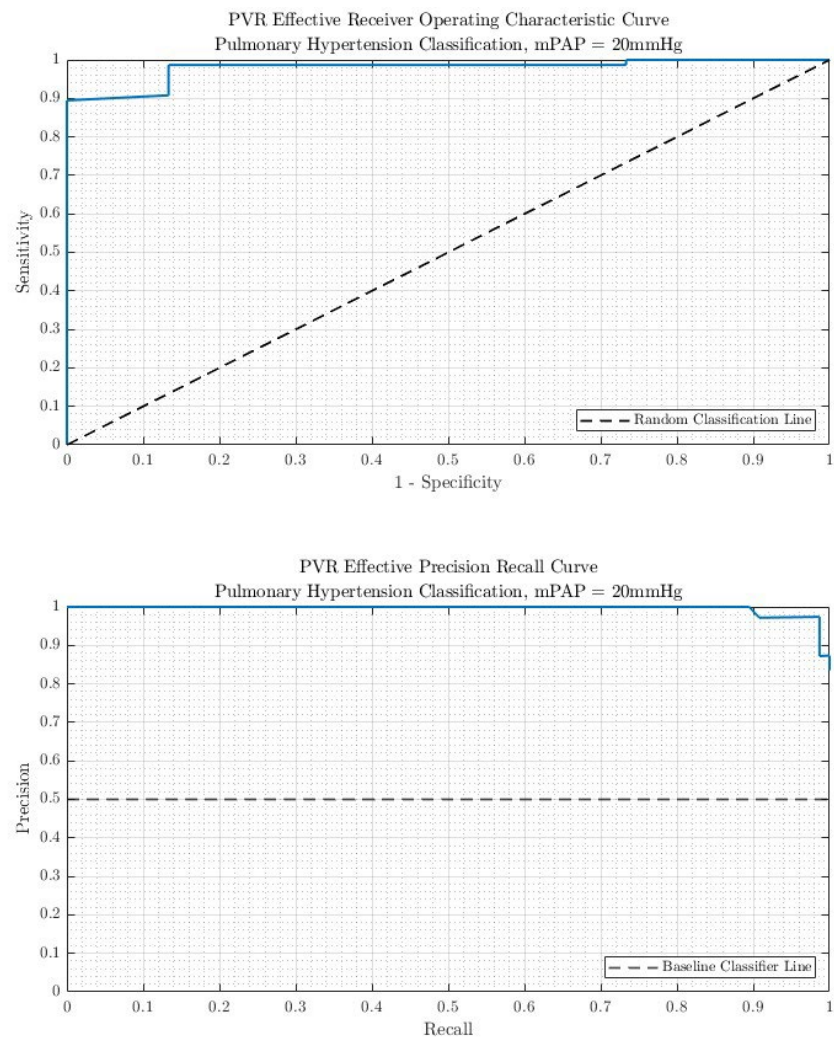
Hence, the input data needs to be tested for these conditions. If any fail, Spearman's Rank Correlation Coefficient can be used. Spearman's correlation does not assume linearity; instead, it measures the strength and direction of a monotonic relationship between two variables. A monotonic relationship means that as one variable increases, the other variable consistently increases or decreases, but not necessarily by a constant amount. Additionally, it does not require normality or continuous data and is less sensitive to outliers.

#### 9.14.10 Alignment

Among the studies reviewed, the Procrustes algorithm alignment method was prominent; however, there were varied approaches to data pre-processing. Medrano-Gracia et al. specified the use of fiducial landmarks for identifying identical key features across all patients to initialize mesh positions before conducting Procrustes alignment (Medrano-Gracia et al., 2014). On the other hand, Folco et al. specified the existence of point-to-point correspondence between meshes before commencing the study,

subsequently employing Procrustes alignment to eliminate translation and rotation disparities (Di Folco et al., 2020). Additionally, Procrustes analysis can standardise patient shapes to uniform sizes, yet most studies clarified that they did not alter the sizes of patient shapes, deeming this aspect crucial for evaluating anatomical shape variations associated with disease (Klingenberg, 2015). However, Medrano-Gracia et al addressed size disparities by scaling the sizes of left ventricles based on each patient's height. This approach facilitated the retention of size differences attributed to unknown causes, such as disease, while mitigating misguiding size variations in patient shapes due to overall patient size differences (Medrano-Gracia et al., 2014).

## 9.15 Appendix N – PVR Effective ROC Curve and PRC



## 9.16 Appendix O – PAA Effective ROC Curve and PRC

